Chaos and Chaos Control in Network Dynamical Systems

Dissertation
zur Erlangung des mathematisch-naturwissenschaftlichen Doktorgrades
"Doctor rerum naturalium"
der Georg–August–Universität Göttingen

im Promotionsprogramm Mathematik
der Georg–August University School of Science (GAUSS)

vorgelegt von
Christian Bick
aus Duisburg

Göttingen, 2012

Betreuungsausschuss

Prof. Dr. Marc Timme, Network Dynamics Group, Max Planck Institute for Dynamics and Self-Organization

Prof. Dr. Laurent Bartholdi, Mathematisches Institut, Georg–August–Universität Göttingen

Mitglieder der Prüfungskommission

Referent: Prof. Dr. Marc Timme, Network Dynamics Group, Max Planck Institute for Dynamics and Self-Organization

Korreferent: Prof. Dr. Laurent Bartholdi, Mathematisches Institut, Georg–August–Universität Göttingen

Weitere Mitglieder der Prüfungskommission:

Prof. Dr. Peter Ashwin, College of Engineering, Mathematics and Physical Sciences, University of Exeter

Prof. Dr. Gert Lube, Institut für Numerische und Angewandte Mathematik, Georg–August–Universität Göttingen

Prof. Dr. Anja Sturm, Institut für Mathematische Stochastik, Georg–August–Universität Göttingen

Prof. Dr. Florentin Wörgötter, III. Physikalisches Institut, Georg–August–Universität Göttingen

Tag der mündlichen Prüfung: 29.11.2012

Contents

In memory of my mother

Introduction

The theory of dynamical systems has its origins in the equations of motion of Newtonian mechanics. Henri Poincaré's initial work [85] laid the foundations for the modern theory of dynamical systems which draws from various mathematical disciplines including topology, geometry, analysis, and algebra [46]. Deterministic dynamical systems describe temporal evolutions on some space Y, that is, an element of Y is assigned to every point in time. This evolution is deterministic in the sense that it is completely determined by a given rule—there is no stochastic component determining these dynamics. In other words, if the present state $y \in Y$ of the system is known any future state can be unambiguously calculated from the present state y using the evolution rule. More formally, any such evolution—the trajectories or orbits of the system—is a function $x : I \to Y$ where $I \subset \mathbb{R}$ is some index set of real numbers $\mathbb{R}$, either discrete or connected [56]. In the former case we say that the dynamical system has discrete time, in the latter the system is referred to as a continuous time dynamical system. We will always assume that $0 \in I$. The value $x(0) = y$ is called the initial condition of the orbit x. If for a given initial condition not only the future but also the past is uniquely determined by a deterministic rule then we call such a dynamical system reversible.

Despite the fact that the future states of the system can be calculated exactly, it turns out that there are dynamical systems which exhibit "complicated" dynamics. Suppose that we have a notion of proximity on the space Y. One property that leads to such complicated dynamics is sensitive dependence on initial conditions. In contrast to the situation where initial conditions close to each other will lead to trajectories that stay close, this means that even the smallest change in initial condition will eventually lead to a separation of trajectories. This property is usually associated with what is referred to as chaotic dynamics. Chaotic dynamical systems exhibit, in spite of their deterministic nature, features of random motion. The so-called maximal Lyapunov exponent [10] is a way to measure the separation for a given orbit; if it takes a positive value then—averaged over time—trajectories close to this orbit drift away exponentially fast. A famous system that can exhibit such chaotic motion is given by the Lorenz equations [65]. Chaotic dynamics have been observed in a wide range of both low and high-dimensional deterministic dynamical systems [76]. An important class of differentiable dynamical systems that may exhibit chaotic dynamics are so-called (uniformly) hyperbolic systems [56, 98]. Here, system is characterized by distinct local expanding and contracting directions at every point of Y and thus the local properties are linked to global features of the dynamical system.

If the rule that defines the evolution of a deterministic dynamical system depends on a parameter, the dynamics of the system may undergo transitions as the parameter is varied. One says that a system bifurcates if its orbits undergo a change in their

dynamical equivalence class as a parameter is changed [42, 60]. In other words, at bifurcation points, the dynamics change qualitatively, for example through the emergence of new particular solutions such as a fixed point (an orbit x with $x(t) = \hat{x}$ for all $t \in I$). For instance, the transition from "simple" to more complex, chaotic dynamics as described above through the variation of a parameter corresponds to one or more bifurcations. These transitions are one of the main topics of this thesis.

The emergence of chaotic dynamics for dynamical systems on some real manifold underlies certain restrictions. Let $\mathbb{R}^N$ denote the N-dimensional vector space over the real numbers and suppose that the space Y is a subset of $\mathbb{R}^N$ of integer dimension. We focus on discrete time dynamical systems whose evolution is given by iterating a function $f : Y \to Y$. For these systems, chaotic dynamics can occur even if Y is one-dimensional. A well known example is the iteration of the logistic family, a collection of maps on the real line that depend on one real parameter [76]. For certain parameter values, its dynamics exhibit exponential separation of trajectories. In fact, the iteration of the logistic map is a special case of a classical topic studied in holomorphic dynamics (complex dynamics): the iteration of complex valued polynomials on the complex plane [71]. In complex dynamics one subdivides the plane into two completely invariant sets: the Fatou set, where trajectories with close initial conditions stay close and its complement, the Julia set, on which the dynamics are chaotic.

For continuous time dynamical systems on subsets $Y \subset \mathbb{R}^N$, the situation is slightly different. We will concentrate on those continuous time dynamical systems for which the dynamics are given by a differential equation. The dynamics of these systems are defined by a field of velocity vectors and its orbits are the integral curves. For example, if Y is some connected compact n-dimensional real manifold, the Poincaré–Bendixon theorem states that for $n < 3$ any solution of a dynamical system on such a manifold must be either periodic or quasiperiodic [56, 97]. Thus, the minimal dimension in which chaotic dynamics can occur is dimension three.

Dynamics and Symmetry

Dynamical systems on some smooth manifold Y may have additional structure such as symmetries. Suppose a group Γ acts on Y. A dynamical system on Y has symmetry group Γ if it is Γ-equivariant, that is, if the action of Γ on Y is "compatible" with the dynamics. When iterating a function f, compatibility corresponds to the condition that the group action commutes with f. For continuous time dynamics given by a system of differential equation on Y of order one, the action has to commute with the vector field that defines the differential equation. The presence of symmetries has several immediate consequences [39, 40]. For any orbit x of the dynamical system, any image of x under the group action is also an orbit of the system. Furthermore, the symmetry gives rise to dynamically invariant subspaces since any fixed point subspace of the group action is dynamically invariant. Hence, the possible dynamics of systems with symmetry may be restricted as the state space Y is subdivided by these flow-invariant subspaces. The study of continuous time dynamical systems with symmetry is the topic of the first part of this thesis.

In particular, we study systems of interacting oscillatory units that are commonly used in the modeling of physical systems. Examples include the dynamics of flashing fireflies, superconducting Josephson junctions, and oscillations in neural networks [82, 105]. A phase oscillator is characterized by a single phase-like variable that takes values on the one-dimensional torus $\mathbb{R}/2\pi\mathbb{Z}$. We consider systems of N interacting oscillators where each oscillator is driven by its own intrinsic frequency and all other oscillators. The interaction of two oscillators is determined by the value of a so-called coupling function of their phase differences. The dynamics are thus given by a differential equation on an N-dimensional torus. Such systems of coupled phase oscillators arise as averaged phase descriptions of weakly coupled, higher-dimensional limit cycle oscillators [7], for instance, neural oscillators [17, 55]. The most famous example of such systems are the Kuramoto equations where the coupling is given by a sine function [1, 59].

The possible dynamics of these coupled phase oscillators depend on both the choice of the intrinsic frequencies and the coupling function. If the intrinsic frequencies are distinct, there is a rich repertoire of possible dynamics including chaos [87]. The situation changes drastically when all intrinsic frequencies are the same. Then the system is symmetric with respect to the permutation of the oscillators as they become indistinguishable. Whereas the dynamics of symmetric higher-dimensional oscillators may be chaotic [74], the dynamics of symmetric phase oscillators with sine coupling becomes highly degenerate as they reduce to an effective two-dimensional system [107, 108]. This is due to the existence of $N-2$ independent constants of motion, the so-called Watanabe–Strogatz constants of motion [68]. If the coupling function contains more than one nontrivial Fourier coefficient, heteroclinic trajectories may occur. Previously, there had not been a single example of a coupling function giving rise to chaotic dynamics for systems of coupled phase oscillators with full permutational symmetry. This provides the main questions to be answered in the first part of this thesis. Are there coupling functions that give rise to chaotic dynamics? From a symmetry point of view, we ask if it is due to symmetry alone that the system cannot be chaotic, or whether it is the rather special form of the coupling that causes the degeneracy.

As the first crucial result, we show that there are in fact families of coupling functions that lead to the emergence of chaos in symmetric coupled phase oscillator systems. Here, chaos is characterized by positive maximal Lyapunov exponents, which were determined numerically. Since the coupling only depends on the phase differences, the N-dimensional system may be reduced to $(N-1)$-dimensional dynamics. We find that chaos in the system of symmetric phase oscillators is not only present in dimension four, the smallest dimension for which chaotic dynamics can occur, but also for some higher-dimensional systems.

The emergence of chaos leads to a number of follow-up questions. Chaotic attractors in dynamical systems with symmetries may have symmetries themselves. We systematically study the symmetries of the chaotic attractors for four oscillators and show that there are attractors of all possible symmetries. Moreover, one may ask which bifurcations lead to the emergence of chaos. A numerical bifurcation analysis shows that there is an abundance of both local and global bifurcations that are linked to the creation and destruction of the chaotic attractors.

The case of even coupling functions requires special attention as they give rise to additional symmetries. Dynamical systems may have so-called time reversing symmetries [61]. Whereas Γ-equivariance says that for any trajectory x and any $\gamma \in \Gamma$ the image γx is also an orbit of the system, the existence of a reversing symmetry ϱ implies that ϱx is a solution when time is reversed. This implies that for any trajectory there is a trajectory with inverse stability properties. Furthermore, the sets of fixed points of reversing symmetries are of interest as they may give rise to certain families of particular solutions [38]. In addition to the equivariance, such reversing symmetries are present in our system of coupled phase oscillators for even coupling functions. An even coupling function is invariant under the reflection in the origin. It is this additional property which implies the existence of reversing symmetries. Furthermore, when solving the equations of motion for a system of four oscillators with even coupling numerically, we observe only periodic orbits. This motivates the main question for the last section of the first part: what are the dynamics of phase oscillators with even coupling functions? Does the existence of reversing symmetries cause degeneracy, for example through constants of motion which lead to the periodic dynamics?

For phase oscillators with even coupling functions there are in fact constants of motion for some coupling topologies. This is the result presented in the last section of the first chapter. Even though the question about the existence of constants of motion of the fully symmetric system in arbitrary dimension is still open, there is a constant of motion for rings of oscillators. The main result may be stated in form of the following theorem.

Theorem A. *There exists a constant of motion for rings of Kuramoto-like phase oscillators of any length N with even coupling. In particular, for $N = 3$ this constant of motion generalizes the Watanabe–Strogatz constant of motion for coupling functions with one nonzero Fourier coefficient to arbitrary even coupling functions.*

See Section 1.3 and in particular Proposition 1.3.3 for a more precise formulation of this statement.

Theory of Chaos Control

Even though deterministic dynamical systems may yield essentially unpredictable long-term dynamics, other properties of such chaotic systems give rise to interesting applications. Within the remainder of this section, we focus on discrete time dynamical systems given by the iteration of some function $f : \mathbb{R}^N \to \mathbb{R}^N$. Furthermore, we suppose that $I \subset \mathbb{Z}$. Recall that a periodic orbit is an orbit that returns to its initial condition after some finite time T, i.e., there exists a $T > 0$ such that $x(t + T) = x(t)$ for all $t \in I$. These periodic orbits may be classified with respect to their local dynamics, i.e., the dynamical behavior of trajectories whose initial conditions are contained in a small neighborhood of the periodic orbit. If there is an open neighborhood of the periodic orbit such that all trajectories with initial conditions within this neighborhood converge to the periodic orbit then it is called stable. Otherwise the periodic orbit is called unstable. Sets supporting chaotic dynamics may contain infinitely many unstable periodic orbits. For example, under some additional conditions, there are explicit

inequalities quantifying the (exponential) growth of periodic orbits in hyperbolic dynamical systems [44, 56]. Moreover, in one complex dimension, Julia sets are actually the closure of the union of all unstable periodic orbits [71].

The basic idea of so-called "chaos control" is to render some of these unstable periodic orbits stable. The method presented in the seminal work by Ott, Grebogi, and Yorke [79] employs arbitrarily small perturbations to an "accessible" system parameter. These perturbations make use of the dynamics in the vicinity of a specific periodic orbit of a certain class, leading to convergence towards the periodic orbit. To apply this control method, both location and stability properties of the unstable periodic orbit have to be known. Hence, for some applications, a different control scheme—Predictive Feedback Control [26]—is better suited as a chaos control method. In Predictive Feedback Control, predictions about the future state of the system are fed back into the dynamics as a control signal. This method requires little a priori knowledge about the system and it is non-invasive, i.e., the control perturbation vanishes upon convergence. At the same time, Predictive Feedback Control provides an easy-to-implement control scheme for the stabilization of unstable periodic orbits.

Although convergence speed may be crucial in applications, most of the existing literature on Predictive Feedback Control ignores this topic. Take, for example, an autonomous robot whose behavior is determined by the dynamics of a single chaotic dynamical system [102]. Depending on the sensory input, the controller stabilizes a periodic orbit of a certain period which is embedded in the original chaotic dynamics. The periodic motion is then translated into movement and gait patterns. In such a setup, the speed of stabilization of periodic orbits is directly related to the reaction time to new sensory inputs. Hence, a fast chaos control method improves the robot's ability to cope with a rapidly changing environment. Speed of convergence is even more important if chaos control is applied in a medical setting; chaos control may be used to restore a periodic rhythm of the heart during an episode of cardiac dysrhythmia [36]. The analysis of this chaos control method with respect to convergence speed is subject of the second half of this thesis.

To solve this problem, we develop an algorithm to adapt the control parameter of Predictive Feedback Control to optimize for convergence speed. Suppose that we want to stabilize a given fixed point. To apply Predictive Feedback Control, a control signal is added to the original function f whose iteration gives rise to chaotic dynamics. The perturbed system corresponds to a function which is a linear interpolation between the map f and the identity map id on $\mathbb{R}^N$ defined by $\mathrm{id}(y) = y$ for all $y \in \mathbb{R}^N$. The control parameter $\mu \in [0, 1]$ determines what point on the interpolating line the system is mapped to; variation of μ leads to bifurcations from regular to chaotic dynamics. At the same time, the choice of control parameter influences convergence speed. There is an interval of control parameters for which the fixed point is stable, so, in order to achieve optimal convergence speed, one would like to pick the value for which convergence is fastest. A main result of Chapter 2 is the development of an adaptive algorithm to optimize convergence speed. The theorem below summarizes the result for the local dynamics.

Theorem B. *Suppose that f is a suitable function whose iteration gives rise to chaotic dynamics on a set $A \subset \mathbb{R}^N$. Then there exists an algorithm that optimizes asymptotic convergence speed by tuning the control parameter online. More precisely, for every stabilizable unstable periodic orbit there exists a neighborhood in which the algorithm maximizes a certain lower bound for asymptotic convergence speed. This lower bound is given by a suitable matrix norm which approximates the spectral radius up to some bounded value and is arbitrarily close at the initial condition.*

See Theorem 2.2.8 for a more precise formulation of this result. This local result may be used to characterize some statistical properties of the dynamics. By assuming the existence of some ergodic invariant measure on the set A, we are able to calculate the probability of convergence towards a given periodic orbit if the control is turned on at an arbitrary point in time. We subsequently apply these results to the logistic family and confirm convergence numerically.

It turns out that Predictive Feedback Control itself suffers from an inherent speed limit. Note that the adaptation algorithm described above optimizes speed within the bounds of Predictive Feedback Control; it acts as a supplement which tunes the control parameter within the regime of stabilization. In hyperbolic systems the strength of local contraction and expansion is determined in a linear approximation by the eigenvalues of the derivative of f at the fixed point. Optimal asymptotic convergence speed for Predictive Feedback Control depends strongly on the largest value associated to the expanding directions; the larger this value, the slower the fastest convergence speed. Since periodic orbits of higher periods—fixed points of the corresponding iterate of f—tend to be more unstable this implies that convergence is slow even if the control parameter is chosen optimally. Is it possible to overcome this inherent limitation of Predictive Feedback Control while maintaining its advantages?

We show in Chapter 3 that it is indeed possible to significantly boost convergence speed, even for periodic orbits of larger periods. The key idea is to "stall" control, i.e., to skip the application of the control perturbation periodically and thus make use of the original uncontrolled dynamics. This works because the slowest direction, which is the leading direction for the convergence, corresponds to a direction of fast attraction of the original dynamics. Balancing repulsion and attraction leads to dynamics which yield fast convergence from all directions and, therefore, fast overall convergence. Since the effect of stalling depends on the local stability properties of a periodic orbit, this aspect is studied systematically in Section 3.2. Thus, choosing the control parameter optimally for stalled control may significantly speed up convergence compared to classical Predictive Feedback Control. Moreover, this Stalled Predictive Feedback Control is not only capable of stabilizing more unstable periodic orbits but the speedup also persists when initial conditions are distributed randomly on the chaotic attractor.

Convergence of Stalled Predictive Feedback Control may be fast when the control parameter is chosen optimally, but how do we find the optimal value? To tackle this problem, we apply and compare different adaptation algorithms for the control parameter of Stalled Predictive Feedback Control. With an objective function that takes local stability into account, standard algorithms may be used to optimize for

convergence speed [35]. As a proof of concept, we develop a hybrid algorithm for the control parameter in order to amend Stalled Predictive Feedback Control. This algorithm increases the control parameter until the dynamics come close to a periodic orbit where it then behaves like gradient descent optimizing for speed. The important result presented towards the end of the last chapter is that the addition of adaptation to Stalled Predictive Feedback Control yields a universal and fast chaos control scheme. While it retains most of the advantages of Predictive Feedback Control, adaptation renders the new control mechanism universally applicable as it lifts the requirement that the parameters be fine-tuned a priori. At the same time, one obtains reliable convergence when control is turned on at an arbitrary point in time.

Structure of this Thesis

In summary, this thesis is split into two parts. In the first part, in Chapter 1, we study the dynamics of symmetrically coupled phase oscillators and show that chaos is indeed possible in such systems. Moreover, we study the dynamical mechanisms that lead to the emergence of chaos. Chapter 1 contains results from a published article [15] as well as a manuscript in preparation [13]. Part II of this thesis is dedicated to the theory of chaos control and the problem of convergence speed. In Chapter 2, we develop an adaptation method that tunes the control parameter of Predictive Feedback Control online to optimize convergence speed. The main results of this chapter are published [14]. In the final Chapter 3, we show that Predictive Feedback Control suffers from an inherent speed limit, in particular, when one tries to stabilize periodic orbits of large period. This speed limit can be overcome by stalling control. Some of the results presented in Chapter 3 have been submitted for publication [11, 12]. In the outlook towards the end of this thesis we summarize some interesting follow-up research questions that are motivated by the results in the main text. Answering these questions will require further effort in the future.

Part I.

Equivariant Dynamical Systems

1. Chaos in Symmetric Oscillator Systems

Models of coupled oscillators describe various collective phenomena in natural and artificial systems, including synchronization of flashing fireflies, and superconducting Josephson junctions, oscillatory activity of neural networks, and oscillations in chemical reaction kinetics [82, 105]. In particular, phase-coupled oscillators arise naturally as the averaged weak coupling limit of more general limit cycle oscillators [7, 106]. The Kuramoto model [59] and its extensions have been successful at suitably describing the dynamics of a variety of real systems, they are extensively studied numerically, and are reasonably well understood analytically [1]. Let $\mathbf{T} := \mathbb{R}/2\pi\mathbb{Z}$ denote the one-dimensional torus and suppose that $g : \mathbf{T} \to \mathbb{R}$ is a 2π-periodic function. The evolution of the phase $\varphi_k(t) \in \mathbf{T}$ of the k-th oscillator is determined by the ordinary differential equation

$$\frac{\mathrm{d}\varphi_k}{\mathrm{d}t} = \omega_k + \frac{1}{N}\sum_{j=1}^{N} g(\varphi_k - \varphi_j) \tag{1.1}$$

where $k \in \{1, \dots, N\}$ and thus g is referred to as the *coupling function*.

For the original Kuramoto model the coupling function g has a single Fourier mode, $g = \sin$. Due to the existence of constants of motion, the dimension of such systems can be reduced to low dimensions [68, 77, 107], implying that solutions are either periodic or quasi-periodic. For coupling functions with two or more Fourier components the collective dynamics may be much more complicated. The emergence of stable heteroclinic switching is one example [5, 6]. While more irregular, chaotic dynamics for identical all-to-all coupled systems appear in amplitude oscillators [74], chaos for phase oscillators (1.5) has only been observed for non-identical phase oscillators [66, 87]. This motivates the main question of this chapter. Are inhomogeneities are necessary for the occurrence of such dynamics in networks of phase oscillators? Until recently there had been no explicit example of a fully symmetric system of phase oscillators that exhibit chaotic dynamics.

One of the central results presented here [15] is the fact that there exist coupling functions g that give rise to chaotic dynamics in homogeneous, globally coupled systems (1.5). Furthermore, for these coupling functions the system exhibits chaotic fluctuations of the order parameter

$$R(t) = \frac{1}{N}\sum_{k=1}^{N} \exp(i\varphi_k). \tag{1.2}$$

where i denotes the imaginary unit. This observable encodes important information about the dynamics, such as the level of synchronization. Moreover, in the classical Kuramoto model, the full complex order parameter (1.2) acts as a mean field variable

enabling closed-form analysis [104]. Generalized order parameters can be used to study synchronization in systems with more general coupling functions [23, 24]. The smallest dimension in which chaotic dynamics can and does occur in such systems is for the case of four oscillators. Attracting chaos is also found for five and seven oscillators and sets with chaotic dynamics for and infinite family of dimensions.

In this chapter, we study the emergence of chaos in symmetrically coupled phase oscillators and the dynamical mechanisms that give rise to such complicated dynamics. This chapter includes and extends upon the recently published preliminary results [15]. After recalling basic definitions and general properties of systems of coupled phase oscillators with symmetry, we give a family of coupling functions that yields chaotic dynamics for four oscillators in Section 1.2. Both local and global bifurcations are involved in the creation of the chaotic attractors and we find examples of attractors of all possible (setwise) symmetries. Attracting chaos is also present for the same family of coupling functions in higher dimensions. At the same time, a bifurcation analysis reveals that the case of even coupling functions is important for the occurrence of chaos. This is studied subsequently in Section 1.3. We discuss the existence of constants of motion for low-dimensional generalized Kuramoto systems before giving some concluding remarks and open questions.

1.1. Equivariant Dynamics

The system of coupled phase oscillators described above is an example of a smooth dynamical system on a real manifold defined by differential equations. In this section, we collect some basic definitions from dynamical systems theory and equivariant dynamics before recalling some properties of the system of phase oscillators on the torus. Let $\mathbb{Z}$, $\mathbb{N}$, and $\mathbb{R}$ denote the sets of integers, natural, and real numbers, respectively. Suppose that $\mathfrak{M}$ is a smooth N-dimensional manifold. Its tangent bundle $T\mathfrak{M}$ is the vector bundle which is the disjoint union of all the tangent spaces $T_p\mathfrak{M}$ for all $p \in \mathfrak{M}$; cf. [62]. Refer, for example, to [10, 42, 56] for a more detailed exposition of the terms introduced below.

Dynamical Systems and Symmetry

A continuous time dynamical system on $\mathfrak{M}$ is defined as follows. A smooth vector field $X : \mathfrak{M} \to T\mathfrak{M}$ assigns to every $p \in \mathfrak{M}$ an element of the corresponding tangent space $T_p\mathfrak{M}$ and these vectors vary smoothly in p. In other words, a vector field X is a section of the tangent bundle. These vectors may be interpreted as "velocity vectors" thus defining an (autonomous) dynamical system through an ordinary differential equation. Solutions $x : \mathbb{R} \to \mathfrak{M}$ that satisfy

$$\frac{\mathrm{d}x}{\mathrm{d}t} = X(x)$$

are called trajectories or orbits. For a set $A \subset \mathfrak{M}$ let $\overline{A}$ denote its topological closure. The long-term dynamics of a given trajectory x are described by its *ω-limit* and *α-limit*

sets,

$$\omega(x) = \bigcap_{\tau\in\mathbb{N}} \overline{\{\, x(t) \mid t > \tau \,\}}, \quad \alpha(x) = \bigcap_{\tau\in\mathbb{N}} \overline{\{\, x(t) \mid t < -\tau \,\}},$$

respectively. A trajectory x is called a fixed point or equilibrium if $x(t) = p$ for all t and a periodic orbit or limit cycle if there exists a $\tau > 0$ such that $x(\tau) = x(0)$. Their stability is determined by the eigenvalues of the linearization of the vector field at the orbit and they are called stable if the real part of all eigenvalues is smaller than zero. Suppose $p, q \in \mathfrak{M}$ are equilibria. A trajectory x is called homoclinic if $\omega(x) = \alpha(x) = \{p\}$ and heteroclinic if $\omega(x) = \{p\}$, $\alpha(x) = \{q\}$; a homoclinic trajectory approaches the same equilibrium in forward and backward time whereas a heteroclinic trajectory "joins" two different equilibria.

The dynamics in the vicinity of a trajectory x are described by the dynamics of the linearized system. Let $\mathrm{d}X(t) = \mathrm{d}X|_{x(t)}$ denote the Jacobian of X at $x(t)$. The temporal evolution $v(t) \in T_{x(t)}\mathfrak{M}$ along a trajectory $x(t)$ of an initial perturbation $v_0 := v(0)$ is given by the variational equation

$$\frac{\mathrm{d}v}{\mathrm{d}t} = \mathrm{d}X(t)v. \tag{1.3}$$

Suppose that $\|\cdot\|_{\mathrm{v}}$ is some suitable vector norm on $T\mathfrak{M}$ (for example, a norm induced by a Riemannian metric) and $\|\cdot\|_{\mathrm{m}}$ is a suitable matrix norm on $\mathbb{R}^{N\times N}$. Suppose that $\sup_{t\in\mathbb{R}} \|\mathrm{d}X(t)\|_{\mathrm{m}} \leq C < \infty$. The Lyapunov exponents are then defined for an initial perturbation v_0 by

$$\lambda(v_0) = \limsup_{t\to\infty} \frac{1}{t} \log \|v(t)\|_{\mathrm{v}}. \tag{1.4}$$

Recall that this function takes up to N different values on $T_{x(0)}\mathfrak{M}$ and its maximum, the maximal Lyapunov exponent $\lambda_{\max}$, is taken for Lebesgue-almost-all initial perturbations v_0. The Lyapunov exponents characterize the average rate of exponential divergence of trajectories along a trajectory. A positive maximal Lyapunov exponent means that the dynamics are sensitive to changes of the initial condition which is a typical feature of chaotic dynamics [33].

Suppose that $U \subset \mathfrak{M}$. In order to define an attractor, recall that a set V is called a neighborhood of V if U is contained in its (topological) interior. Moreover, $A \subset \mathfrak{M}$ is called *Lyapunov-stable* for a dynamical system on $\mathfrak{M}$ if for every neighborhood V of A there exists an open neighborhood W of A such that for any trajectory x with initial condition $x(0) \in W$ we have $x(t) \in V$ for all $t > 0$.

Definition 1.1.1 (as in [39]). *Suppose a differential equation defines a dynamical system on a smooth manifold $\mathfrak{M}$. A set $A \subset \mathfrak{M}$ is an attractor if it is Lyapunov-stable, closed, connected, and the ω-limit set of a trajectory.*

A symmetry is additional property of the dynamical system and imposes restrictions not only on the possible solutions but also on the bifurcations in such systems; see for example [39, 40] for more details. Suppose Γ is a group that acts on the manifold $\mathfrak{M}$.

Definition 1.1.2. *A vector field X on $\mathfrak{M}$ is called Γ-equivariant if X "commutes" with the action of Γ, i.e., $X \circ \gamma = \mathrm{d}\gamma \circ X$ for all $\gamma \in \Gamma$ where $\mathrm{d}\gamma$ denotes the induced action on the tangent bundle.*

A dynamical system that is defined by a Γ-equivariant vector field is also called a Γ-equivariant dynamical system. The group Γ determines the symmetry of the system itself and an immediate consequence is that for every solution x of a Γ-equivariant dynamical system γx is also a solution for every $\gamma \in \Gamma$. Furthermore, equivariance gives rise to flow-invariant subspaces. For every subgroup $\Delta \subset \Gamma$ the corresponding fixed point subspace $\mathrm{Fix}(\Delta) := \{\, p \in \mathfrak{M} \mid \gamma p = p \text{ for all } \gamma \in \Delta \,\}$ are dynamically invariant. Equivariant dynamical systems may give rise to solutions that have symmetries themselves. We thus define the symmetries of a specific set $A \subset \mathfrak{M}$ as follows.

Definition 1.1.3. *The subgroup $\mathrm{Stab}(A) := \{\, \gamma \in \Gamma \mid \gamma(a) = a \text{ for all } a \in A \,\}$ is called the group of instantaneous symmetries and $\Sigma(A) := \{\, \gamma \in \Gamma \mid \gamma(A) = A \,\}$ is the group of symmetries on average of A.*

Remark 1.1.4. These subgroups are typically referred to as (pointwise) stabilizers or fixators in the literature on group theory.

The instantaneous symmetries $\mathrm{Stab}(A)$ keep every point in A fixed at each point in time whereas symmetries on average preserve the set as a whole. Clearly, we have $\mathrm{Stab}(A) \subset \Sigma(A)$ as a subgroup. Recall that the group of instantaneous symmetries is constant along a trajectory. This implies that the group of instantaneous symmetries of an attractor as defined above is generically the same. This fact indicates that the definition of an attractor given in Definition 1.1.1 is rather restrictive; Milnor attractors [69, 70] may display a wider range of symmetries, including the possibility of several different instantaneous symmetries at the same time.

Symmetries of dynamical systems may be intertwined with the temporal evolution of the system. There may be additional (time) reversing symmetries [61]. Dynamical systems with reversing symmetries are related to both Hamiltonian and equivariant dynamics.

Definition 1.1.5. *A dynamical system defined by a vector field X on a smooth manifold $\mathfrak{M}$ is said to have reversing symmetry $\varrho : \mathfrak{M} \to \mathfrak{M}$ if ϱ is invertible and*

$$\frac{\mathrm{d}\varrho(x)}{\mathrm{d}t} = -X(\varrho(x)).$$

In contrast to a Γ-equivariant dynamical system where for every solution x the group translate γx is also a solution for any $\gamma \in \Gamma$, the presence of a (time) reversing symmetry has a slightly different implication. Suppose that a dynamical system has a reversing symmetry ϱ. Then for any solution x the image under the reversing symmetry ϱx is a solution when time is reversed. Thus, for any attractor A there is a repeller $\varrho(A)$ and any solution that lies on the fixed point sets must have stability properties compatible with the symmetry, e.g., there are no sinks or sources.

Equivariant Systems of Phase Oscillators

This terminology now applies to the dynamical system defined through the ordinary differential equations (1.1) on the N-dimensional torus $\mathbf{T}^N$. We focus on the homogenous system, i.e., let us assume that $\omega_k = \omega$ for all $k \in \{1, \dots, N\}$ for the remainder of this chapter. First, we collect some basic properties of this system as presented in [7]. As a consequence, we obtain a first observation: chaos can only occur in systems of four or more oscillators.

Let S_N denote the group of permutations of N symbols and write $\Upsilon = (\Upsilon_1, \dots, \Upsilon_N)$ for $\Upsilon \in \{\varphi, \psi, \Phi, \Psi\}$. The dynamical system defined by

$$\frac{\mathrm{d}\varphi_k}{\mathrm{d}t} = \omega + \frac{1}{N}\sum_{j=1}^{N} g(\varphi_k - \varphi_j) =: \Phi_k(\varphi) \tag{1.5}$$

for $k = 1, \dots, N$ is $S_N \times \mathbf{T}^1$ equivariant where S_N acts by permuting indices and $\mathbf{T}^1$ through a phase shift [72]. Introducing phase differences $\psi_j := \varphi_j - \varphi_1$ for each $j \in \{1, \dots, N\}$ eliminates the phase-shift symmetry. The reduced system on $\mathbf{T}^{N-1}$ is given by

$$\frac{\mathrm{d}\psi_k}{\mathrm{d}t} = \frac{1}{N}\left(\sum_{j=1}^{N} g(\psi_k - \psi_j) - \sum_{j=1}^{N} g(-\psi_j)\right) =: \Psi_k(\psi). \tag{1.6}$$

for $k = 2, \dots, N$.

Suppose $P = \{P_1, \dots, P_m\}$ is a partition of $\{1, \dots, N\}$, that is $P_r \subset \{1, \dots, N\}$, $\bigcup_{j=1}^{m} P_j = \{1, \dots, N\}$, and $P_r \cap P_s = \emptyset$ for $r \neq s$. For all partitions P the subspaces

$$F_P := \{\, \varphi \mid \varphi_j = \varphi_k \text{ if } j, k \in P_r \text{ for each } r \,\} \subset \mathbf{T}^N \tag{1.7}$$

are flow-invariant as fixed point subspaces of some action of a subgroup of S_N on the indices. The subspaces divide $\mathbf{T}^{N-1}$ in $(N-1)!$ invariant $(N-1)$-dimensional simplices [7], each one corresponding to a specific ordering of the phases modulo 2π. We refer to one of these subspaces

$$\mathcal{C} := \{\, \psi \mid 0 = \psi_1 < \psi_2 < \cdots < \psi_N < 2\pi \,\} \subset \mathbf{T}^{N-1} \tag{1.8}$$

as the *canonical invariant region*; cf. Figure 1.1. There is a $\mathbb{Z}/N\mathbb{Z}$ symmetry on the canonical invariant region that is generated by

$$\xi : (0, \psi_2, \dots, \psi_N) \mapsto (0, \psi_3 - \psi_2, \dots, \psi_N - \psi_2, 2\pi - \psi_2)\,. \tag{1.9}$$

and the "splay state" φ^{splay}, i.e., the phase-locked solution with $\psi_{j+1} = \frac{2\pi j}{N}$ for $j = 1, \dots, N-1$ in reduced coordinates, is the only fixed point of this action at the centroid of this region.

As a first observation, we note that chaos cannot occur for systems of three or fewer oscillators. The reduced system for $N = 2, 3$ evolves on a one- resp. two-dimensional torus. Hence, the minimal dimension for the system to exhibit chaotic dynamics is $N = 4$ according to the Poincaré–Bendixon theorem [97] which states that every solution of a continuous time dynamical system on manifolds of dimension less than three, which are smooth, compact, and connected, must be either periodic or quasiperiodic.

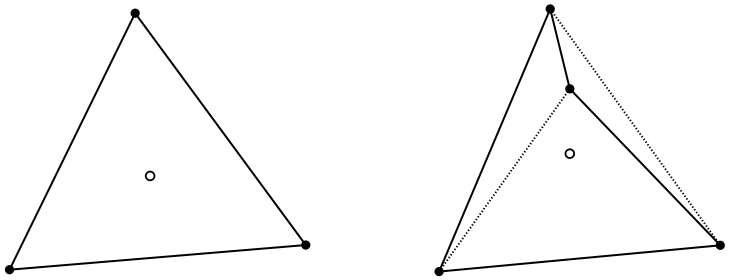

(a) $N = 3$ (b) $N = 4$

Figure 1.1.: The canonical invariant region $\mathcal{C}$ is an $(N-1)$-dimensional simplex and its faces $B \subset \mathbf{T}^{N-1}$ have $\mathrm{Stab}(B) = S_2$. The solid dots represent the fully synchronized solution and the empty dots the splay state at the centroid. Solid lines represent subsets A of $\mathbf{T}^{N-1}$ with $\mathrm{Stab}(A) = S_{N-1}$, i.e., all but one oscillator are synchronized, and dotted lines subsets with $\mathrm{Stab}(A) = S_{N/2} \times S_{N/2}$, that is, two pairs of $N/2$ synchronized oscillators. The group $\mathbb{Z}/N\mathbb{Z}$ acts by "rotating" the simplex along the solid lines; cf. Appendix A.1.

1.2. Chaos in Symmetric Oscillators

Chaotic dynamics can only occur in systems of four or more oscillators. In this section, we show that there are families of coupling functions that give rise to chaotic dynamics in four dimensions. In addition, we study the symmetry properties of the chaotic attractors found in these systems and the bifurcations that lead to the appearance of chaos. In the last part of this section we present results on chaotic dynamics for five and more oscillators.

Chaos for Four Oscillators

We choose a parametrization of the coupling function g in (1.5) by considering a truncated Fourier series

$$g(\varphi) = \sum_{k=1}^{4} a_k \cos(k\varphi + \xi_k). \tag{1.10}$$

with constant parameters $a_1 = -2$, $a_2 = -2$, $a_3 = -1$, and $a_4 = -0.88$. In particular, we restrict ourselves to the two-parameter family given by the parametrization

$$(\xi_1, \xi_2, \xi_3, \xi_4) = (\eta_1, -\eta_1, \eta_1 + \eta_2, \eta_1 + \eta_2) \tag{1.11}$$

where η_1 and η_2 are real valued parameters.

We find that for this family of coupling functions there is a region in parameter space where the dynamics are chaotic. Within this chapter, chaos is characterized by a positive value of the numerically computed maximal Lyapunov exponent $\lambda_{\max}$. The function $\hat{\lambda}_{\max} := \max\{\lambda_{\max}, 0\}$ is depicted in Figure 1.2 (and 1.5). The maximal

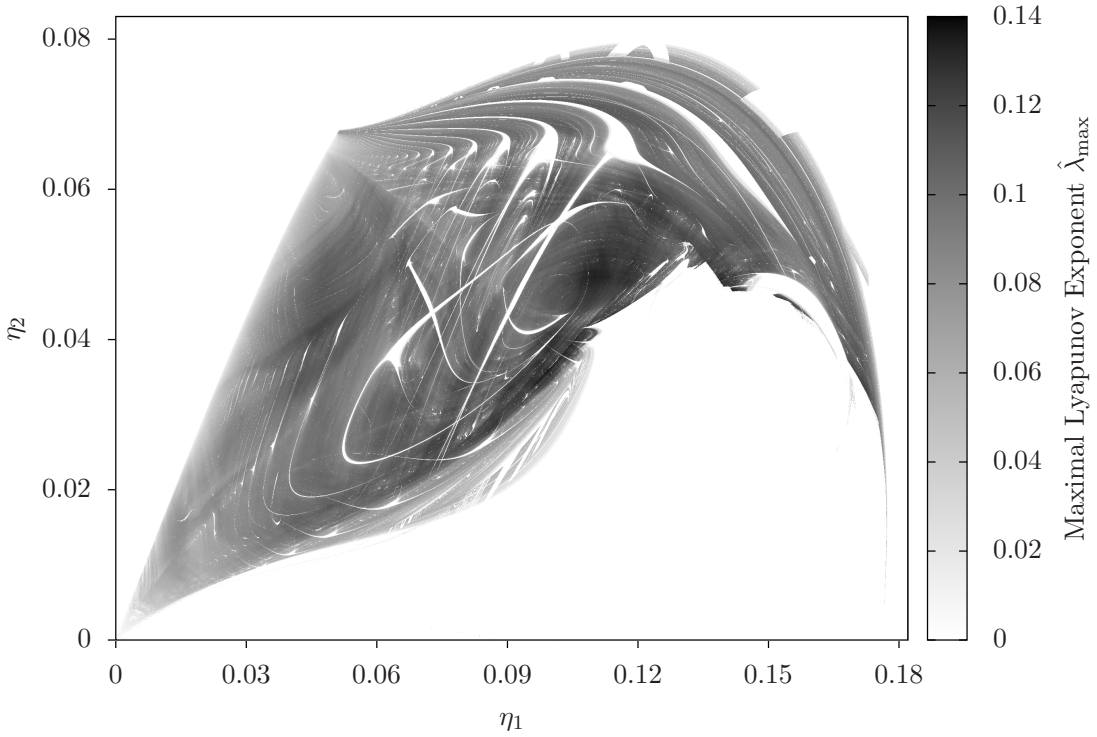

Figure 1.2.: Chaos for $N = 4$. The maximal Lyapunov exponent is positive in a region of parameter space. The coupling function parametrized by (1.11) and the initial condition was fixed.

Lyapunov exponents were calculated by integrating the variational equation (1.3) and integration ranged over tens of thousands of time units after discarding a transient of several thousand time units; cf. Appendix A.1 for details.

What are the possible symmetries of chaotic attractors A for systems of coupled phase oscillators (1.5)? By definition, the symmetry group of A is a subgroup of $\Gamma = S_N \times \mathbf{T}$. Suppose that $A \subset \mathbf{T}^N$ is an attractor with trivial instantaneous symmetry. Since the flow-invariant subspaces, which divide $\mathbf{T}^N$ into the canonical invariant region and its images under the group action, have nontrivial instantaneous symmetry we have $\Sigma(A) \subset \mathbb{Z}/N\mathbb{Z}$ as a subgroup. In particular, for $N = 4$ any chaotic attractor must have trivial instantaneous symmetry because all subsets of $\mathbf{T}^4$ with nontrivial instantaneous symmetry are of dimension two or smaller. For four oscillators, the setwise symmetries of any chaotic attractor therefore must be one of the four subgroups of $\mathbb{Z}/4\mathbb{Z}$ (up to conjugacy).

By the use of so-called detectives, i.e., by encoding the symmetry properties of dynamics in a suitably large space on which Γ acts, the symmetry groups of the chaotic attractors may be calculated systematically [4, 39]. Here, we employed the $\Gamma = \mathbb{Z}/4\mathbb{Z}$

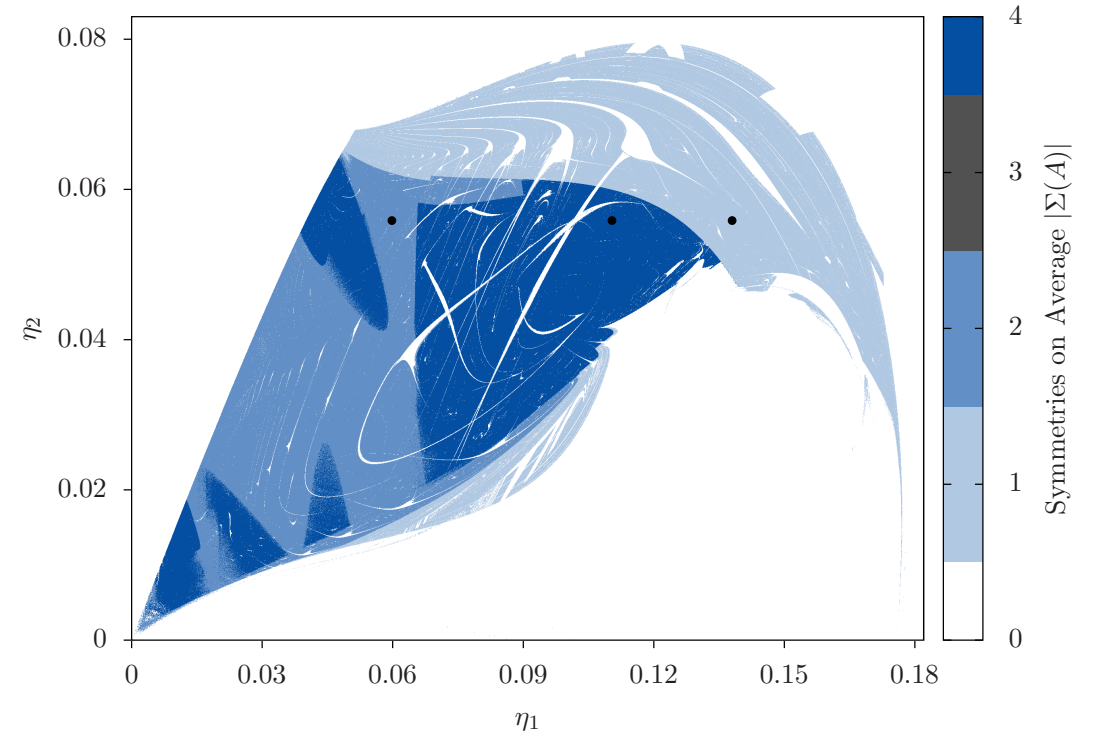

(a) Size of the symmetry group with respect to the parametrization (1.11)

(b) $\Sigma(A) = 1$ (c) $\Sigma(A) = \mathbb{Z}/2\mathbb{Z}$ (d) $\Sigma(A) = \mathbb{Z}/4\mathbb{Z}$

Figure 1.3.: All possible symmetries of the chaotic attractors are present for $N = 4$. Panel (a) shows the parameter dependence of the cardinality of the group $\Sigma(A)$ if $\lambda_{\max} > 0.01$ and zero otherwise for fixed initial condition; cf. Figure 1.2. Panels (b)–(d) show attractors with different symmetries for the parameter values indicated by black dots in Panel (a). We have $\eta_1 = 0.138$ in Panel (a), $\eta_1 = 0.0598$ in Panel (b), $\eta_1 = 0.1104$ in Panel (c), and $\eta_2 = 0.05586$ in all panels.

equivariant map

$$y : \mathbf{T}^N \to \mathbb{R}^2, \quad \varphi \mapsto (y_1(\varphi), y_2(\varphi)) = (\sin(\varphi_1 - \varphi_3), \sin(\varphi_2 - \varphi_4)) \tag{1.12}$$

to calculate the symmetry properties of minimal distances to the points $(1,1)$, $(-1,1)$, $(-1,-1)$, and $(1,-1)$; cf. Appendix A.1. The resulting cardinalities of $\Sigma(A)$ for chaotic attractors, i.e., when the maximal Lyapunov exponent $\lambda_{\max}$ exceeds a threshold of 0.01, are plotted in Figure 1.3(a) in dependence on the values of the parameters (η_1, η_2). In fact, there are chaotic attractors of all possible symmetries on average. Some examples are shown in Figure 1.3 by use of the $\mathbb{Z}/4\mathbb{Z}$-equivariant projection

$$\begin{aligned} \Pi : \mathcal{C} &\to \mathbb{R}^2 \times \mathbb{R}, \\ \psi &\mapsto (y, |R|), \end{aligned} \tag{1.13}$$

where R is the complex valued order parameter (1.2). On the image of the canonical invariant region under the projection, the group $\mathbb{Z}/4\mathbb{Z}$ acts by rotating around the axis $(0,0,\mathbb{R})$; cf. Appendix A.1.

Chaos persists if the coupling function is replaced by a piecewise affine one (not shown). Calculation of the maximal Lyapunov exponent reveals a region in parameter space where $\lambda_{\max}$ is positive when replacing cos in (1.10) by the continuous piecewise affine 2π-periodic function function defined by

$$\operatorname{coz}(\phi) = \begin{cases} 1 & \text{for } \phi \in [0, \frac{\pi}{2} - 1), \\ \frac{\pi}{2} - \phi & \text{for } \phi \in [\frac{\pi}{2} - 1, \frac{\pi}{2} + 1), \\ -1 & \text{for } \phi \in [\frac{\pi}{2} + 1, \frac{3\pi}{2} - 1), \\ -\frac{3\pi}{2} + \phi & \text{for } \phi \in [\frac{3\pi}{2} - 1, \frac{3\pi}{2} + 1), \\ 1 & \text{for } \phi \in [\frac{3\pi}{2} + 1, 2\pi). \end{cases}$$

However, in contrast to smooth coupling functions, we only found examples of chaotic attractors with trivial and $\mathbb{Z}/2\mathbb{Z}$ symmetry.

Bifurcation analysis. A parameter-dependent dynamical system undergoes a bifurcation if the dynamics change qualitatively, i.e., its dynamic equivalence class changes, as parameters are varied smoothly. An example is the period doubling of a stable periodic orbit; at the bifurcation point the existing periodic orbit becomes unstable and a new periodic orbit emerges with a period twice as large as the original periodic orbit; cf. Figure 1.4. In particular, a dynamical system undergoes one or more bifurcations when stable dynamics disappear and chaotic attractors emerge. Hence, a bifurcation analysis is essential in the understanding of the transition to chaos. For example, a typical route to chaos is through an infinite sequence of period doublings. Details on bifurcation theory may be found, for example, in [42, 60].

Note that the parametrization (1.11) gives rise to a symmetry in parameter space when reflecting in the origin $(\eta_1, \eta_2) = (0,0)$ given by the map $(\eta_1, \eta_2) \mapsto (-\eta_1, -\eta_2)$ and reversing time. Let Φ^{η_1,η_2} denote the vector field Φ for the coupling function

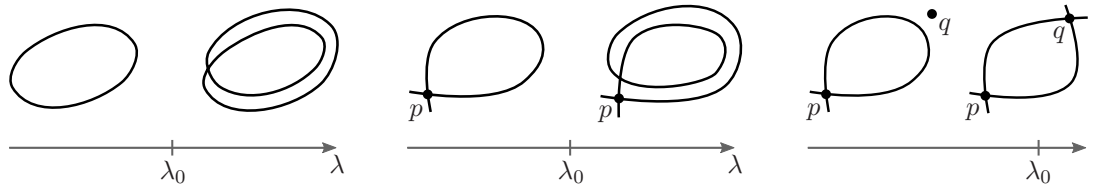

(a) Period doubling (b) Homoclinic doubling (c) Two heteroclinics

Figure 1.4.: Overly simplified sketch of some bifurcations. The bifurcation parameter is denoted by λ with bifurcation taking place at λ_0, and p, q are equilibria. Period doubling and homoclinic doubling are depicted in Panels (a) and (b), respectively. Panel (c) shows the existence of two heteroclincs at λ_0 which leads to two branches of heteroclinc orbits.

given by the truncated Fourier series (1.10) with parametrization (1.11). Suppose $\varphi = (\varphi_1, \ldots, \varphi_N)$ is a solution of (1.5) with right hand side given by Φ^{η_1,η_2}. We have

$$\frac{\mathrm{d}(-\varphi_k)}{\mathrm{d}t} = -\Phi_k^{\eta_1,\eta_2}(\varphi) = -\Phi_k^{-\eta_1,-\eta_2}(-\varphi) \tag{1.14}$$

for $k = 1, \ldots, N$ and therefore $-\varphi$ is a solution of the system with parameters $(-\eta_1, -\eta_2)$ when time is reversed. In other words, every solution for (η_1, η_2) has a corresponding solution for $(-\eta_1, -\eta_2)$ with inverse stability properties and therefore every bifurcation point has a symmetric counterpart.

We calculated bifurcation lines numerically by using the numerical continuation software AUTO/HomCont[1]. Figure 1.5 shows an overlay of some of the bifurcation lines with the values for the maximal Lyapunov exponent when initial conditions were chosen randomly on the canonical invariant region. Chaos arises through different period doubling cascades and vanishes at a saddle-node bifurcation of periodic trajectories, i.e., where two periodic trajectories of opposite stability annihilate each other. Recall that homoclinic trajectories, similar to periodic ones, may "double" [47, 49]; additional "revolutions" are added before the homoclinic loop is closed; cf. Figure 1.4. Such bifurcations may occur at homoclinic flip bifurcation where the exact nature of the bifurcation depends on the eigenvalues at the equilibrium [48]. In our system, the bifurcation lines that bound the chaotic region from the left and top emanate from a homoclinic flip bifurcation with an inclination flip (Figure 1.5, Label A). Here the eigenvalues at the equilibrium of the reduced system are such that infinitely many higher homoclinics and period doubling curves emanate from this bifurcation point. We find and continue the 2- and 3-homoclinics, as shown in Figure 1.5.

Choosing initial conditions randomly (in contrast to fixed initial conditions as in Figure 1.2) reveals a large part of parameter space with multistability as depicted in

[1] Numerical continuation of the bifurcations was done with AUTO-07p by E. J. Doedel et. al. [29, 30] (available at `http://indy.cs.concordia.ca/auto/`) which includes HomCont and an implementation of Lin's method [64] to find higher homoclinics.

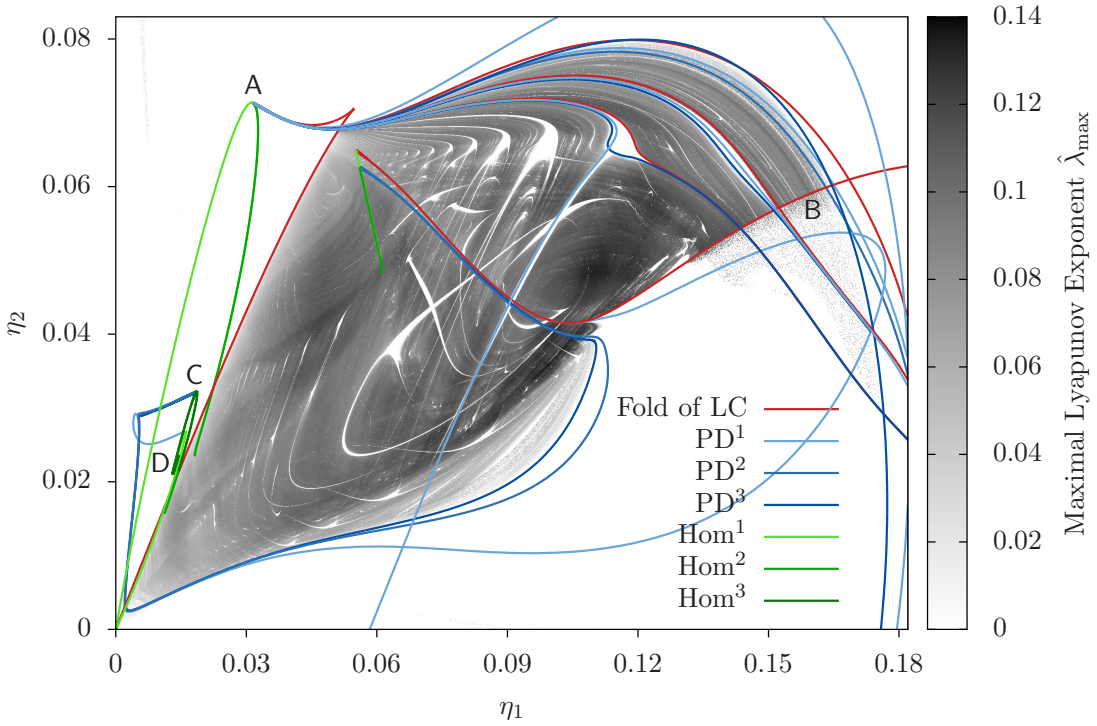

Figure 1.5.: Chaos for $N = 4$ overlaid with the numerically calculated bifurcation lines. Here, initial conditions were chosen randomly on the canonical invariant region for every pair (η_1, η_2). In "sprinkled" regions, for example close to Label B, stable and chaotic dynamics coexist. PD^k are period doubling lines of the kth doubling in a given period doubling cascade. Hom^k are the k-homoclinics either emanating from the homoclinic flip bifurcation or from the heteroclinic bifurcation. Note that there are multiple bifurcation lines passing through $(\eta_1, \eta_2) = 0$. Refer to the main text for a detailed explanation of the labels A–D.

Figure 1.5. Here, attracting chaos coexists with one or more stable periodic trajectories. The bifurcation analysis shows how these stable limit cycles are related to other global bifurcations in the system. The region of multistability on the right hand side of the chaotic region close to Label B is due to the existence of a stable limit cycle that is destroyed in a saddle node bifurcation of limit cycles (Figure 1.5, Label B). This stable limit cycle undergoes period doubling, yielding the bifurcation lines that bound the lower part of the chaotic region. The period doubling lines bifurcate in global bifurcations, both homoclinic and heteroclinic [49]. They end in homoclinic bifurcations (Figure 1.5, Label C) which collide with another fixed point to give multiple heteroclinic loops (Figure 1.5, Label D); cf. Figure 1.4(c). The two heteroclinic trajectories which are present at the bifurcation point may be continued separately (not shown).

Note that the lines corresponding to both the homoclinic flip bifurcation and the homoclinic-to-heteroclinic bifurcations emanate from the origin in (η_1, η_2) parameter

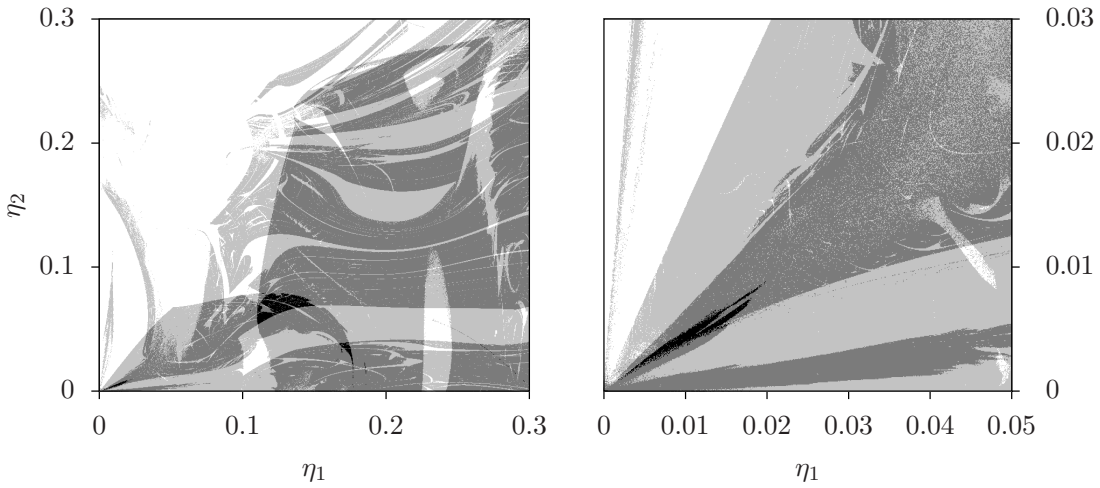

(a) Overlapping regions (b) Magnification

Figure 1.6.: Emergence of chaos in higher-dimensional systems. Overlapping regions where the maximal Lyapunov exponent exceeds 0.01 for $N \in \{4, 5, 7\}$. The darker the color, the more N for which the condition holds. The magnification in Panel (b) shows that there is a wedge-like region pointing towards $(\eta_1, \eta_2) = 0$ of positive maximal Lyapunov exponents for every N.

space. As discussed above, these bifurcation lines are linked to the main lines involved in the emergence and destruction of the chaotic dynamics. This indicates that at the origin there may be the crucial bifurcation which gives rise to the bifurcation structure involved in the emergence of chaos for systems of four oscillators.

Chaos for Five or More Oscillators

Analyzing the same region of parameter space for $N > 4$ yields attracting chaos in systems of $N = 5$ and $N = 7$ oscillators in large regions. Figure 1.6 shows an overlay of regions for three different N; regions are shaded where the Lyapunov exponent exceeds 0.01 and darker areas indicate that several N satisfy this condition. Clearly, there is a single coupling function for which attracting chaos is present for all $N = 4$, $N = 5$, and $N = 7$. Intriguingly, we did not find chaotic attractors for any $N \in \{6, 8, 9, \ldots, 13\}$ in the entire region of parameter space considered in Figure 1.6(a).

The parametrization of the coupling function by a truncated Fourier series raises the question how many Fourier components the coupling function needs to contain for chaos to occur. For $N = 5$ we also measured positive Lyapunov exponents when the coupling was chosen to be through the simpler coupling function

$$g(\phi) = -0.2\cos(\phi + \delta_1) - 0.04\cos(2\phi - \delta_2)$$

where δ_1, δ_2 are real parameters as in [6]. Hence, in dimension five, coupling functions with only two Fourier components suffice to generate chaotic dynamics whereas for

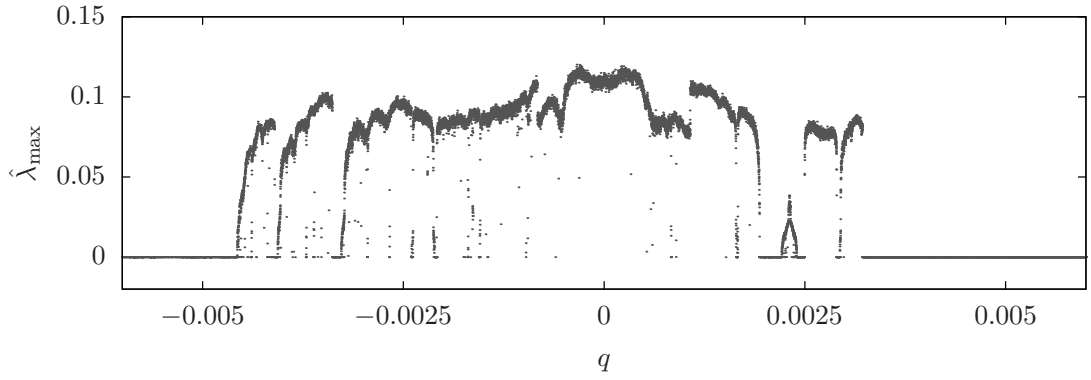

Figure 1.7.: Positive maximal Lyapunov exponents for asymmetric 4-cluster states for large systems, $N = KM + L(q, M) \gg 4$. Here, the parameter q parametrizes the deviation from the symmetric cluster state and L is the corresponding integer dimension (coupling function (1.11) with $\eta_1 = 0.1104$ and $\eta_2 = 0.05586$).

$N = 4$, we did not find an example with less than four components. In particular, using $\eta = \eta_1 = \eta_2$ and a_4 as parameters for $N = 4$, we found that the onset of chaos occurs for values of a_4 larger than one half (not shown), i.e., for coupling functions (1.10) the amplitude of the fourth harmonic has to be large enough for chaos to occur.

From the above, it is clear that for systems of size $N = KM$ with $K \in \{4, 5, 7\}$ there are chaotic invariant sets lying in flow-invariant subspaces for coupling functions yielding positive maximal Lyapunov exponents $\lambda_{\max}$; cf. Figure 1.6. For instance, for $K = 4$, these spaces are given by partitions $P = \{P_1, \ldots, P_4\}$ with $|P_j| = M$ for $j \in \{1, \ldots, 4\}$. For N large, cluster states close to the symmetric four-cluster state may be parametrized by partitions $P = \{P_1, \ldots, P_4\}$ with $\frac{|P_1|}{N} = \frac{1}{4} + q$ and $\frac{|P_j|}{N} = \frac{1}{4} - \frac{q}{3}$ for $j \in \{2, 3, 4\}$ where the parameter q characterizes the deviation from the symmetric state. We calculated positive maximal Lyapunov exponents for the system reduced to these near-symmetric cluster states as depicted in Figure 1.7. However, the dynamics on flow-invariant surfaces may have a variety of stability properties with respect to the dynamics of the full system [3]. Hence, these chaotic invariant sets in subspaces close to the symmetric cluster state may be transversally repelling, possibly yielding non-chaotic long-term dynamics.

The origin $(\eta_1, \eta_2) = 0$ of parameter space where the phase shift parameters are zero, i.e., where the coupling function (1.10) is even, plays a special role in the emergence of chaos. As discussed above, for the considered systems of four oscillators, many of the lines corresponding to bifurcations that are involved in the appearance of chaos emanate from the origin. Furthermore, for both cases $N = 5$ and $N = 7$ in which attracting chaos was found, positive maximal Lyapunov exponents are measured in a wedge-like region close to the origin; cf. Figure 1.6(b). Thus, the bifurcations taking place at the origin seem to be important for the appearance of chaos not only for four but also for a larger number of oscillators.

1.3. Dynamics for Even Coupling Functions

An even coupling function g is a function that is invariant under the reflection $-\phi \mapsto \phi$, i.e., $g(-\phi) = g(\phi)$. This symmetry of the coupling function itself has implications for the dynamics of the generalized Kuramoto equations (1.5) as it imposes additional constraints on the dynamics. At the same time, for an even coupling function, the fully synchronized solution $\varphi^{\text{sync}}(t) = (\omega t, \dots, \omega t)$ bifurcates as all eigenvalues of the linearization pass through zero [7]. First, we study special properties of the system of symmetric phase oscillators if the coupling function is even. We show that there are constants of motion for rings of coupled phase oscillators and discuss the implications of these results for fully coupled systems towards the end of this section.

For a dynamical system defined by a vector field X on a smooth manifold $\mathfrak{M}$ recall the following estimate for the sum of all Lyapunov exponents (1.4) as given, for example, in [10].

Lemma 1.3.1. *Suppose that the vector field X defines a differential equation on a smooth manifold $\mathfrak{M}$ and x is a solution thereof with initial condition $x(0)$. For any basis $(v_1, \dots, v_n)$ of the tangent space $V := T_{x(0)}\mathfrak{M}$ we have*

$$\limsup_{t\to\infty} \frac{1}{t} \operatorname{Re}\left(\int_0^t \operatorname{trace}\left(\mathrm{d}X(t)\right)\right) \leq \sum_{j=1}^{n} \lambda(v_j) =: \bar{\lambda}.$$

In particular, the basis of V can be chosen such that $\lambda(v_k)$ evaluate to the r distinct values of the Lyapunov exponent, i.e., $\bar{\lambda}$ can be interpreted as the mean Lyapunov exponent.

We apply this lemma to the generalized Kuramoto equations (1.5) with an even coupling function g.

Corollary 1.3.2. *If the coupling of the generalized Kuramoto equations (1.5) is given by an even coupling function g then the mean Lyapunov exponent is bounded from below by zero, $0 \leq \bar{\lambda}$.*

Proof. The Jacobian of the generalized Kuramoto equations (1.5) with an even coupling function g at $\varphi \in \mathbf{T}^N$ is given by

$$\left.\frac{\partial \Phi_k}{\partial \varphi_\ell}\right|_\varphi = \begin{cases} \sum_{j\neq k} g'(\varphi_k - \varphi_j) & \text{for } k = \ell \\ -g'(\varphi_k - \varphi_\ell) & \text{otherwise} \end{cases} \tag{1.15}$$

where the prime denotes differentiation with respect to the argument. Note that the derivative g' is odd and therefore the trace of the Jacobian is equal to zero. The inequality of Lemma 1.3.1 proves the assertion. □

Hence, either all Lyapunov exponents vanish or there is at least one positive Lyapunov exponent. In other words, the dynamics are either degenerate or chaotic.

If the coupling function is even then there are reversing symmetries for the generalized Kuramoto system (1.5). For any $\alpha \in \mathbf{T}^1$, the map $\varrho_\alpha : \varphi \mapsto -\varphi + \alpha$ is a reversing symmetry. For coupling functions that can be written as (1.10) this reversing symmetry corresponds to the degenerate point $(\eta_1, \eta_2) = 0 = (-\eta_1, -\eta_2)$ of the symmetry (1.14) of parameter space.

Consider the reduced dynamics of the phase differences ψ as given by (1.6). For even coupling functions g the system has a reversing symmetry $\varrho : \psi \mapsto -\psi$ since $\Psi(\psi) = \Psi(-\psi)$ and therefore

$$\frac{\mathrm{d}\varrho(\psi)}{\mathrm{d}t} = -\frac{\mathrm{d}\psi}{\mathrm{d}t} = -\Psi(\psi) = -\Psi(\varrho(\psi)).$$

Of particular interest are the fixed point subspaces

$$\mathrm{Fix}(\varrho) = \left\{ \psi \in \mathbf{T}^{N-1} \;\middle|\; \varrho(\psi) = \psi \right\} = \{0, \pi\}^{N-1}$$

as they give rise to particular solutions such as homoclinic and heteroclinic orbits. Moreover, equilibria in $\mathrm{Fix}(\varrho)$ may locally give rise to specific families of periodic solutions [38]. For $N > 2$ we have $\mathrm{Fix}(\varrho) \cap \overline{\mathcal{C}} =: \mathrm{Fix}_{\mathcal{C}}(\varrho) \subset \partial\mathcal{C}$ where ∂ denotes the topological boundary of a set. Hence, any ϱ-invariant point lies on the boundary of the canonical invariant region, which consists of the flow-invariant subspaces F_P for certain partitions P. Furthermore, as the cardinality of $\mathrm{Fix}(\varrho)$ is finite, there are only finitely many trajectories that pass through this fixed point space.

The additional symmetries for even coupling functions and in particular the consequences of Corollary 1.3.2 motivate the question of whether the dynamics are degenerate for such coupling functions. This would be the case if there were constants of motion.

Dynamics of Three Oscillators and Rings

Consider a system of N nearest neighbor coupled phase oscillators on the N-torus $\mathbf{T}^N$ with coupling given by a 2π-periodic real-valued coupling function g. The evolution of the phases $\varphi(t) = (\varphi_1(t), \ldots, \varphi_N(t)) \in \mathbf{T}^N$ is governed by the ordinary differential equations

$$\frac{\mathrm{d}\varphi_k}{\mathrm{d}t} = \omega + g(\varphi_k - \varphi_{k-1}) + g(\varphi_k - \varphi_{k+1}) \tag{1.16}$$

for $k = 0, \ldots, N-1$ (with indices taken modulo N). Let $\mathbb{Z}/N\mathbb{Z}$ act on the phases φ by permuting indices. The dynamical system defined by (1.16) is $\Gamma = \mathbb{Z}/N\mathbb{Z} \times \mathbf{T}$ equivariant.

Proposition 1.3.3. *Consider the dynamics of a ring of oscillators as given by (1.16) and suppose that the coupling function g is even. Let f be an antiderivative of g, i.e., $f' = g$. Then*

$$V_N = \sum_{\mathfrak{p} \in \mathbb{Z}/N\mathbb{Z}} f\left(\varphi_{\mathfrak{p}(1)} - \varphi_{\mathfrak{p}(2)}\right) \tag{1.17}$$

is a constant of motion, i.e., its value is constant along any trajectory.

Proof. Define the shorthand notation $\mathbf{g}_{j,k} := g(\varphi_j - \varphi_k)$. Without loss of generality we consider the dynamics in a "rotating frame," i.e., $\omega = 0$. Since g is even we have $\mathbf{g}_{k,l} = \mathbf{g}_{l,k}$. Taking the derivative with respect to φ_k yields

$$\frac{\partial V_N}{\partial \varphi_k}\dot{\varphi}_k = \left(\mathbf{g}_{k,k+1} - \mathbf{g}_{k,k-1}\right)\left(\mathbf{g}_{k,k+1} + \mathbf{g}_{k,k-1}\right) = \mathbf{g}_{k,k+1}^2 - \mathbf{g}_{k,k-1}^2 \,.$$

The derivative

$$\frac{\mathrm{d}V_N}{\mathrm{d}t} = \sum_{k=0}^{N-1} \frac{\partial V_N}{\partial \varphi_k}\frac{\mathrm{d}\varphi_k}{\mathrm{d}t} = 0$$

vanishes as every $\mathbf{g}_{l,l+1}$ appears twice in the sum, once with a positive and once with a negative sign. Thus, V_N is constant along trajectories. □

Remark 1.3.4. This constant of motion is very similar to the constant of motion found for finite lattices of phase oscillators [81]. In fact, rings of coupled phase oscillators (1.16) are also Hamiltonian systems [32].

For three oscillators, $N = 3$, the dynamical equations for the all-to-all coupled generalized Kuramoto equations (1.5) and the ring coupling topology (1.16) coincide. Thus, V_3 is a constant of motion for the $(S_3 \times \mathbf{T})$-equivariant system (1.5). Define $\mathbf{s}_{jk}^{\kappa} = \sin\left(\frac{\kappa}{2}(\varphi_j - \varphi_k)\right)$, $\mathbf{s}_{jk} = \mathbf{s}_{jk}^{1}$ for $j, k \in \mathbb{N}, \kappa \in \mathbb{R}$, and the cyclic products $\mathcal{S}^{\kappa} = \mathbf{s}_{12}^{\kappa}\,\mathbf{s}_{23}^{\kappa}\,\mathbf{s}_{31}^{\kappa}$. If functions $W_1, W_2 : \mathbf{T}^N \to \mathbb{R}$ differ only by an invertible affine transformation, i.e., if there exists an invertible affine map τ such that $\tau(W_1) = W_2$, write $W_1 \equiv W_2$. Suppose that the even coupling function is given in the form of a Fourier series

$$g(\phi) = \sum_{k=0}^{\infty} a_k \cos(k\phi). \tag{1.18}$$

Since $\mathcal{S}^{\kappa}$ may be written as a sum of cosines by using basic trigonometric identities, we find that

$$\widetilde{V}_3 = \sum_{k=1}^{\infty} \frac{a_k}{k}\mathcal{S}^k \tag{1.19}$$

satisfies $V_3 \equiv \widetilde{V}_3$. Note that the constant of motion $\widetilde{V}_3$ vanishes on the boundary of the canonical invariant region $\mathcal{C}$. Figure 1.8 shows contour lines of this constant of motion for some coupling functions.

At the same time, it is well known that (1.5) has constants of motion for coupling functions with only one nonzero Fourier coefficient and any number N of oscillators [108]. One of these Watanabe-Strogatz (WS) constants of motion is given by

$$V_N^{\mathrm{WS}} = \prod_{\mathfrak{p}\in\mathbb{Z}/N\mathbb{Z}} \sin\left(\frac{\varphi_{\mathfrak{p}(1)} - \varphi_{\mathfrak{p}(2)}}{2}\right) = \prod_{\mathfrak{p}\in\mathbb{Z}/N\mathbb{Z}} \mathbf{s}_{\mathfrak{p}(1)\mathfrak{p}(2)} \,. \tag{1.20}$$

For $N = 3$ and a coupling function with only one nonzero Fourier coefficient a_K with $K \in \mathbb{N}$, the WS constant of motion and V_3 are equivalent since $V_3^{\mathrm{WS}} = \mathcal{S}^1$ and therefore

$$V_3 \equiv V_3^{\mathrm{WS}}$$

after rescaling time. Hence, the constant of motion for rings of three oscillators and Watanabe–Strogatz constant of motion are essentially the same.

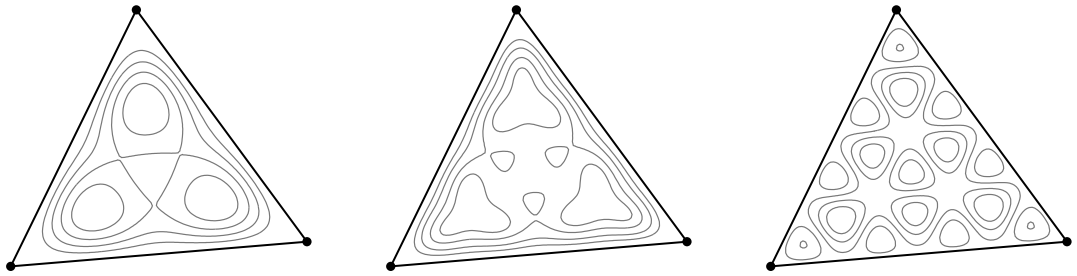

(a) (b) (c)

Figure 1.8.: Some contour lines of the constant of motion $\widetilde{V}_3$ for three oscillators for some even coupling functions (1.18) on the canonical invariant region $\mathcal{C}$; cf. Figure 1.1(a). Recall that the canonical invariant region is a two-dimensional simplex given by the ordering $0 = \psi_1 < \psi_2 < \psi_3$ with vertices $(0, 0, 0)$, $(0, 0, 2\pi)$ and $(0, 2\pi, 2\pi)$, i.e., the fully synchronized state. The nontrivial Fourier coefficients of the coupling function are $a_1 = 1$ and $a_2 = 1$ in Panel (a), $a_1 = -2$, $a_2 = -2$, $a_3 = -1$, and $a_4 = -0.88$ as in (1.10) in Panel (b), and $a_1 = -2$, $a_2 = -2$, $a_3 = -1$, and $a_4 = 10$ in Panel (c).

Four Oscillators

For four all-to-all coupled oscillators with dynamics given by (1.5) the situation is different; in contrast to the ring topology the "cross coupling terms" $g(\varphi_1 - \varphi_3)$ and $g(\varphi_2 - \varphi_4)$ enter the dynamical equations. For three oscillators, the constant of motion interpolates the Watanabe–Strogatz constant of motion for a single Fourier component. For $N = 4$ and coupling function $g = \cos$, this constant of motion evaluates to

$$V_4^{\mathrm{WS}} = \prod_{\mathfrak{p}\in\mathbb{Z}/4\mathbb{Z}} \mathrm{s}_{\mathfrak{p}(1)\mathfrak{p}(2)} = \prod_{\mathfrak{p}\in\mathbb{Z}/4\mathbb{Z}} \sin\left(\frac{\varphi_{\mathfrak{p}(1)} - \varphi_{\mathfrak{p}(2)}}{2}\right) \tag{1.21}$$

$$\equiv \sum_{\mathfrak{p}\in\mathbb{Z}/4\mathbb{Z}} \cos\left(\varphi_{\mathfrak{p}(1)} - \varphi_{\mathfrak{p}(2)}\right) - \cos(\varphi_1 - \varphi_3) - \cos(\varphi_2 - \varphi_4) - \cos(\varphi_1 - \varphi_2 + \varphi_3 - \varphi_4). \tag{1.22}$$

Note that, in addition to the extra terms that involve the cross coupling phase differences, the functions constituting the constant of motion have the same symmetry properties as the coupling function itself. By contrast, for three oscillators this function was odd as the integral of cos. So far, we have not been able to find a constant of motion for $N = 4$.

However, there is numerical evidence that a constant of motion may exist even for four oscillators and an arbitrary even coupling function. Solving the equations of motion for even coupling functions shows that the orbits are periodic. Examples of such periodic orbits for the coupling function given by (1.10) with phase shift parameters $\xi_j = 0$ for all j are shown in Figure 1.9. At the same time, the calculation of the entire

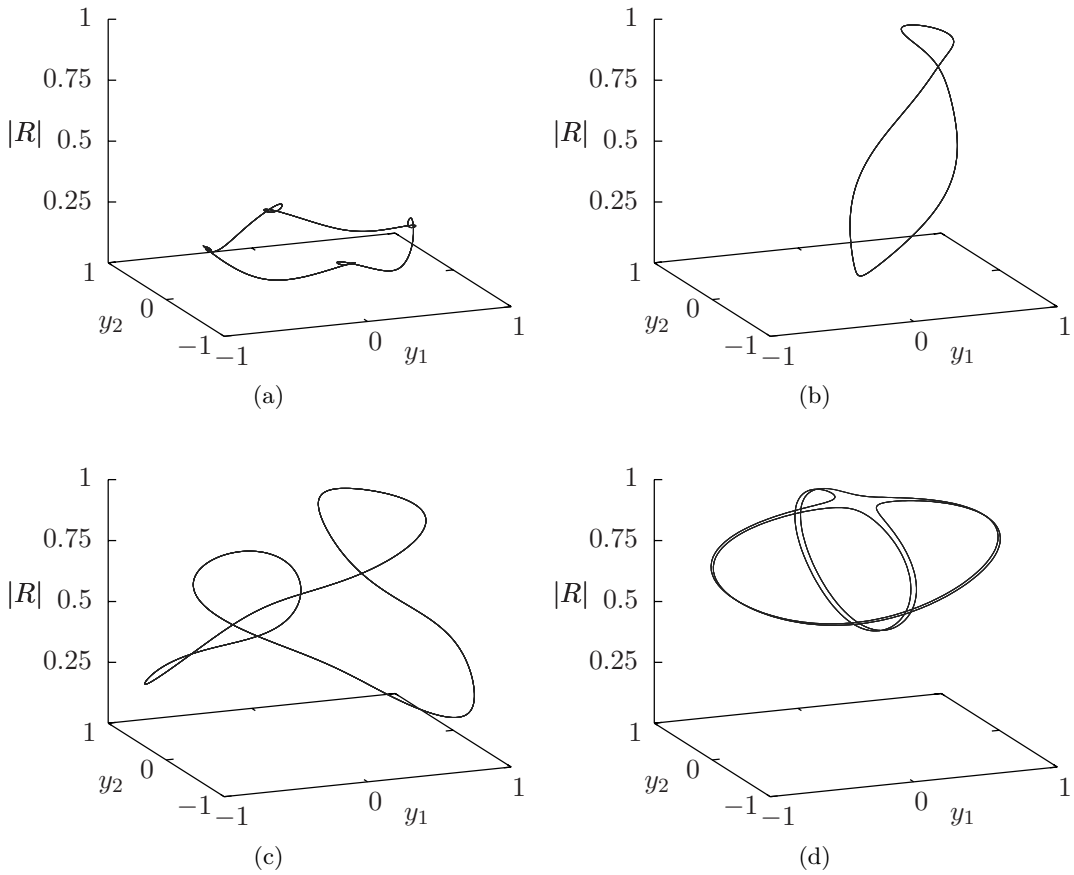

Figure 1.9.: Regular dynamics for four all-to-all coupled oscillators and an even coupling function (1.18). All solutions are periodic and have different symmetries on average depending on initial conditions. The projection is through the equivariant projection (1.13).

Lyapunov spectrum shows convergence of all Lyapunov exponents to zero for various even coupling functions (not shown).

Even though we only found periodic orbits for four phase oscillators with even coupling, these may be quite complicated[2]. For an even coupling function with four nontrivial Fourier modes, that is with g as (1.10) with $\xi_j = 0$ for all j, and parameters $a_1 = -2$, $a_2 = -2$, $a_3 = -1$, and $a_4 = 10$ there are various periodic orbits that exhibit "spiraling" motion[3] as shown in Figure (1.10). The dynamical origin of these periodic orbits for even coupling functions is still unknown.

[2]This observation is due to Pete Ashwin.

[3]Note that for these parameter values the parameters for the numerical solver have to be chosen carefully to obtain proper solutions, in particular with respect to the time step.

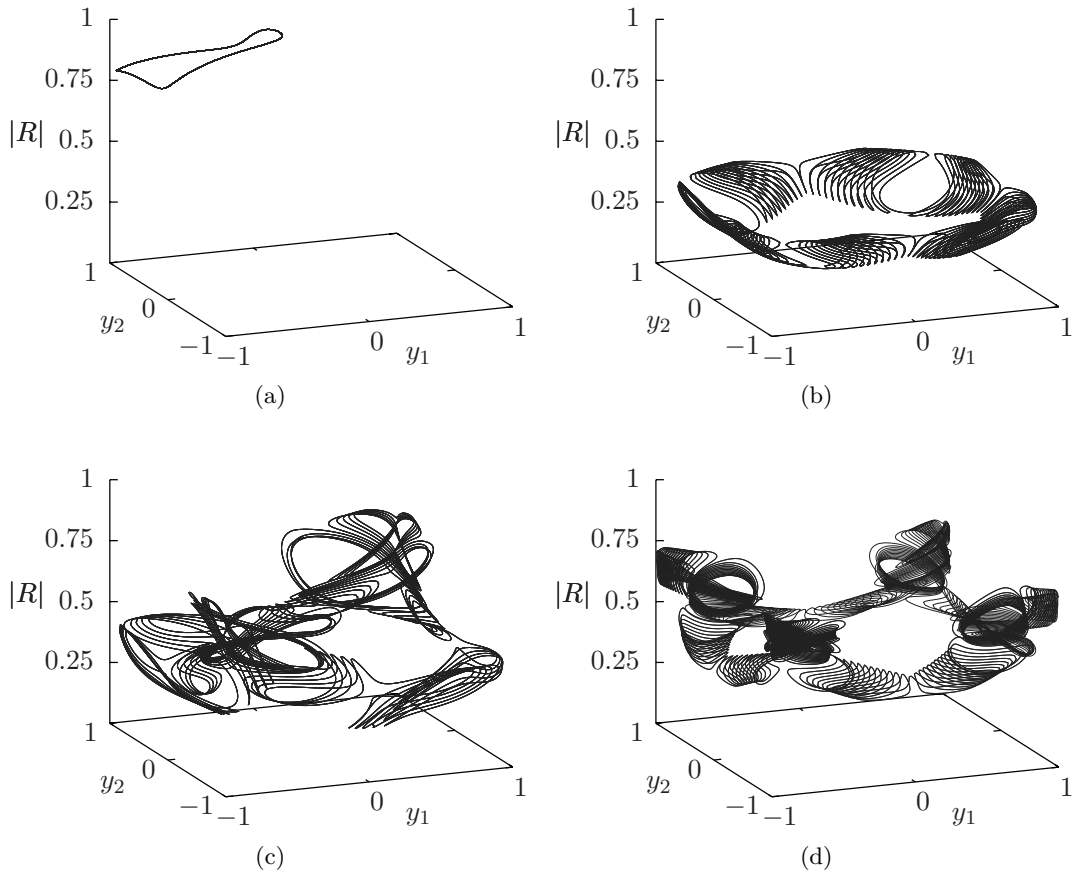

Figure 1.10.: Changing one amplitude parameter, a_4, of the coupling function (1.18) to $a_4 = 10$ yields complicated periodic trajectories for some initial conditions in addition to "simple" periodic orbits. Initial conditions are $\varphi(0) = (0, 4.8188, 4.8862, 5.0751)$ in Panel (a), $\varphi(0) = (0, 4.8238, 3.8251, 2.0564)$ in Panel (b), $\varphi(0) = (0, 1.6756, 5.0189, 5.3693)$ in Panel (c), and $\varphi(0) = (0, 0.9361, 2.2935, 5.9977)$ in Panel (d). The projection is given by the equivariant projection (1.13).

1.4. Discussion

We showed that chaotic dynamics and also chaotic fluctuations of the order parameter are possible for systems of phase coupled oscillators in the presence of full $S_N \times \mathbf{T}$-symmetry. Chaos is found not only for the smallest dimension in which chaos can occur, $N = 4$, but also for larger numbers of oscillators. The same family of coupling functions also yields attracting chaos for $N = 5$ and $N = 7$ but, interestingly, not for any other N less than fourteen. Note that the regions for which the maximal Lyapunov exponent is positive for $N \in \{4, 5, 7\}$ in (η_1, η_2) parameter space differ drastically; cf. Figure 1.6. Furthermore, chaotic dynamics are found on flow-invariant subspaces for an infinite family of dimensions N_k where $k \in \mathbb{N}$. The question whether there are coupling functions that gives rise to attracting chaos for $N = 6$ or $N \geq 8$ is still open. At the same time, one might ask whether there exists a single coupling function g that gives rise to chaotic attractors for all, or at least an infinite number of dimensions N, acting as a "universal chaos function."

That chaotic dynamics are possible for symmetrically coupled phase oscillators has implications for some applications. For example, the observation of chaotic dynamics in experimental setups of phase oscillators (see for example [58]) cannot necessarily traced back to inhomogeneities induced by the experimental setup and environmental noise. It might rather be an intrinsic property of the system itself.

For an even coupling function the system has additional (reversing) symmetries. For three oscillators the dynamics are determined by a constant of motion. This constant of motion is not only a generalization of the constant of motion found by Watanabe and Strogatz [108] for the classical Kuramoto equations to general coupling functions but it is also related to constants of motion found for rings of identical oscillators [81]. It hence describes a link between two previously unrelated quantities, at least for $N = 3$. At the same time, writing this constant of motion in the form (1.19) provides a direct relationship between the dynamics and the coupling function; note that the appearance of the Fourier coefficients of the coupling function somewhat justifies the ansatz of expanding the coupling function as a Fourier series rather than choosing some other basis. The existence of a similar expression for larger dimensions N might give insight into what features of the coupling function are crucial for the emergence of chaos as the system bifurcates from the even coupling case. This way one might obtain a hint at how to construct a "universal coupling function" as discussed above.

In particular, the existence of a single constant of motion for four oscillators with even coupling would imply non-chaotic dynamics as the effective dimension of the system is reduced to two. An expression for such a constant of motion (if it exists) could also clarify the role of the origin of parameter space as the crucial bifurcation point for emergence of chaotic dynamics; it may indicate which bifurcations happen close to this point. A similar line of argumentation applies if there was a constant of motion for a larger number of oscillators leading to a system that is at least partially integrable. Unfortunately, the efforts to find such a constant of motion for just $N = 4$ have been unsuccessful so far, motivating the question whether it exists at all and, if it does, what role the "cross coupling terms" play. At the same time, the existence of rather

complicated periodic orbits, as depicted in Figure 1.10, is an indication that even if a constant of motion exists, it might not be possible to find a simple expression for it.

For the classical Kuramoto equations, the continuum limit, i.e., the limit as $N \to \infty$, and the finite dimensional system are closely related. In the Kuramoto system, the coupling function has only one nontrivial Fourier component and for both finite N and the continuum limit, the system reduces to effectively two-dimensional dynamics [68, 77]. Thus, chaotic dynamics cannot occur. This relationship, however, depends on the special form of the coupling function which implies that the case of a general coupling function is more subtle. The question remains whether chaotic dynamics are possible in the continuum limit of (1.5)? And if so, how would that relate to systems of finitely many oscillators studied in this thesis?

Coupled phase oscillators arise naturally as the averaged limit of weakly coupled limit cycle oscillators [7]. Chaotic dynamics are observed for ensembles of globally coupled identical Ginzburg–Landau oscillators [43, 75] but it was believed that the amplitude degree of freedom is crucial for the emergence of these chaotic dynamics. Our results show that this is in fact not the case because even for phase oscillators, i.e., in the absence of any amplitude degree of freedom, chaos can occur. Conversely, the possibility of chaos in the limiting case of symmetrically coupled phase oscillators suggests that ensembles of higher-dimensional limit cycle oscillators support a wide range of intricate dynamics, including chaos.

Compared to the classical Kuramoto equations, the dynamics of identical, globally coupled phase oscillators with more general coupling functions remain poorly understood. We demonstrated that they may support rather complicated dynamics and investigated the mechanisms involved in the emergence of such dynamics. Finally, we highlighted some of the important research questions motivated by our findings. Even though these questions are beyond the scope of this thesis, tackling them may lead to a better understanding of the dynamics of symmetrically coupled phase oscillators.

Part II.

Theory of Chaos Control

2. Adaptation for Predictive Feedback Control

Typically, chaotic attractors contain infinitely many unstable periodic orbits [56]. These can be seen as a "skeleton" for the chaotic attractor [8, 21, 22], therefore revealing important information about the dynamics of the system itself. By suitable perturbations the stability of these unstable periodic points can be changed; a control perturbation may render them stable. Apart from its theoretical importance, such "chaos control" has not only been hypothesized to be a mechanism exploited in biological neural networks [91] but has also found its way into many applications [95] including chaotic lasers, stabilization of cardiac rhythms [36], and more recently into the control of autonomous robots [94, 102].

In the last twenty years, different methods for stabilizing unstable periodic orbits have been suggested. The seminal work by Ott, Grebogi, and Yorke (OGY) [79] and its implementations employ arbitrarily small perturbations of a parameter of the system to stabilize a known unstable periodic orbit of a discrete time dynamical system. A successful application of the OGY method, however, requires prior knowledge about or online analysis of the dynamics (for example by analyzing the evolution of the system [100]) to determine fixed points and their stability properties.

A different approach is given by Predictive Feedback Control (PFC) [26, 86] which overcomes this disadvantage. In this approach, the future state of the dynamics, which is calculated from the current state, is fed back into the system to stabilize a periodic orbit. This is similar to time-delayed feedback control [89] with the difference that a prediction about the future state (rather than a past state) is used for the control signal. Predictive Feedback Control is noninvasive, i.e., the control strength vanishes upon convergence, and is extremely easy to implement. In fact, it is a special case of a recent effort to stabilize all periodic points of a discrete time dynamical system [92, 93] which is also closely related to nonlinear successive overrelaxation methods [16, 109]. It has been extensively studied [19, 20, 28, 83, 84] and extended [25, 31, 57] with respect to its original purpose as a tool for examining the structure of chaotic attractors.

In any real-world application, not only the existence of parameters for which stabilization takes place but also speed of convergence is of crucial importance. For example, if a robot is controlled by stabilizing periodic orbits in a chaotic attractor [102], the time it needs to react to a changing environment is bounded by the time the system needs to converge to a periodic point of a given period. Hence, for Predictive Feedback Control one desires to tune the control parameter such that the spectral radius of the unknown periodic point to which the system converges is minimized. Previous works

on feedback chaos control have not considered convergence speed while maintaining its simplicity in terms of implementation. Adaptation of the control parameter has an impact on convergence speed. However, existing adaptation mechanisms [63, 102] have two major shortcomings: they do not optimize for speed, and, for adaptation of a heuristic nature, they may adapt the parameter to regimes where stabilization fails.

To approach the problem of optimizing convergence speed, we introduce an adaptation method that overcomes these shortcomings. It is defined within the framework of Predictive Feedback Control and adaptively tunes the control parameter online to achieve optimal asymptotic convergence speed. In the following section we review the Predictive Feedback Control method and introduce the notation that will be used throughout this chapter. In Section 2.2 we present our adaptation method and prove its convergence properties. As an example, the well-known logistic map is studied both analytically and numerically in the two subsequent Sections 2.4 and 2.5. Finally, we give some concluding remarks. The results presented in this chapter are published in [14].

2.1. Predictive Feedback Control

In this section we give some basic definitions and recall some facts about Predictive Feedback Control to set the stage for the results presented in the sections to come. A differentiable map $f : \mathbb{R}^N \to \mathbb{R}^N$ gives rise to a discrete time dynamical system through the evolution equation

$$x_{k+1} = f(x_k) \tag{2.1}$$

with $x_k \in \mathbb{R}^N$ for all $k \in \mathbb{Z}$. Let

$$f^{\circ p} = \underbrace{f \circ f \circ \cdots \circ f}_{p \text{ times}}$$

denote the p-fold composition of f. The sequence x_k with $k \in \mathbb{N}$ is called an orbit of the dynamical system with initial condition x_0. If $f^{\circ p}(x_k) = x_k$ for all $k \geq 0$, we say that the orbit is periodic with period p. As above, let

$$\mathrm{Fix}(f) := \{x \in \mathbb{R}^N \mid f(x) = x\}$$

be the set of fixed points, i.e., periodic points of period one. Note that any periodic orbit of period p is a fixed point of the pth iterate of the map f so within this chapter we will use the expressions "fixed point" and "periodic orbit" interchangeably.

Let $A \subset \mathbb{R}^N$ be a compact forward invariant subset of $\mathbb{R}^N$ with respect to f, i.e., $f(A) \subset A$. If periodic points are dense in A and f maps transitively, i.e., for every pair of non-empty open sets $U, V \subset A$, there is a non-negative integer n such that $f^{\circ n}(U) \cap V \neq \emptyset$, then we call A a *chaotic set*. Julia sets [71] in one complex dimension, as described below, are examples of such chaotic sets. Let $\mathrm{d}f|_x$ denote the derivative of f at $x \in \mathbb{R}^N$ and let $\mathrm{id} : \mathbb{R}^N \to \mathbb{R}^N$ denote the identity map.

Definition 2.1.1. *A fixed point $x^* \in \mathrm{Fix}(f)$ is called attractive or stable if all eigenvalues of $\mathrm{d}f|_{x^*}$ are of absolute value smaller than one, i.e., if the spectral radius of the matrix $\mathrm{d}f|_{x^*}$ is smaller than one. The value of the spectral radius is referred to as the asymptotic convergence rate towards an attractive fixed point.*

Remark 2.1.2. If ρ is the convergence rate of a stable fixed point, then convergence is fast for small ρ. In the following, we will mostly talk about asymptotic convergence speed which will be either $1-\rho$ or ρ^{-1} depending on what is convenient in the context. Either one of these quantities coincides with the traditional notion of speed, i.e., convergence is fast if the value is large.

For a fixed point x^* let $\mathcal{B}(x^*) = \{x_0 \in \mathbb{R}^N \mid f^{\circ k}(x_0) = x_k \to x^* \text{ as } k \to \infty\}$ denote its basin of attraction. If x^* is stable then there is an open neighborhood V of x^* with $V \subset \mathcal{B}(x^*)$. Attractive periodic orbits of period p are attractive fixed points of $f^{\circ p}$; the stability properties of $x^* \in \mathrm{Fix}(f^{\circ p})$ are determined by the eigenvalues of $\mathrm{d}(f^{\circ p})|_{x^*}$. By the chain rule, the stability properties are the same for any point $x^*, f(x^*), \ldots, f^{\circ(p-1)}(x^*)$ of the periodic orbit.

The results of [93] are now summarized as follows.

Proposition 2.1.3. *Suppose that $x^* \in \mathrm{Fix}(f)$ and the matrices $\mathrm{d}f|_{x^*}$ and $\mathrm{d}f|_{x^*} - \mathrm{id}$ are real, nonsingular, and diagonalizable. If g_μ is the map obtained from f through the transformation*

$$S(\mu, M_k) : f \mapsto \mathrm{id} + \mu M_k(f - \mathrm{id}) =: g_\mu$$

then there exist a parameter $\mu > 0$ and an orthogonal matrix $M_k \in O(n)$ such that x^* is an attractive fixed point of g_μ. In particular, for $\mu \neq 0$ the transformation $S(\mu, M_k)$ preserves the set of fixed points, that is, $\mathrm{Fix}(f) = \mathrm{Fix}(g_\mu)$.

In fact, it can be shown that the number of matrices M_k needed to stabilize all fixed points of a given map f is quite limited [19]. The choice of M_k depends on the local stability properties of fixed points and there are types of fixed points that can be stabilized for $M_k \in \{\pm \mathrm{id}\}$. Let $\mathbb{C}$ denote the set of complex numbers and suppose that $\chi_j \in \mathbb{C}$ where $j \in \{1, \ldots, n\}$ are the eigenvalues of $\mathrm{d}g_\mu|_{x^*}$ for a given $x^* \in \mathrm{Fix}(f)$. We denote by

$$\varrho_{x^*}(\mu) := \max_{j \in \{1,\ldots,n\}} \{|\chi_j|\}$$

the spectral radius of $\mathrm{d}g_\mu|_{x^*}$, i.e., the maximum of the absolute values of the eigenvalues of the derivative of g_μ at x^*. We have

$$\mathrm{d}g_\mu|_x = \mathrm{id} + \mu M_k(\mathrm{d}f|_x - \mathrm{id}). \tag{2.2}$$

for all $x \in \mathbb{R}^N$. In other words, the proposition above ensures the existence of μ and $M_k(x^*)$ for a given $x^* \in \mathrm{Fix}(f)$ such that the transformation $S(\mu, M_k)$ gives $\varrho_{x^*}(\mu) < 1$; cf. Figure 2.1. Therefore, with these parameters, the fixed point x^* of f is an attracting fixed point for g_μ.

The results above are directly related to predictive feedback chaos control methods. A transformation $T_\eta : f \mapsto g$ is called a *chaos control transformation* if g can be written

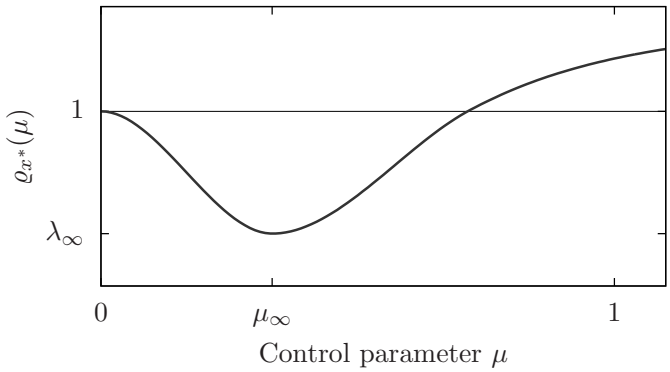

Figure 2.1.: Sketch of the dependence of the spectral radius $\varrho_{x^*}(\mu)$ on μ for some fixed point x^* according to Proposition 2.1.3.

as $g = f + \eta c$ with *control perturbation* $c : \mathbb{R}^N \to \mathbb{R}^N$ and $\eta \in \mathbb{R}$. Note that for $M_k \in \{\pm \mathrm{id}\}$ the transformations $S(M_k, \mu)$ are chaos control transformations since

$$g_\mu = f + (1 \mp \mu)(\mathrm{id} - f) \tag{2.3}$$

with $\eta = 1 \mp \mu$. Therefore, we will refer to these transformations $S(\mu, M_k)$ as PFC transformations. In fact, we may treat $M_k \in \{\pm \mathrm{id}\}$ simultaneously by considering $M_k = \mathrm{id}$ and choosing the parameter μ from the interval $[-1, 1]$.

The results of Proposition 2.1.3, however, give little information about the speed of convergence, except for the fact that when decreasing μ towards zero, convergence takes longer and longer as the spectral radius approaches one. In the vicinity of a stabilized fixed point, convergence is at least linear and the rate of convergence is bounded from above by the quantity $\varrho_{x^*}(\mu)$. In order to obtain an adaptation method that increases the speed of convergence, we therefore have to minimize $\varrho_{x^*}(\mu)$ using the control parameter μ. For a random initial condition, we do not know to which fixed point x^* (if any) the trajectory will converge. We only have a converging sequence $x_k \to x^*$. In other words, we are looking for a way to obtain a sequence $\mu_k \to \mu_\infty$ where

$$\mu_\infty = \sup \left\{ \mu > 0 \;\middle|\; \forall \hat{\mu} > 0 : \varrho_{x^*}(\mu) \leq \varrho_{x^*}(\hat{\mu}) \;\; \begin{array}{l} \text{and assumptions of} \\ \text{Prop. 2.1.3 are satisfied} \end{array} \right\} \tag{2.4}$$

is the optimal μ to minimize $\varrho_{x^*}(\mu)$. Define $\lambda_\infty := \varrho_{x^*}(\mu_\infty)$. In applications, the control parameter μ plays a double role; on the one hand, it can be used to turn chaos control on and off, $\mu = 1$, and on the other hand, it is the crucial parameter for stabilizing the periodic orbits and determining the speed of convergence.

Let card denote the cardinality of a set. For parameters $p \in \mathbb{N}$ and $\mu_0 > 0$ define the class of functions

$$\mathcal{F}(\mu_0, p) := \{\, f \mid \mathrm{card}\,(\{\, x^* \in \mathrm{Fix}(f^{\circ p}) \mid \varrho_{x^*}(\mu_0) < 1 \text{ for } M_k = \mathrm{id} \,\}) > 0 \,\}\,.$$

The sets $\mathcal{F}(\mu_0, p)$ are the functions f with a chaotic set that have at least one periodic orbit of period p which can be stabilized for the given parameters.

2.2. An Adaptation Method for Accelerating Chaos Control

Predictive Feedback Control is a chaos control scheme that depends on one real parameter, the control parameter μ. For a certain class of fixed points, there exists a value of μ such that these fixed points are stable fixed points of the PFC-transformed dynamical system. At the same time, the choice of control parameter influences the speed of convergence. In this section, we develop an adaptive algorithm which tunes the control parameter to achieve optimal convergence speed. After proving the local convergence properties of the resulting chaos control method, we discuss how to determine features of the global dynamics from invariant measures on the chaotic attractor.

Within this section suppose that $f \in \mathcal{F}(\mu_0, p)$ for some $\mu_0 > 0$ and, without loss of generality, we may assume $p = 1$ since we can replace f with the pth iterate. Suppose that g_μ is the transformed map after applying $S(\mu, \mathrm{id})$. Furthermore, we assume that for all times $k < 0$ the system evolves according to Equation (2.1), i.e., with $\eta = 1 - \mu = 0$, along a trajectory of points in the chaotic set A. At time $k = 0$ the control parameter μ is set to μ_0. Therefore, because of the assumptions on f, there is at least one periodic orbit of period p on the chaotic attractor which is now an attracting periodic orbit. Let $\mathrm{Fix}^\bullet(f)$ denote the set of these stabilized fixed points.

Close to a Fixed Point

Recall two facts: first, for any contraction h on a Banach space $(Y, \|\cdot\|)$, i.e., a map that satisfies

$$\|h(x) - h(y)\| \leq L \|x - y\|$$

with a Lipschitz constant $L < 1$, the Banach Fixed Point Theorem gives the existence of a unique fixed point x^*. For an initial condition $x_0 \in Y$ and $x_k = h^{\circ k}(x_0)$ we have the error estimates $\|x^* - x_k\| \leq \frac{L^k}{1-L} \|x_0 - x_1\|$ and $\|x_{k+1} - x_k\| \leq L \|x_k - x_{k-1}\|$. Second, if $h : U \to \mathbb{R}^N$ is a differentiable map on an open set $U \subset \mathbb{R}^N$ then it is is Lipschitz continuous on any compact $C \subset U$. Let $\|\cdot\|_C$ denote the supremum of the operator norms induced by a norm $\|\cdot\|$ on C and $\mathrm{d}h$ denotes the total derivative. We have

$$\|h(x) - h(y)\| \leq \|\mathrm{d}h\|_C \cdot \|x - y\|,$$

for all $x, y \in C$.

Let $x^* \in \mathrm{Fix}^\bullet(f)$ be fixed. According to Proposition 2.1.3 there exists a $\lambda_0 < 1$ for $\mu = \mu_0$ sufficiently small such that $\varrho_{x^*}(\mu_0) < \lambda_0$. Therefore, there exists a vector norm $\|\cdot\|$ such that we have $\|\mathrm{d}g_\mu|_{x^*}\|_{\mathrm{op}} \leq \lambda_0$ for the induced operator norm; cf. Figure 2.2(a). We will omit the index indicating the operator norm when it is clear from the context. Henceforth all norms denote this vector norm and the induced operator norm, respectively.

Let $B(r, x)$ denote a ball of radius $r > 0$ centered at x and by $\overline{B(r, x)}$ denote its closure. Assume that for $\hat{\varepsilon}$ small enough there is a constant $K \geq 0$ such that

$$\Big| \|\mathrm{d}g_\mu|_{x^*}\| - \|\mathrm{d}g_\mu|_x\| \Big| \leq K \|x^* - x\| \tag{2.5}$$

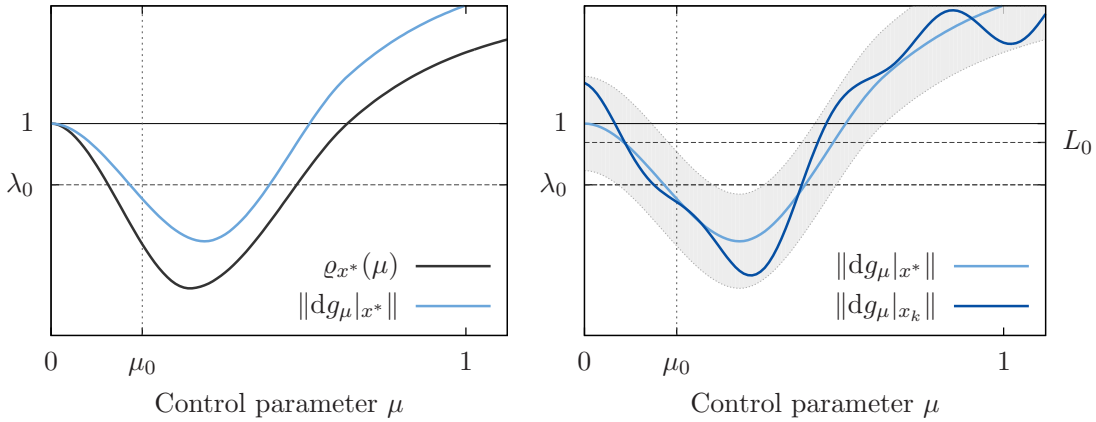

Figure 2.2.: (a) An appropriately chosen norm approximates the spectral radius from above with $\varrho_{x^*}(\mu_0) \leq \|\mathrm{d}g_{\mu_0}|_{x^*}\| \leq \lambda_0$. (b) According to Condition (2.5), $\|\mathrm{d}g_\mu|_{x_k}\|$ lies in a $K\,\|x^* - x_k\|$-tube around $\|\mathrm{d}g_\mu|_{x^*}\|$. While iterating, this tube becomes smaller and smaller. As another consequence of (2.5), we have $\|\mathrm{d}g_\mu|_x\|_{\overline{B(\varepsilon,x^*)}}$ in a $K\varepsilon$-tube around $\|\mathrm{d}g_\mu|_{x^*}\|$. Therefore, for ε small enough, there is $L_0 < 1$ such that $\|\mathrm{d}g_{\mu_0}|_x\|_{\overline{B(\varepsilon,x^*)}} \leq L_0$.

for all x with $\|x^* - x\| < \hat{\varepsilon}$ independent of μ. This condition is depicted in Figure 2.2(b). Now we can choose $\varepsilon \leq \hat{\varepsilon}$ such that $\|\mathrm{d}g_{\mu_0}|_x\|_{\overline{B(\varepsilon,x^*)}} < 1$. In other words, for sufficiently small $\delta_0 > 0$ there exists an $\varepsilon \in (0, \hat{\varepsilon})$ such that

$$\|\mathrm{d}g_{\mu_0}|_x\|_{\overline{B(\varepsilon,x^*)}} \leq \lambda_0 + \delta_0 < 1.$$

The choice of ε (corresponding to the size of the ball around x^*) depends on λ_0, μ_0, and δ_0.

Definition 2.2.1. *A function $f \in \mathcal{F}(\mu_0, 1)$ that satisfies Condition (2.5) is called admissible with initial control parameter μ_0 (or simply μ_0-admissible). For such a function f, the tuple $(\mu_0, K, \varepsilon, \lambda_0, \delta_0)$ defined above is referred to as initial adaptation parameters for x^*. The ball $B(\varepsilon, x^*)$ is called the initial adaptation neighborhood.*

Remark 2.2.2. Condition (2.5) is satisfied if f has a bounded second derivative on $\mathrm{Fix}^\bullet(f)$ due to the functional dependence of the derivative of g_μ on μ as given by (2.2) and the reverse triangle inequality.

Algorithm 2.2.3. *Suppose that f is a μ_0-admissible function with $x^* \in \mathrm{Fix}^\bullet(f)$ and let $(\mu_0, K, \varepsilon, \lambda_0, \delta_0)$ be initial adaptation parameters. Define the convergence acceleration algorithm for initial conditions $x_0 \in B(\varepsilon, x^*)$ by the following steps:*

Step 1 (iterate)*: Calculate $x_1 = g_{\mu_0}(x_0)$.*

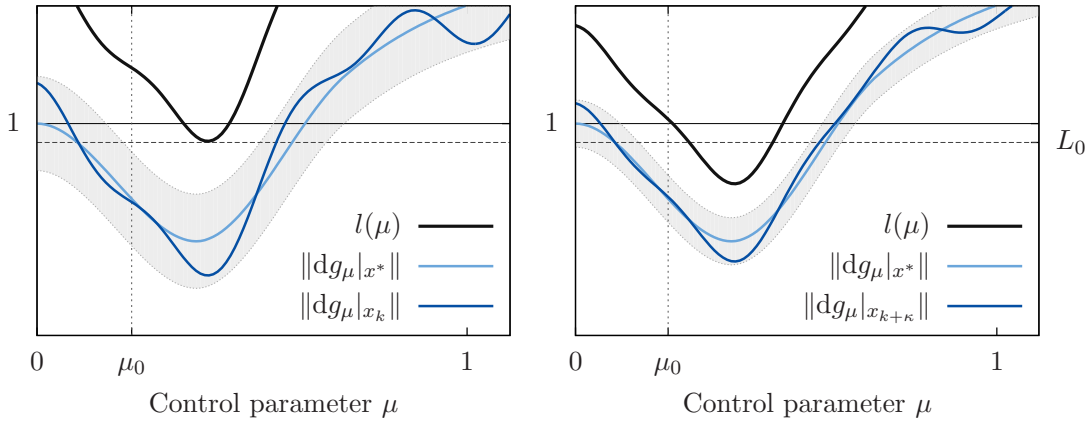

Figure 2.3.: (a) Inequality (2.6a) does not always have to be satisfied. (b) After a finite time κ the function $l(\mu)$ is below L_0 for some μ since $x_k \to x^*$.

Step 2 (optimize μ)*: Set* $L_0 := \lambda_0 + \delta_0$*. Minimize the "cost function"* $\|\mathrm{d}g_\mu|_{x_1}\|$ *with respect to* $\mu \in (0,1)$ *under the conditions*

$$l(\mu) := \|\mathrm{d}g_\mu|_{x_1}\| + \left(\frac{2KL_0}{1-L_0}\right)\|x_0 - x_1\| < L_0, \tag{2.6a}$$

$$\mu \text{ maximal}; \tag{2.6b}$$

cf. Figure 2.3.

Step 3 (set quantities)*: If the minimization under constraints of Step 2 returns a result* μ_{opt}*, then set*

$$\begin{aligned}
\mu_1 &:= \mu_{\mathrm{opt}},\\
\lambda_1 &:= \|\mathrm{d}g_\mu|_{x_1}\| + \left(\frac{KL_0}{1-L_0}\right)\|x_0 - x_1\|,\\
\delta_1 &:= \left(\frac{KL_0}{1-L_0}\right)\|x_0 - x_1\|, \text{ and}\\
L_1 &:= \lambda_1 + \delta_1.
\end{aligned}$$

Otherwise set $\mu_1 := \mu_0, \lambda_1 := \lambda_0, \delta_1 := \delta_0$*, and* $L_1 := L_0$*.*

Repeat these steps with all indices increased by one.

The goal now is to prove the applicability and convergence of this adaptive algorithm. First, we prove that Algorithm 2.2.3 yields a sequence x_k with $k \in \mathbb{N}$ that converges to the specified fixed point.

Lemma 2.2.4. *Suppose that* f *is admissible and* $x^* \in \mathrm{Fix}^\bullet(f)$*. For all initial conditions* x_0 *in the initial adaptation neighborhood* $B(\varepsilon, x^*)$ *the iteration according to*

Algorithm 2.2.3 yields a trajectory $x_k \to x^*$ as $k \to \infty$ which converges to the fixed point.

Proof. If the optimization process does not give a result, convergence is ensured by Proposition 2.1.3 and the Banach Fixed Point Theorem.

Without loss of generality, suppose that optimization yields a result for $k = 1$. Then because of (2.5), (2.6a), and the error estimate of the Banach Fixed Point Theorem we have

$$\begin{aligned}\|\mathrm{d}g_{\mu_1}|_x\|_{\overline{B(\|x_1-x^*\|,x^*)}} &\leq \|\mathrm{d}g_{\mu_1}|_{x^*}\| + K\,\|x_1 - x^*\| \\ &\leq \|\mathrm{d}g_{\mu_1}|_{x_1}\| + 2K\,\|x_1 - x^*\| \\ &\leq \|\mathrm{d}g_{\mu_1}|_{x_1}\| + \left(\frac{2KL_0}{1-L_0}\right)\|x_1 - x_0\| \\ &= L_1 \leq L_0 < 1.\end{aligned}$$

Therefore, the point x_1 is contained in a ball around the fixed point x^* on which the map g_{μ_1} is a contraction with contraction coefficient L_1. An analogous calculation is valid for subsequent optimization steps for $k > 1$. □

The lemma above ensures that the adaptation does not compromise convergence against the stabilized fixed point. But will optimization actually take place? For a map with $K = 0$, adaptation is not necessary since $\|\mathrm{d}g_\mu|_{x^*}\| = \|\mathrm{d}g_\mu|_{x_k}\|$ and therefore we can set μ straight to the optimal value.

Lemma 2.2.5. *Suppose that f is admissible with initial control parameter μ_0 and let $(\mu_0, K, \varepsilon, \lambda_0, \delta_0)$ be initial adaptation parameters for $x^* \in \mathrm{Fix}^\bullet(f)$. If x_0 is an element of the initial adaptation neighborhood $B(\varepsilon, x^*)$ then, while iterating according to Algorithm 2.2.3, Inequality (2.6a)*

$$\|\mathrm{d}g_\mu|_{x_{k+1}}\| + \left(\frac{2KL_k}{1-L_k}\right)\|x_k - x_{k+1}\| < L_k$$

is be satisfied for infinitely many $k \in \mathbb{N}$.

Proof. By definition we have $\|\mathrm{d}g_{\mu_0}|_{x_0}\| \leq L_0 = \lambda_0 + \delta_0$ with $\delta_0 > 0$. Hence, we have $\|\mathrm{d}g_{\mu_0}|_{x^*}\| < L_0$. Suppose that k_0 is the first index for which the optimization under constraints yields a result. Note that $L_k = L_0$ for $k < k_0$.

Let $\zeta > 0$ be such that $\zeta < L_0 - \|\mathrm{d}g_{\mu_0}|_{x^*}\|$. Since $x_k \to x^*$ as $k \to \infty$ according to Lemma 2.2.4, the sequence x_k is a Cauchy sequence with respect to $\|\cdot\|$. Moreover, we have $\|\mathrm{d}g_{\mu_0}|_{x_k}\| \to \|\mathrm{d}g_{\mu_0}|_{x^*}\|$. Therefore, there exists an $\kappa \in \mathbb{N}$ such that $\left(\frac{2KL_0}{1-L_0}\right)\|x_{\kappa+1} - x_\kappa\| < \frac{\zeta}{2}$ and $\left|\|\mathrm{d}g_{\mu_0}|_{x^*}\| - \|\mathrm{d}g_{\mu_0}|_{x_{\kappa+1}}\|\right| < \frac{\zeta}{2}$. We obtain

$$\|\mathrm{d}g_{\mu_0}|_{x_{\kappa+1}}\| + \left(\frac{2KL_0}{1-L_0}\right)\|x_{\kappa+1} - x_\kappa\| < \|\mathrm{d}g_{\mu_0}|_{x^*}\| + \frac{\zeta}{2} + \frac{\zeta}{2} < \|\mathrm{d}g_{\mu_0}|_{x^*}\| + \zeta < L_0.$$

Therefore, Inequality (2.6a) will be satisfied after maximally $\kappa =: \kappa_0$ steps.

By increasing all indices above by κ_0, the same argument gives a κ_1 for which optimization of Step 2 yields a result. Inductively, we obtain a sequence κ_l with $l \in \mathbb{N}$ of indices for which Inequality (2.6a) is satisfied. This completes the proof of the assertion. □

Remark 2.2.6. Although the adaptation method gives a sequence μ_k that minimizes the norm while ensuring convergence, it is not clear how often optimization yields a result. Additional conditions on the map f, such as requiring monotonicity of $\|\mathrm{d}g_\mu|_{x_k}\|$ in x_k, influence how often the parameter μ will be adapted. On the other hand, additional constraints make the theory less broadly applicable.

If Inequality (2.6a) is satisfied for some $k > 0$, then, because $\|\mathrm{d}g_\mu|_{x^*}\|$ depends continuously on μ, it holds for a whole closed neighborhood of μ_k. This gives μ_{k+1} with $\|\mathrm{d}g_{\mu_{k+1}}|_{x^*}\| < \|\mathrm{d}g_{\mu_k}|_{x^*}\|$ unless $\|\mathrm{d}g_\mu|_{x^*}\|$ is constant on that interval.

Definition 2.2.7 ([50]). *Let $\varrho(M)$ denote the spectral radius of a matrix $M \in \mathbb{R}^{N\times N}$. A matrix norm $\|\cdot\|$ on $\mathbb{R}^{N\times N}$ is called minimal for M if $\varrho(M) = \|M\|$.*

The following theorem summarizes the results we have obtained so far on the convergence properties of the adaptation algorithm.

Theorem 2.2.8. *Suppose that f is admissible with initial control parameter μ_0 and suppose that $x^* \in \mathrm{Fix}^\bullet(f)$ with initial adaptation parameters $(\mu_0, K, \varepsilon, \lambda_0, \delta_0)$. Then, for any initial condition $x_0 \in B(\varepsilon, x^*)$ in the initial adaptation neighborhood, Algorithm 2.2.3 minimizes an upper bound for the spectral radius $\varrho_{x^*}(\mu)$.*

In particular, if the induced operator norm $\|\cdot\|_{op}$ is minimal for $\mathrm{d}g_{\mu_\infty}|_{x^*}$, it converges at least linearly with asymptotic convergence rate λ_∞.

Remark 2.2.9. For dimension $N = 1$, the Euclidean norm is minimal for any matrix.

Proof of Theorem 2.2.8. Lemmas 2.2.4 and 2.2.5 ensure convergence against the fixed point x^* and adaptation of the control parameter μ after a maximum of finitely many iterations.

By construction, μ_k tends to a value which minimizes the norm of the derivative of g_μ at x^* as $k \to \infty$. For arbitrary dimension N we have $\varrho_{x^*}(\mu_k) \leq \|\mathrm{d}g_{\mu_k}|_{x^*}\|$. If in addition the norm is minimal, in the limit the spectral radius is minimized, yielding optimal asymptotic convergence speed, i.e., $\mu_k \to \mu_\infty$. □

Remark 2.2.10. One could also use convergence acceleration transformations [99] in order to get a better approximation to $\varrho_{x^*}(\mu)$. However, to exploit the acceleration within the framework of this theory, one would have to have suitable error estimates for the transformed sequence.

The choice of the size of the ball $B(\varepsilon, x^*)$ depends on the desired estimate of the contraction constant. It is clearly bounded from above since we have to make sure that there is a contraction. On the other hand, it is desirable to take a neighborhood as large as possible to make the method applicable to as many initial conditions as possible.

From Local to Global

Consider the situation where the control is turned on at an arbitrary point in time. We choose indices such that this time is $k = 0$. In general, the initial condition x_0

for the adaptation method is unknown, and it is likely to be outside of the initial adaptation neighborhood $B(\varepsilon, x^*)$. One possible scenario is the existence of a chaotic attractor that makes up part of the old chaotic attractor and ending up in its basin of attraction when the control is turned on. Another likely scenario is to have x_0 close to the boundary of the basin of attraction of one of the stabilized fixed points. An initial condition close to the basin boundary implies a long transient iteration before the adaptation method becomes applicable.

We want to quantify the latter scenario. We may assume that the initial condition x_0 is distributed according to some ergodic f-invariant measure on A [33]. This implies in particular that x_0 does not lie on any periodic orbit; see also [56, 67] for other measure theoretic aspects of dynamical systems. This approximates the situation in which the dynamics evolved on the chaotic set for "a long time," $x_k = f(x_{k-1})$ for $k \leq 0$, after having been initialized with a generic initial condition. Thus, $m(U)$ is the probability that $x_0 \in U$ at time $k = 0$ for any measurable subset $U \subset A$.

Let $B(\varepsilon(x^*), x^*)$ denote the initial adaptation neighborhood for $x^* \in \mathrm{Fix}^\bullet(f)$ as defined above. Since we assume f to be μ_0-admissible, there is at least one such ball of positive radius. Define

$$V_0 := V = \left(\bigcup_{x^* \in \mathrm{Fix}^\bullet(f)} B(\varepsilon(x^*), x^*) \right) \cap A$$

to be the part of the union of all these neighborhoods on the attractor. Thus, if V is measurable, $m(V)$ is a lower bound for the probability that the adaptation method described above converges if the dynamics evolved on the chaotic set before the parameter μ is set to μ_0 at a random point in time. Furthermore, we define

$$V_k := \left(\bigcup_{l \leq k} g_{\mu_0}^{\circ(-l)}(V) \right) \cap A.$$

By definition, $P_k = m(V_k)$ is a lower bound on the probability that the algorithm will converge after letting the transformed system evolve for k time steps after being initialized with $\mu = \mu_0$ at time $k = 0$.

As k tends to infinity, the set V_k will converge to the union of the basins of attraction of the stabilized fixed points. Hence, we obtain a function

$$\varphi(\mu_0) := \lim_{k \to \infty} m(V_k)$$

depending on the initial parameter μ_0. The value $\hat{\varphi} = \liminf_{\mu_0 \to 0} \varphi(\mu_0)$ for some $\hat{\varphi} \in [0, 1]$ determines the size of the basin of attraction of the stabilized fixed points.

2.3. Adaptive Predictive Feedback Control for the Logistic Family

As an example, we apply the PFC transformation to the family of logistic maps given by the quadratic polynomials $\ell_r(x) = rx(1 - x)$ with the real parameter $1 < r \leq 4$. It

is well known that there are parameter values for which the dynamics are chaotic on some subset A of the unit interval $I = [0, 1]$. In particular, for $r = 4$ the whole unit interval is a chaotic set. Here, we study the period one orbits; higher periods can be treated similarly.

Calculating the Adaptation Parameters

First, we want to calculate the initial adaptation parameters for the adaptation method described in the previous section. The second derivative of ℓ_r exists everywhere on $\mathbb{R}$ and is bounded on compact subsets. Within this section let h' denote the derivative of a differentiable function h. Here, we treat the two cases $M_k \in \{\pm \mathrm{id}\}$ simultaneously by taking $\mu \in [-1, 1]$ for the transformed function

$$g_{\mu,r}(x) = S(\mu, M_k)(\ell_r)(x) = x + \mu(\ell_r(x) - x).$$

For $\mu = 1$ we obtain the original system and around $\mu = 0$ either of the two cases, that is $M_k = \mathrm{id}$ when μ is positive and $M_k = -\mathrm{id}$ when μ is negative.

Since $|g''_{\mu,r}(x)| = |\mu|\,|\ell''_r(x)| = 2r\,|\mu|$ for all $x \in I$, the maximum of $|g''_{\mu,r}|$ in μ is taken for $|\mu| = 1$. We have

$$\Big||g'_{\mu,r}(x)| - |g'_{\mu,r}(y)|\Big| \le |g'_{\mu,r}(x) - g'_{\mu,r}(y)| \le \max_{a\in I} |g''_{\mu,r}(a)|\,|x - y|$$

for all $x, y \in I$ which implies that Condition (2.5) is fulfilled for a constant $K = 8$, which is independent of the parameter r and the sign of M_k.

The two fixed points of ℓ_r are $x^* = 0$ and $x^* = \frac{r-1}{r}$. The derivatives at the fixed points are $g'_{\mu,r}(0) = 1 + \mu(r - 1)$ and $g'_{\mu,r}(\frac{r-1}{r}) = 1 - \mu(r - 1)$. Hence, $x^* = 0$ is stable for negative μ ($M_k = -\mathrm{id}$) and $x^* = \frac{r-1}{r}$ for positive μ ($M_k = \mathrm{id}$). To apply the adaptive method, the initial parameters need to be determined as in Section 2.2: for a given μ_0 the bound λ_0 can be calculated directly from the derivative $g'_{\mu_0,r}$. Furthermore, we have to find ε that defines the initial adaptation neighborhood of x^* for the initial condition x_0 and a given initial μ_0. From the local stability and (2.5) we obtain that convergence is ensured if

$$\lambda_0 = 1 + |\mu_0|\,(r - 1) > -1, \tag{2.7a}$$

$$K\varepsilon - |\mu_0|\,(r - 1) < 0, \tag{2.7b}$$

$$K\varepsilon + |\mu_0|\,(r - 1) < 2. \tag{2.7c}$$

For either x^* this gives $|\mu_0| < \frac{2}{r-1}$. This results in a bound for the size of the neighborhood of x^* in which the map is a contraction,

$$\varepsilon < \min\left\{\frac{2 - \mu_0(r - 1)}{K}, \frac{\mu_0(r - 1)}{K}\right\}. \tag{2.8}$$

The optimal bound $\varepsilon < \frac{1}{K}$ is achieved for $\mu_0(r - 1) = 1$.

It is desirable to choose ε as large as possible (to cover as many initial conditions as possible) while keeping the whole expression on the left-hand side of Inequality (2.7a) as small as possible (a smaller contraction constant L_0 leads to stronger contraction). This choice depends on the initial guess μ_0, cf. Inequality (2.8).

Remark 2.3.1. The chaotic set A depends on the choice of the parameter r, so we obtain a family of chaotic sets A_r. Note that we do not necessarily have $0 \in A_r$ or $\frac{r-1}{r} \in A_r$. We have $A_4 = I$ so that the two fixed points are contained in A_4. Otherwise, for a given fixed point x^*, the value of ε has to be chosen large enough such that $A_r \cap B(\varepsilon, x^*) \neq \emptyset$.

The constant parameters $K = 8$ and μ_0, λ_0, and ε as given by (2.7) together with an approximation of the measure on A are the basis of the calculations of lower bounds for the probability of convergence in the following section.

PFC on the Complex Plane

The quadratic polynomial defining the logistic map can also be seen as a polynomial over the complex numbers. Iteration of complex polynomials is a classical example in one-dimensional complex analytic dynamics, and the theory developed there can tell us something about the effect of the PFC transformation $S(\mu, M_k)$ for $M_k \in \{\pm \mathrm{id}\}$. Here, this geometric point of view allows us to calculate the full basin of attraction of the stabilized fixed points. In particular, we also obtain convergence for general, complex valued initial conditions in a neighborhood of the periodic orbits in the complex plane.

Recall some notions from one-dimensional complex dynamics [71]. Suppose $f : \mathbb{C} \to \mathbb{C}$ is holomorphic. A point $z \in \hat{\mathbb{C}} = \mathbb{C} \cup \{\infty\}$ is said to be in the *Fatou set* $F(f)$ if there is an open neighborhood U of z on which the family of iterates $\mathcal{G} := \{f^{\circ k} \mid k \in \mathbb{N}\}$ is normal, i.e., for every sequence in $\mathcal{G}$ there is a subsequence that converges uniformly on compact subsets of U. Its complement is called the *Julia set* $J(f)$ and constitutes the boundary of all Fatou components which contain any stable periodic orbit. Both of these sets are forward and backward invariant with respect to the map f. The Julia set is a chaotic set in our sense. Henceforth, we denote the complex variable by z.

Let $f \in \mathbb{C}[z]$ be a complex polynomial. Note that the PFC transformed map g_μ again is a polynomial of the same degree as f in the complex variable z unless f is constant or $\mu = 0$. A member of the logistic family is given by a polynomial of degree two. The dynamics of quadratic polynomials are conjugate to the dynamics of a polynomial z^2+c, where $c \in \mathbb{C}$ is a parameter. Recall that $w \in \mathbb{C}$ is a critical point of f if $f'(w) = 0$. For a quadratic polynomial, the complex valued parameter c may be characterized in terms of the orbit of the only finite critical point $w = 0$; the points for which that orbit is bounded constitute the *Mandelbrot set* $\mathcal{M}$. For $c \in \mathcal{M}$ there can be bounded Fatou components corresponding to the basin of attraction of a stable periodic orbit.

The logistic family described above is dynamically conjugate to polynomials z^2+c with $c \in [-2, \frac{1}{4}]$, the intersection of $\mathcal{M}$ with the real axis. The PFC transformed map $g_{\mu,r}$ for ℓ_r is again is a quadratic polynomial with real coefficients. For the logistic family, any $g_{\mu,r}$ is therefore conjugated to a quadratic polynomial $z^2 + c$ with real parameter c since only those polynomials keep the real axis invariant. By conjugation with a Möbius transformation ϑ, i.e., solving $\vartheta \circ g_{\mu,r} \circ \vartheta^{-1} = z^2 + c_r(\mu)$, one obtains the relationship between the real parameter c and the control parameter $\mu \neq 0$ for a given r. A quick

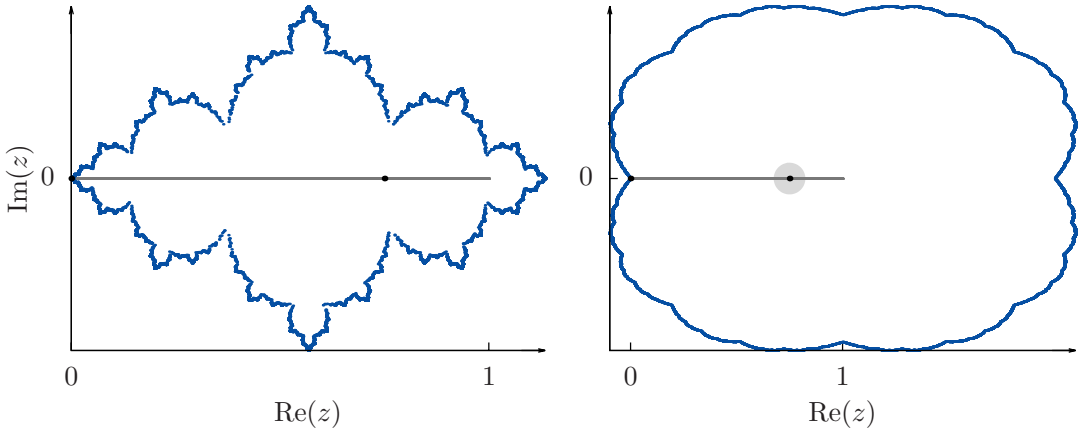

Figure 2.4.: Julia sets for parameters $\mu = -0.65$ (left) and $\mu = -0.2$ (right) for $M_k = -\mathrm{id}$. The Julia set of $g_{\mu,4}$ is depicted in blue, whereas the Julia set of the original map, i.e., the unit interval, is depicted in gray. The fixed points $z^* = 0$ and $z^* = \frac{3}{4}$ are marked by black dots. Shaded circles indicate $B(\varepsilon, z^*)$ for $\mu_0 = \mu$.

calculation yields

$$c_r(\mu) = \frac{1}{4}\left(1 - \mu^2(r-1)^2\right).$$

Hence, varying the parameter μ results in a "shift" of the dynamics up the real axis until it approaches $c = \frac{1}{4}$ as $\mu \to 0$. From the equation above, one can also see that the dynamics of $g_{\mu,r}$ are conjugated for $\mu = 1$ and $\mu = -1$, the former case corresponding to the unperturbed system.

What does stabilization of fixed points mean in terms of complex analytic dynamics? An unstable fixed point is contained in the Julia set. The goal of stabilization is to turn this fixed point into a stable one, i.e., so that it now belongs to a bounded Fatou component. In other words, the transformation should deform the Julia set in such a way that it does not contain the targeted periodic point anymore.

Let us consider the logistic map for $r = 4$ in more detail. The Julia set $J(\ell_{r=4}) = I$ is equal to the whole unit interval. The probability distribution m is given by a beta distribution with both parameters equal to $\frac{1}{2}$ (see, for example, [27]), i.e., with probability density function

$$p(x) = \left(\pi x^{\frac{1}{2}}(1-x)^{\frac{1}{2}}\right)^{-1}.$$

Suppose $M_k = \mathrm{id}$ and μ is small enough. Now $z^* = \frac{3}{4}$ is the stabilized fixed point. In the previous section we calculated the maximum size of the ball around the fixed point for which the adaptation method works straight away. This radius is given by $\varepsilon < \frac{1}{8}$

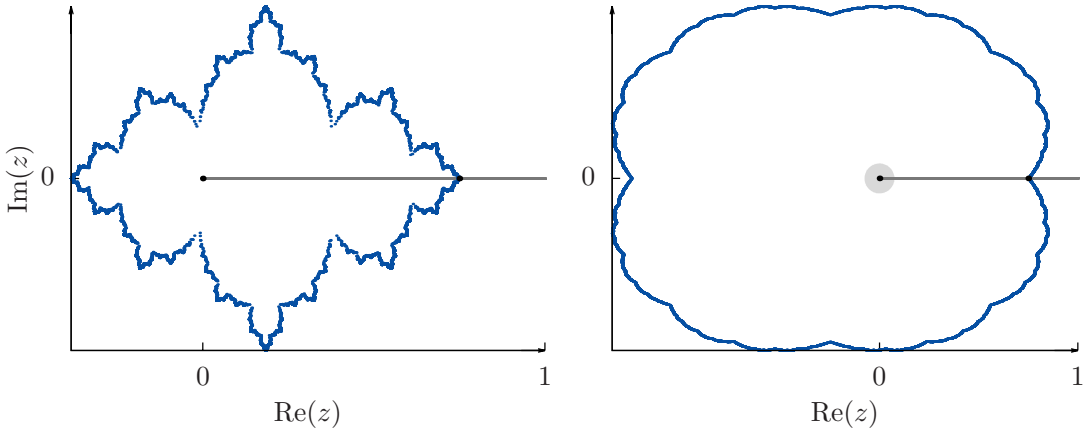

Figure 2.5.: Julia sets for parameters $\mu = -0.65$ (left) and $\mu = -0.2$ (right) for $M_k = \mathrm{id}$. The Julia set of $g_{\mu,4}$ is depicted in blue, whereas the Julia set of the original map, i.e., the unit interval, is depicted in gray. The fixed points $z^* = 0$ and $z^* = \frac{3}{4}$ are marked by black dots. Shaded circles indicate $B(\varepsilon, z^*)$ for $\mu_0 = \mu$.

and

$$P_0 = m(V_0) \leq m(B(\varepsilon, z^*) \cap I) = m\left(\left[\frac{5}{8}, \frac{7}{8}\right]\right) = \int_{\frac{5}{8}}^{\frac{7}{8}} \frac{\mathrm{d}x}{\pi x^{\frac{1}{2}}(1-x)^{\frac{1}{2}}}$$
$$= \frac{2}{\pi}\left(\arctan\left(\sqrt{\frac{3}{5}}\right) - \operatorname{arccot}\left(\sqrt{7}\right)\right) \approx 0.1895.$$

In Figure 2.4, one can see that the whole unit interval is contained in the bounded Fatou component. Backward iteration takes this set closer to the boundary of this Fatou component. For μ_0 small, we therefore have

$$\varphi(\mu_0) = 1,$$

$P_0 \leq P_k = m(V_k) \leq 1$, and $\hat{\varphi} = 1$. This means that the whole unit interval I is contained in the basin of attraction of the stabilized fixed point. In other words, for an initial condition distributed on I according to the distribution m, the orbit will converge to the stabilized periodic point with probability one.

The picture is slightly different for $M_k = -\mathrm{id}$ and μ small enough. Now, $z^* = 0$ is the stabilized fixed point. Again we have $\varepsilon < \frac{1}{8}$ and therefore

$$P_0 = m(V_0) \leq m(B(\varepsilon, z^*) \cap I) = m\left(\left[0, \frac{1}{8}\right]\right) = \int_{0}^{\frac{1}{8}} \frac{\mathrm{d}x}{\pi x^{\frac{1}{2}}(1-x)^{\frac{1}{2}}}$$
$$= \frac{2}{\pi}\operatorname{arccot}\left(\sqrt{7}\right) \approx 0.2301.$$

In this case backward iteration yields a different result, as can be seen in Figure 2.5. Part of the set of initial conditions I is in the basin of attraction of infinity, and

the intersection with the Julia set is exactly the fixed point $z^* = \frac{3}{4}$. Therefore, the probability of convergence with a random initial condition distributed on I according to m is less than one. Integrating the probability density function gives

$$\varphi(\mu_0) = \int_0^{\frac{3}{4}} \frac{\mathrm{d}x}{\pi x^{\frac{1}{2}}(1-x)^{\frac{1}{2}}} = \frac{2}{3}.$$

Therefore, we have $\hat{\varphi} = \frac{2}{3}$ and $P_0 \leq m(V_k) \leq \frac{2}{3}$. In contrast to the case $M_k = \mathrm{id}$, this means that for $M_k = \mathrm{id}$ and $z^* = 0$ a trajectory with an initial condition on I distributed according to m will diverge with a probability of one-third.

When considering higher periods of such a polynomial map, the Julia sets are more complicated as the degree of the iterated polynomial rises exponentially with increasing period. The situation changes qualitatively when considering the Predictive Feedback Control dynamics of higher-dimensional maps $f : \mathbb{R}^N \to \mathbb{R}^N$ by interpreting them as functions $f : \mathbb{C}^N \to \mathbb{C}^N$. In general, the dynamics of holomorphic, higher-dimensional maps are more diverse since even low-dimensional invertible maps give rise to rich dynamics [52].

2.4. Numerical Results

To compare the speed of the adaptive method (ACC) with the original PFC chaos control in a real-world application, we performed numerical simulations for the logistic map ℓ_4. The results for $M_k = \mathrm{id}$, $\mu_0 \in [0, 1]$, and periods one and two are summarized in Figure 2.6. One can clearly see that for most initial values of the control parameter, the adaptive method yields an increase in convergence speed. The results for $M_k = -\mathrm{id}$ and period one are similar, but the convergence probability is lower (not shown) in accordance with the results of the previous section; cf. Figure 2.5. There is only one orbit of period $p = 2$ which is stabilized for $\mu > 0$. Thus, when attempting to stabilize a period two orbit for $\mu < 0$, trajectories will converge to one of the fixed points. A nonoptimized, ad hoc choice of parameters for the adaptive method of $K = 8$ and $L_0 = 0.99$ (independent of the initial condition) was employed in the simulations. The criterion for convergence time T was given by $|x_T - x_{T-1}| \leq 10^{-10}$. Reliability was determined after convergence by checking for the correct (targeted) period.

The convergence reliability, i.e., the fraction of trials where the above criterion is fulfilled after some time T, is not improved by the adaptive method. However, it is possible to amend the adaptation method to lead to convergence for most initial conditions x_0 within the convergent regime, independent of the initial value of the control parameter μ_0 (the modified method is denoted by ACCD). When adapting, the ACC method has to check whether Criterion (2.6a) is fulfilled. If this is not the case after R iterations, the modified method simply scales μ by a certain factor $v < 1$. To prevent μ from becoming too small, we impose a threshold $\theta > 0$ below which μ cannot decay. In other words, the modified method ACCD will automatically decrease μ towards zero to reach the convergence regime if Inequality (2.6a) is not satisfied within a given number of steps.

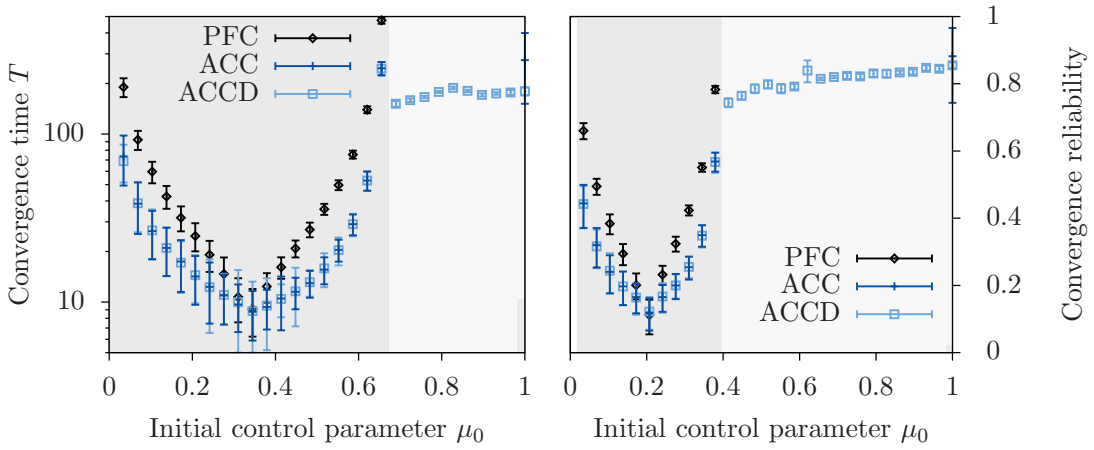

Figure 2.6.: Speed and reliability comparison of the original PFC chaos control ($\mu = \mu_0$ fixed) and both ACC and ACCD for the logistic map ℓ_4 with $p = 1$ (left) and $p = 2$ (right). Times are plotted only if more than 1% of initial values lead to convergence to the correct period. Gray shading indicates the convergence reliability; dark gray corresponds to all methods converging, and light gray to the reliability of ACCD. Convergence time T is given by $|x_T - x_{T-1}| \leq 10^{-10}$ calculated for 1000 random initial conditions after a transient of random length.

The modified method ACCD behaves like the original ACC method for initial values of μ_0 in the convergent regime while leading to convergence outside of it; cf. Figure 2.6 (here $R = 50$, $v = 0.7$, $\theta = 0.1$ for period $p = 1$, and $\theta = 0.05$ for period $p = 2$). Failure of convergence that is due to the existence of a range of diverging initial conditions, however, will persist, even with the decay. The results are similar for a broad parameter range (e.g., decay rate $v \in [0.65, 0.99]$ and decay kick-in time $R \in [10, 100]$). For a decay rate too close to one or a too large decay kick-in time, it will take many iterations to reach the convergent interval. On the other hand, if the decay kick-in time is too small or does not exist at all, the sequence of control parameters μ_k decreases even if it is in the convergent interval as Inequality (2.6a) is not fulfilled all the time, unnecessarily increasing convergence time.

2.5. Discussion

In this chapter, we presented an adaptive method to optimize the control parameter of Predictive Feedback Control for optimal convergence speed. Since Predictive Feedback Control provides a one-parameter control scheme to stabilize periodic orbits, which is noninvasive and easy to implement, the addition of adaptation retains the advantages of the control method. In contrast to ad hoc or heuristic adaptation methods, we prove that our adaptive method leads to convergence to a periodic orbit. Adaptive Predictive Feedback Control ensures convergence in a neighborhood of a periodic orbit which was stabilized by the PFC transformation. Assuming the existence of an ergodic invariant

measure on the chaotic set, one obtains a bound on the probability of convergence if control is switched on at an arbitrary point in time. Such an estimate does not only reveal some global features of the dynamics and the control method as will be discussed below, but is also useful for applications. The logistic family provided an example for which the adaptation parameters may be calculated explicitly. Note that even though these results are stated in the framework of discrete time dynamical systems, they may also be applied to stabilizing continuous time systems after discretization such as taking Poincaré sections.

Our method was stated in the general context of "chaotic sets." In general, such sets do not need to be local or even global attractors of the dynamical system. In fact, the Julia sets considered in the example are repelling rather than attracting. In applications, however, an attractor would be desirable such that the process of stabilization becomes repeatable. That is, after the control perturbation is turned off by choosing the appropriate value for the control parameter, the dynamics would return to the attractor and the process could be started over again.

Apart from its importance for the adaptive algorithm, the probabilities given in Section 2.2 reveal information about the chaos control method itself. It allowed us to calculate the size of the basin of attraction for varying μ in our example. Decreasing μ always leads to slower convergence since the eigenvalues approach one as $\mu \to 0$. So is it possible to find an optimal μ_0 for a given map? Since any adaptation method increases the computational cost of the chaos control method, a priori estimates of such crucial quantities are of importance. Furthermore, the choice of the stabilization matrix M_k depends on the type of fixed points in the chaotic attractor. Hence, global statistics for a given map f of the periodic orbits and their stability properties might yield some a priori estimates.

Our numerical studies of the logistic family suggest that it is possible to get reliable convergence without a priori knowledge of the exact values for the parameters. A slight modification of the method yields a hybrid method that finds the regime of control parameter in which the dynamics converge online before adapting the parameter to the optimal value. This simplification, however, comes at a cost in convergence speed. By definition, PFC cannot distinguish between periodic orbits of periods p and q if q is a divisor of p. Our numerical calculations, however, indicate that this does not influence reliability of the chaos control method. This is most likely caused by the exponential growth of the number of periodic orbits. In the future, it would be desirable to add a mechanism that rigorously distinguishes between the target period and its divisors to prove optimal convergence.

An adaptation method for chaos control is a step towards solving the intuitively contradictory problem of optimizing speed while maintaining simplicity in the implementation of the control. By leaving the actual control method unchanged, however, one may optimize convergence speed only within the inherent limitations of the control scheme. What is the best convergence speed that may be achieved by using adaptation? It turns out that the restrictions imposed by Predictive Feedback Control are rather severe. In particular, the increasing instability of periodic orbits of higher peri-

ods lead to a slowdown in optimal convergence speed. This problem will be addressed in the following chapter.

3. Stalling Predictive Feedback Control

We have seen that Predictive Feedback Control [26, 86] is well suited for applications. It requires little to no prior knowledge about the system to be controlled, it is non-invasive (i.e., control strength vanishes upon convergence) and it is very easy to implement due to the nature of the control transformation which is determined by a prediction about the future state of the system. It hence overcomes some of the shortcomings of, for example, the control method proposed by Ott, Grebogi, and Yorke [79]. The speed of convergence to a stabilized fixed point depends on the control parameter of Predictive Feedback Control. In the previous chapter, it was shown that this control parameter can be tuned online for optimal convergence speed, which means that in the best case the control parameter converges to the value for which the highest asymptotic convergence speed is achieved.

But how fast is the best asymptotic convergence speed actually? It turns out that for a given fixed point the convergence speed at the optimal value of the control parameter strongly depends on the local stability properties of the fixed point. In particular, the larger the absolute value of the eigenvalue corresponding to the strongest repelling direction, the slower the asymptotic convergence speed becomes even when the control parameter is chosen optimally. Considering that unstable periodic orbits in chaotic attractors typically become more and more unstable with increasing period [22], this implies that Predictive Feedback Control suffers from an inherent "speed limit" as convergence to periodic orbits of larger period becomes slower and slower. For applications this implies that stabilization of highly unstable periodic orbits is difficult. In particular, any method optimizing speed within the PFC framework, for instance the adaptation presented in Chapter 2, is therefore subject to the same limitation.

In this chapter we introduce Stalled Predictive Feedback Control (SPFC), an extension of Predictive Feedback Control, which can overcome this "speed limit" while maintaining most of the advantages of Predictive Feedback Control. We derive conditions for the local stability properties of periodic orbits that imply stabilizability and evaluate them for some specific examples. Furthermore, we propose an adaptation mechanism that is capable of tuning the control parameter online to the regime where convergence can take place and converging to the value for best asymptotic convergence speed. The resulting adaptive SPFC is an easy-to-implement, non-invasive, and broadly applicable chaos control method that stabilizes even periodic orbits of large periods reliably without the need to fine-tune parameter values.

This chapter extends work recently submitted for publication [12] and is organized as follows. In the next section, we adapt the notation from the previous chapter and illustrate the limitations of Predictive Feedback Control. In the second section, Stalled Predictive Feedback Control is defined and we identify regimes in parameter space in

which stabilization is successful. In Section 3.3, we apply our algorithm to some maps with chaotic dynamics and calculate and compare convergence speeds across different control methods. Adaptive methods for the control parameter are explored in Section 3.4 before giving some concluding remarks.

3.1. Limitations of Predictive Feedback Control

In this section, we adapt the notation from Section 2.1 in order to be more explicit about the period dependency and discuss the limitations of Predictive Feedback Control. Suppose that $f : \mathbb{R}^N \to \mathbb{R}^N$ is a chaotic map, i.e., f is differentiable and its iteration given by the evolution equation $x_{k+1} = f(x_k)$ gives rise to a set $A \subset \mathbb{R}^N$ with a dense set of unstable periodic orbits. Recall that $\mathrm{Fix}(f) = \{x^* \in \mathbb{R}^N \mid f(x^*) = x^*\}$ is the set of fixed points of f and id the identity map on $\mathbb{R}^N$. The main result motivating Predictive Feedback Control, Proposition 2.1.3 in the previous chapter, can be restated as follows.

Proposition 3.1.1. *Suppose that* $\mathrm{Fix}^*(f) \subset \mathrm{Fix}(f)$ *is the set of fixed points for which both* $\mathrm{d}f|_{x^*}$ *and* $\mathrm{d}f|_{x^*} - \mathrm{id}$ *are nonsingular and diagonalizable (over* $\mathbb{C}$*). For some matrix* $M \in \mathbb{R}^{N\times N}$ *let* $\mathrm{Fx}(f, M) \subset \mathrm{Fix}^*(f)$ *denote the set of fixed points such that for each* $x^* \in \mathrm{Fx}(f, M)$ *there exists* $\mu \in (0, 1)$ *for which* x^* *is a stable fixed point of the map* $g_{\mu,1}$ *obtained by the transformation*

$$S(\mu, M) : f \mapsto \mathrm{id} + \mu M(f - \mathrm{id}) = g_{\mu,1}. \tag{3.1}$$

There exist finitely many orthogonal matrices M_k *with* $k = 1, \ldots, K$ *such that*

$$\mathrm{Fix}^*(f) = \bigcup_{k=1}^{K} \mathrm{Fx}(f, M_k).$$

Write $f_p := f^{\circ p}$ for the pth iterate of f where $p \in \mathbb{N}$. Again, we use the terms fixed point and periodic orbit interchangeably depending on what is convenient in the context. Define the set of periodic orbits of minimal period p as $\mathrm{Fix}(f, p) = \{\, x^* \in \mathrm{Fix}(f_p) \mid f^{\circ q}(x^*) \neq x^* \text{ for } q < p \,\}$. Furthermore, define $\mathrm{Fix}^*(f, p) = \mathrm{Fix}(f, p) \cap \mathrm{Fix}^*(f_p)$ and

$$\mathrm{Fix}^*_g(f, p) := \mathrm{Fix}^*(f, p) \cap \left(\mathrm{Fx}(f_p, \mathrm{id}) \cup \mathrm{Fx}(f_p, -\mathrm{id})\right).$$

Predictive Feedback Control is a consequence of Proposition 3.1.1 when f is being replaced by f_p; cf. Chapter 2.

Corollary 3.1.2. *Let* $p \in \mathbb{N}$*. For every* $x^* \in \mathrm{Fix}^*_g(f, p)$ *there exists a* $\mu \in (-1, 1)$ *such that* x^* *is a stable fixed point of the Predictive Feedback Control method given by the iteration*

$$x_{k+1} = g_{\mu,p}(x_k) := f_p(x_k) + \eta(x_k - f_p(x_k))$$

with $\eta = 1 - \mu$ *and control perturbation* $c_{\mu,p}(x) = \eta\,(x_k - f_p(x_k))$.

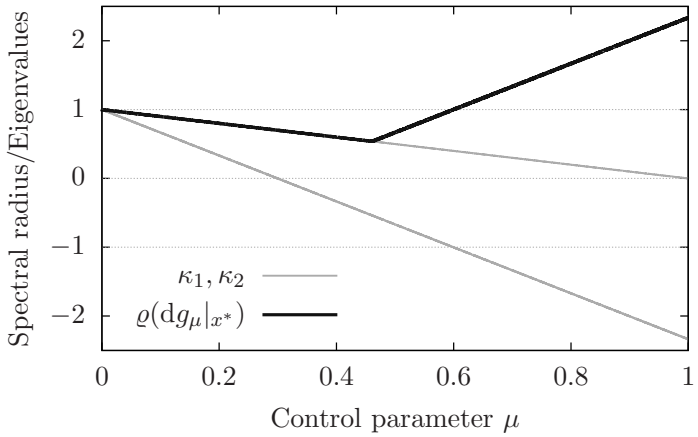

Figure 3.1.: The local stability properties around a "typical" periodic orbit of the two-dimensional system (3.4) of the controlled system depend (piecewise) linearly on the control parameter μ.

The elements of $\mathrm{Fix}^*_g(f,p)$ are referred to as *PFC-stabilizable* periodic orbits of period p. The cardinality of the set $\mathrm{Fix}^*_g(f,p)$ depends on the chaotic map f and contains roughly half of the periodic orbits of a given period in two-dimensional systems [84, 93].

Since the function $g_{\mu,p}$ is a linear interpolation between f_p and id in the space of differentiable functions, the derivative of $g_{\mu,p}$ at $x \in \mathbb{R}^N$ is given by (2.2),

$$\mathrm{d}g_{\mu,p}|_x = \mathrm{id} + \mu(\mathrm{d}f_p|_x - \mathrm{id}).$$

Fix a point $x^* \in \mathrm{Fix}^*(f,p)$. Suppose that λ_j denote the eigenvalues of $\mathrm{d}f_p|_{x^*}$ where $j = 1,\ldots,N$. The local stability of g_μ at x^* is readily computed; the eigenvalues of $\mathrm{d}g_{\mu,p}|_{x^*}$ are

$$\kappa_j(\mu) = 1 + \mu(\lambda_j - 1) \tag{3.2}$$

for $j = 1,\ldots,N$. Hence, we have $x^* \in \mathrm{Fix}^*_g(f,p)$ iff there exists a $\mu_0 \in (-1,1)$ such that the spectral radius $\varrho(\mathrm{d}g_{\mu_0,p}|_{x^*}) = \max_{j=1,\ldots,N} |\kappa_j(\mu_0)|$ is smaller than one. In particular, for a two-dimensional system these are the periodic orbits of saddle type with local dynamics given by the eigenvalues $\lambda_1 \in (-1,1)$ and $\lambda_2 < -1$ [84]. The dependency of the local stability properties on the control parameter μ and the resulting spectral radius for a typical periodic orbit is depicted in Figure 3.2. Note that optimal convergence speed is achieved for the value of μ that corresponds to the minimal spectral radius.

The crucial observation now is that convergence speed becomes increasingly slow for increasing instability. Suppose that x^* is a PFC-stabilizable fixed point of a two-dimensional system with stability determined by λ_1, λ_2 as above, we have

$$\inf_{\{\,\mu \mid \varrho(\mathrm{d}g_{\mu,p}|_{x^*})<1\,\}} \varrho\left(\mathrm{d}g_{\mu,p}|_{x^*}\right) \to 1 \quad \text{as} \quad \lambda_2 \to -\infty.$$

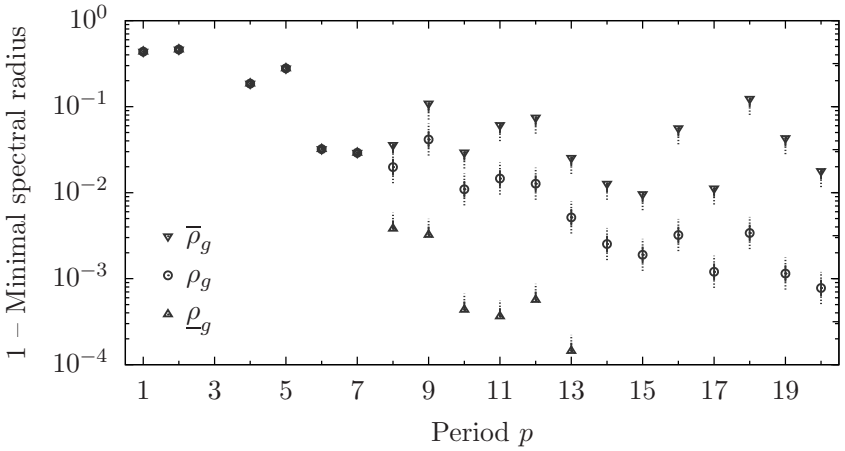

Figure 3.2.: Best, average, and worst asymptotic convergence speed for periodic orbits of the two-dimensional map (3.4) approach one exponentially with increasing period p.

The same argument holds in higher dimensions if the fixed point to stabilize has both repelling and attracting directions. As the periodic orbits become increasingly unstable on average for large periods [22], asymptotic convergence speed decreases. Let $\varrho^g_{\min}(x^*) = \inf_\mu \varrho(\mathrm{d}g_{\mu,p}|_{x^*})$ denote the spectral radius of the linearization at a periodic orbit x^* for the optimal parameter value and card the cardinality of a set. The slowdown can be explicitly calculated by evaluating the functions

$$\overline{\rho}_g(p) = 1 - \min_{x^* \in \mathrm{Fix}^*_g(f,p)} \varrho^g_{\min}(x^*), \tag{3.3a}$$

$$\rho_g(p) = 1 - \frac{1}{\mathrm{card}(\mathrm{Fix}^*_g(f,p))} \sum_{x^* \in \mathrm{Fix}^*_g(f,p)} \varrho^g_{\min}(x^*), \tag{3.3b}$$

$$\underline{\rho}_g(p) = 1 - \max_{x^* \in \mathrm{Fix}^*_g(f,p)} \varrho^g_{\min}(x^*), \tag{3.3c}$$

that correspond to the best, average, and worst asymptotic convergence speed for all periodic orbits of a given period respectively.

Remark 3.1.3. Note that all convergence times and speeds for a period p orbit presented in this chapter are scaled to evaluations of f_p. Therefore, with respect to the number of evaluations of the map f, one has to keep in mind that they increase linearly with increasing period.

Suppose that $l_{11} = -22, l_{12} = 5.9, l_{21} = -6.6$, and $l_{22} = 0$ and define the sigmoidal function $\sigma(x) = (1 + \exp(-x))^{-1}$. Consider the map $f : \mathbb{R}^2 \to \mathbb{R}^2$ given by

$$f(x_1, x_2) = (l_{11}\sigma(x_1) + l_{12}\sigma(x_2) - 3.4, l_{21}\sigma(x_1) + l_{22}\sigma(x_2) + 3.8). \tag{3.4}$$

Iteration of this map describes the evolution of a two-dimensional neuromodule and gives rise to a chaotic attractor [80]. The values of the functions (3.3) are depicted in

Figure 3.2. One can clearly see that even the lower bound on asymptotic convergence speed for the PFC method, corresponding to the smallest spectral radius as determined by $1 - \overline{\rho}_g$, approaches one on average for increasing periods.

3.2. Stalled Predictive Feedback Control

Is there a method that is capable of stabilizing highly unstable periodic orbits while maintaining the advantages of Predictive Feedback Control? The main result presented in this chapter is that the origin of the slowdown motivates a modified chaos control method. In this section we introduce Stalled Predictive Feedback Control and study the local stability of unstable periodic orbits with respect to this method. By looking at the geometry of the local dynamics, one obtains an intuitive explanation for the increased performance of the new control method.

Stalled Predictive Feedback Control provides an extension of standard Predictive Feedback Control which is capable of overcoming this speed limit. Define $\psi^{\circ 0} := \mathrm{id}$ for a map ψ.

Definition 3.2.1. *Suppose that the iteration of $F : \mathbb{R}^N \to \mathbb{R}^N$ defines a dynamical system. For $M_k \in \{\pm \mathrm{id}\}$ and $\mu \in \mathbb{R}$ let $S(\mu, M_k)(F) = \mathrm{id} + \mu M_k(F - \mathrm{id}) =: G_\mu$ denote the map obtained by applying the Predictive Feedback Control transformation; cf. Proposition 3.1.1. For parameters $m, n \in \mathbb{N}_0 = \mathbb{N} \cup \{0\}$ and $\mu \in \mathbb{R}$, the iteration of*

$$H_\mu^{(m,n)} = (F)^{\circ n} \circ (G_\mu)^{\circ m} . \tag{3.5}$$

is referred to as Stalled Predictive Feedback Control.

Remark 3.2.2. The function $H_\mu^{(m,n)}$ defined above stalls Predictive Feedback Control in the following sense. In the PFC method, the control signal is applied at every point in time. By iterating $H_\mu^{(m,n)}$ we "stall" the application of the control perturbation by adding extra evaluations of the original, uncontrolled map F.

For the rest of this chapter, we adopt the period-dependent notation of the previous section where the uncontrolled dynamics were given by iterating $f : \mathbb{R}^N \to \mathbb{R}^N$. Stalled Predictive Feedback Control is given by the iteration of

$$h_{\mu,p} = h_{\mu,p}^{(m,n)} := (f_p)^{\circ n} \circ (g_{\mu,p})^{\circ m} , \tag{3.6}$$

where $m, n \in \mathbb{N}_0$ are the parameters. By definition, we have $h_{\mu,p}^{(0,1)} = f_p$ and we recover the original PFC method for $h_{\mu,p}^{(1,0)} = g_{\mu,p}$. In general, we will omit the superscript (m, n) unless the choice is important.

Local Stability of Periodic Orbits for $h_{\mu,p}$

The local stability properties of $h_{\mu,p}$ can be calculated from f_p and $g_{\mu,p}$. By definition we have $\mathrm{Fix}(f_p) \subset \mathrm{Fix}(h_{\mu,p})$. Suppose that $x^* \in \mathrm{Fix}^*(f, p)$ and the eigenvalues of $\mathrm{d}f_p|_{x^*}$

are given by λ_j where $j = 1, \ldots, N$. Note that the eigenvectors of $\mathrm{d}g_{\mu,p}|_{x^*}$ and $\mathrm{d}f_p|_{x^*}$ are the same. Hence, the local stability properties of $h_{\mu,p}$ are readily computed from the λ_j and the local stability properties of the PFC transformed map $g_{\mu,p}$ as given by (3.2). The eigenvalues of the Jacobian of $h_{\mu,p}$ at x^* evaluate to

$$\Lambda_j = \lambda_j^n \kappa_j(\mu)^m = \lambda_j^n \left(1 + \mu(\lambda_j - 1)\right)^m$$

for $j = 1, \ldots, N$. Hence, local stability at x^* is given by the spectral radius

$$\varrho(\mathrm{d}h_{\mu,p}|_{x^*}) = \max_{j=1,\ldots,N} |\Lambda_j| .$$

If all eigenvalues are of modulus smaller than one, the fixed point x^* is stable for $h_{\mu,p}$.

Definition 3.2.3. *A periodic orbit $x^* \in \mathrm{Fix}^*(f,p)$ is called SPFC-stabilizable if there are parameters $m, n \in \mathbb{N}_0$ and $\mu \in (-1, 1)$ such that*

$$\varrho(\mathrm{d}h_{\mu,p}^{(m,n)}|_{x^*}) < 1.$$

Let $\mathrm{Fix}_h^*(f,p)$ denote the set of SPFC-stabilizable periodic orbits, and, clearly,

$$\mathrm{Fix}_g^*(f,p) \subset \mathrm{Fix}_h^*(f,p),$$

that is every PFC-stabilizable periodic orbit is also SPFC-stabilizable.

To compare the "performance" of Stalled Predictive Feedback Control with that of original Predictive Feedback Control we have to rescale the stability properties. Since $h_{\mu,p}^{(m,n)}$ contains $n + m$ evaluations of f_p we take the $(m+n)$th root to obtain functions

$$\hat{l}_j(m, n, \mu) = \left| \lambda_j^n \left(1 + \mu(\lambda_j - 1)\right)^m \right|^{\frac{1}{m+n}},$$

where $j = 1, \ldots, N$. With the parameter $\alpha = \frac{n}{m+n}$ we thus obtain an equivalent set of functions

$$l_j(\alpha, \mu) = |\lambda_j|^{\alpha} \left|(1 + \mu(\lambda_j - 1))\right|^{1-\alpha} \tag{3.7}$$

for $j = 1, \ldots, N$ which determine the local stability properties of $h_{\mu,p}$ rescaled to a single evaluation of f_p. Conversely, for any rational $\alpha \in [0, 1] \cap \mathbb{Q}$ we obtain a pair (m, n). In the following, we refer to both α and m, n as *stalling parameters*, depending what is convenient in the context. When using the stalling parameter α, we may also write $h_{\mu,p}^{\alpha}$.

Rescaled local stability of Stalled Predictive Feedback Control for a given periodic orbit $x^* \in \mathrm{Fix}^*(f,p)$ of period p is hence determined by the *stability function*

$$\varrho_{x^*}(\alpha, \mu) = \max_{j=1,\ldots,N} l_j(\alpha, \mu). \tag{3.8}$$

In comparison to the original Predictive Feedback Control, Stalled Predictive Feedback Control depends on two parameters: the control parameter μ and the stalling parameter α.

Conditions for Stabilizability

To derive conditions for SPFC-stabilizability, consider some general properties of functions of type (3.7). Fix $w \in \mathbb{C}^\times := \mathbb{C}\setminus\{0\}$. Let $\mathbf{S}^1 := \{\, z \in \mathbb{C} \mid |z| = 1 \,\} = \mathbb{R}/2\pi\mathbb{Z}$ denote the unit circle. We will choose a realization to describe elements of $\mathbf{S}^1$ depending on what is convenient in the context. Consider the function $L_w : \mathbb{R}^2 \to \mathbb{R}$ given by

$$L_w(\alpha, \mu) := |w|^\alpha \, |1 + \mu(w-1)|^{1-\alpha}\,.$$

By definition, we have $L_w(0,0) = 1$ and in a sufficiently small open ball V around $(0,0)$ the function L_w is differentiable and the derivative is bounded away from zero. Hence, in this ball the curve defined by

$$V_0 := \{\, (\alpha,\mu) \in V \mid L_w(\alpha,\mu) = 1 \,\}$$

is a one-dimensional submanifold of $\mathbb{R}^2$. If V is chosen small enough, it may be written as a disjoint union

$$V = V_0 \cup V_+ \cup V_-$$

where $V_+ = \{\, (\alpha,\mu) \in V \mid L_w(\alpha,\mu) > 1 \,\}$ and $V_- = \{\, (\alpha,\mu) \in V \mid L_w(\alpha,\mu) < 1 \,\}$.

The goal is to get a linearized description close to the origin. Let grad denote the gradient and $\langle\,\cdot\,,\cdot\,\rangle$ the usual Euclidean scalar product. Define the line

$$\gamma(w) = \Big\{\, x \in \mathbb{R}^2 \;\Big|\; \langle \operatorname{grad}(L_w)|_{(0,0)}, x\rangle = 0 \,\Big\} \tag{3.9}$$

which is tangent to V_0 at the origin. Let

$$\mathcal{H} := \{x \in \mathbb{R}^2 \mid \langle \operatorname{grad}(L_w)|_{(0,0)}, x\rangle < 0\}$$

denote one of the half planes defined by the line $\gamma(w)$. Moreover, the sets $Q_j := (\frac{(j-1)\pi}{2}, \frac{j\pi}{2})$ denote the open segments of $\mathbf{S}^1$ that lie in one of the four quadrants of $\mathbb{R}^2$.

Definition 3.2.4. *Suppose that $w \in \mathbb{C}^\times$. The connected subset $C_w := \mathcal{H} \cap \mathbf{S}^1$ is called the domain of stability of w. For a tuple $\tilde{w} = (w_1, \ldots, w_N) \in (\mathbb{C}^\times)^N$ define the domain of stability to be*

$$C_{\tilde{w}} := \bigcap_{j=1}^{N} C_{w_j}. \tag{3.10}$$

If $C_{\tilde{w}} \cap \overline{(Q_1 \cup Q_4)} \neq \emptyset$ then the tuple $\tilde{w}$ is called stabilizable.

In a sufficiently small neighborhood $U \subset V$ of the origin, the "linearized" version of V_- is given by the set $\mathcal{H} \cap U$.

Lemma 3.2.5. *If the domain of stablity C_w of a tuple $w = (w_1, \ldots, w_N) \in (\mathbb{C}^\times)^N$ is nonempty then there exist (μ_0, α_0) such that $L_{w_j}(\mu_0, \alpha_0) < 1$ for all $j = 1, \ldots, N$. If the tuple w is stabilizable then then α_0 may be chosen such that $\alpha_0 \geq 0$.*

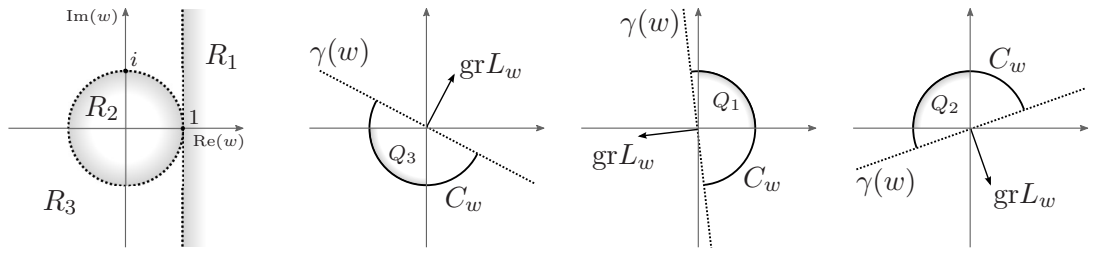

(a) Parameter $w \in \mathbb{C}$ (b) $w \in R_1$ (c) $w \in R_2$ (d) $w \in R_3$

Figure 3.3.: Stabilizability regions for $w \in \mathbb{C}$ are shown in Panel (a) and the corresponding domains of stability C_w, as given by (3.10), for each R_k in Panels (b)–(d). Here, we use the abbreviation $\mathrm{gr}L_w = \mathrm{grad}(L_w)|_{(0,0)}$.

Proof. Suppose that V_- and $\mathcal{H}$ are defined as above. Because of continuity, for every $w \in \mathbb{C}^\times$ there exists an open ball $B_w \subset V_- \cap \mathcal{H}$ that is tangent to the origin. If a tuple $\tilde{w} = (w_1, \ldots, w_N)$ has nonempty domain of stability $C_{\tilde{w}}$ then

$$B := \bigcap_{j=1}^{N} B_{w_j} \neq \emptyset.$$

By construction, any $(\mu_0, \alpha_0) \in B$ has the desired property.

If in addition w is stabilizable then the intersection $B \cap \{\, (x,y) \in \mathbb{R}^2 \mid x \geq 0 \,\}$ is not empty. This proves the second assertion. □

The domain of stability is determined by the gradient of L_w at the origin. Let ln denote the (real) natural logarithm. We have $\mathrm{grad}(L_w)|_{(0,0)} = (\ln|w|, \mathrm{Re}(w) - 1)$. Define

$$\begin{aligned} R_1 &:= \{\, z \in \mathbb{C} \mid \mathrm{Re}(z) > 1 \,\}, \\ R_2 &:= \{\, z \in \mathbb{C} \mid |z| < 1 \,\}, \\ R_3 &:= \{\, z \in \mathbb{C} \mid |z| > 1,\ \mathrm{Re}(z) < 1 \,\}. \end{aligned}$$

These regions are sketched in Figure 3.3(a). If $w \in R_1$ then $\|\mathrm{grad}(L_w)|_{(0,0)}\|^{-1} \cdot \mathrm{grad}(L_w)|_{(0,0)} \in Q_1$ and therefore $Q_3 \subset C_w$. Similarly, if $w \in R_2$ then $Q_1 \subset C_w$ and if $w \in R_3$ then $Q_2 \subset C_w$ (Figure 3.3(b)–(d)). For w on the boundary of the R_k the gradient lies on one of the coordinate axes and we obtain similar conditions.

These observations have implications for stabilizability for a tuple $(w_1, \ldots, w_N)$: if for any fixed $k \in \{1,2,3\}$ all $w_j \in R_k$ for $j = 1, \ldots, N$ then the tuple is stabilizable. Furthermore, if either $w_j \in R_1 \cup R_3$ or $w_j \in R_2 \cup R_3$ for all $j = 1, \ldots, N$ then the tuple is stabilizable. For any other combination the condition of stabilizability is more difficult; in two dimensions linear dependence of the gradients tells us for (w_1, w_2) with $w_1 \in R_1$ and $w_2 \in R_2$ the tuple is stabilizable iff

$$\ln(|w_2|)\,\mathrm{Re}(w_1) \neq \ln(|w_1|)\,\mathrm{Re}(w_2). \tag{3.11}$$

Note that this condition is satisfied for a set of zero Lebesgue measure.

Remark 3.2.6. Note that stabilizability is not affected by taking the complex conjugate. Hence, conjugate complex numbers have the same stabilizability properties.

For $w = 0$ the function L_0 has a discontinuity at $\alpha = 0$. In case $\alpha > 0$ we have $L_0(\alpha, \mu) = 0$ and for $\alpha = 0$ and $\mu \in (-1, 1)$ we have $L_0(0, \mu) = 1 - \mu$. Therefore, define the domain of stabilizability of zero to be $C_0 = \{0, \frac{\pi}{2}\} \cup Q_1 \cup Q_4$. For $\alpha > 0$, stabilizability of a tuple with one component equal to zero may be reduced to stabilizability of the "reduced" tuple where the zero entry is omitted.

With the notation as above, we are now able to relate these general results to the local stability properties of a given periodic orbit.

Definition 3.2.7. *Suppose that $x^* \in \mathrm{Fix}^*(f, p)$ is a periodic orbit of f and suppose that the eigenvalues of $\mathrm{d}f_p|_{x^*}$ are given by λ_j with $j = 1, \ldots, N$. The periodic orbit is called locally stabilizable if the tuple $\lambda = (\lambda_1, \ldots, \lambda_N)$ is stabilizable as a tuple, as defined in Definition 3.2.4.*

This definition links the notion of stabilizability of a tuple defined above and the local dynamics close to a periodic orbit. Recall the notion of uniform hyperbolicity [56]. Suppose that a differentiable function f defines a discrete time dynamical system on $\mathbb{R}^N$. We call an f-invariant set $A \subset \mathbb{R}^N$ hyperbolic if for every $x \in A$ no eigenvalue of $\mathrm{d}f|_x$ is of absolute value one; refer to the Outlook for a more detailed discussion of hyperbolicity.

Proposition 3.2.8. *Suppose that the chaotic map $f : \mathbb{R}^N \to \mathbb{R}^N$ gives rise to a hyperbolic attractor and for $x^* \in \mathrm{Fix}^*(f, p)$ let $\lambda = (\lambda_1, \ldots, \lambda_N)$ denote the eigenvalues of $\mathrm{d}f_p|_{x^*}$. If x^* is locally stabilizable then x^* is SPFC-stabilizable. Moreover, if the domain of stability C_λ satisfies*

$$\left\{\frac{\pi}{2}, \frac{3\pi}{2}\right\} \cap C_\lambda \neq \emptyset$$

then x^* is PFC-stabilizable.

Proof. If a periodic orbit x^* is locally stabilizable, then tuple λ is stabilizable. Thus, according to Lemma 3.2.5, there are parameters (α_0, μ_0) such that $L_{\lambda_j}(\alpha_0, \mu_0) < 1$ for all $j = 1, \ldots, N$ simultaneously. Recall that local stability of $h^{\alpha_0}_{\mu_0, p}$ at x^* is given by $l_j(\alpha, \mu) = L_{\lambda_j}(\alpha, \mu)$ according to Equation (3.7). Therefore, local stability of a periodic orbit is equivalent to the existence of parameters (α_0, μ_0) with $\alpha_0 \geq 0$ and

$$\varrho(\mathrm{d}h^{\alpha_0}_{\mu_0, p}|_{x^*}) < 1.$$

which proves the first statement.

If $\{\frac{\pi}{2}, \frac{3\pi}{2}\} \cap C_\lambda \neq \emptyset$ then there exists a parameter μ_0 such that $\varrho(\mathrm{d}h^0_{\mu_0, p}|_{x^*}) < 1$. Since Stalled Predictive Feedback Control reduces to classical Predictive Feedback Control for a stalling parameter of $\alpha = 0$, the claim follows. □

The conditions derived for stabilizability of tuples translate directly into conditions on the local stability properties of a periodic orbit. For dynamics in two dimensions we obtain the following immediate consequence.

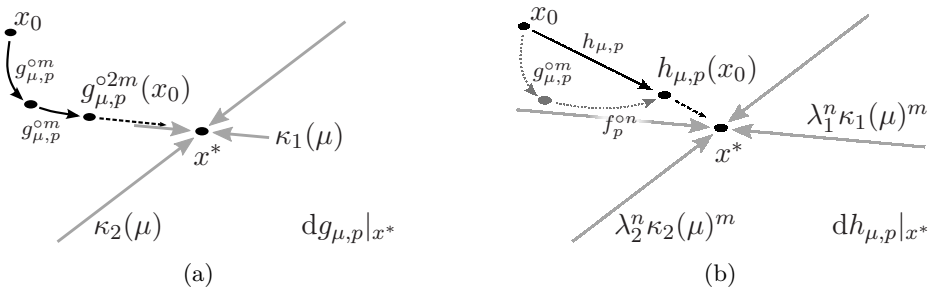

Figure 3.4.: Local stability explains why stalling chaos control speeds up convergence. Iteration of $g_{\mu,p}$ takes a trajectory to the periodic orbit x^* along the (weakly stable) direction of the originally stable manifold (Panel (a)). Stalling control accelerates convergence by taking advantage of the fast convergence speed along the stable manifold (Panel (b)) leading to fast overall convergence speed. The length of the gray arrows scale inversely with the corresponding value of the eigenvalue and illustrate convergence speed.

Corollary 3.2.9. *Suppose that $f : \mathbb{R}^2 \to \mathbb{R}^2$ is a chaotic map where all periodic orbits are of saddle type with eigenvalues λ_1, λ_2 that satisfy condition (3.11), i.e., we have*

$$\ln(|\lambda_2|)\,\mathrm{Re}(\lambda_1) \neq \ln(|\lambda_1|)\,\mathrm{Re}(\lambda_2).$$

Then all periodic orbits are SPFC-stabilizable.

Remark 3.2.10. The number of constraints for stabilizability grows with increasing dimension of the dynamical system. In order to determine the absolute number of periodic orbits which are stabilizable for higher dimensional systems, a more detailed knowledge about the "average" local stability properties of periodic orbits is needed.

Since the system is real, complex eigenvalues of the derivative will always come in complex conjugate pairs. According to Remark 3.2.6 above, this actually results in an effective decrease of the number of constraints.

A Geometric Interpretation

Why does Stalled Predictive Feedback Control increase asymptotic convergence speed? Consider a periodic orbit x^* of saddle type in a two-dimensional system where contraction along the stable direction is given by $\lambda_1 \in (-1, 1)$ and expansion along the unstable manifold by $\lambda_2 < -1$. As discussed in Section 3.1, these are the PFC-stabilizable periodic orbits. Suppose that $\mu_{\mathrm{opt}} > 0$ is the value of the control parameter for which the spectral radius of the linearization of the PFC-transformed map $g_{\mu,p}$ takes its minimum. For $\lambda_2 \ll -1$ we have $\mu_{\mathrm{opt}} \approx 0$ and therefore $\kappa_1(\mu_{\mathrm{opt}}) \approx 1$ determines the asymptotic convergence speed of the dominating direction if the periodic orbit is stabilized. Therefore the trajectory will approach the periodic orbit along the direction corresponding to λ_1; cf. Figure 3.4. The slowdown of Predictive Feedback Control is

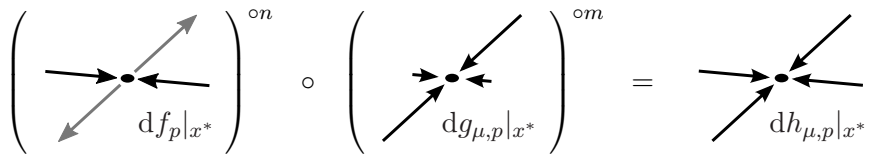

Figure 3.5.: Stalling PFC leads to fast convergence from all directions to a periodic orbit x^* for small μ. In this cartoon for two dimensions the direction of the arrows indicates stability and the length the absolute value of the corresponding eigenvalue.

caused by the fact that for highly unstable periodic orbits, the trajectories converge to the originally stable manifold along which convergence is slow in the transformed system.

Stalling PFC exploits exactly this property. First, iteration of $g_{\mu,p}$ takes the trajectory closer to the stable manifold. Second, iteration of f_p leads to fast convergence along the stable manifold while diverging from the stable manifold; cf. Figure 3.4. Thus, asymptotic convergence speed of $h_{\mu,p}$ is increased by making use of the (increasing) stability of the stable direction. For given stalling parameters m, n the optimal value of the control parameter μ is close to the zero of $\kappa_2(\mu)$. For this value, convergence to the stable direction is strongest, taking full advantage of the fast convergence given by λ_1 along the stable manifold of the chaotic map f. The resulting local stability properties are sketched in Figure 3.5. The question of how to chose the stalling parameters m, n will be addressed in the following section.

3.3. Convergence Speed for Chaotic Maps

In the previous section we analyzed the stability properties of the SPFC method for periodic orbits in dependence of their stability properties. The improvements due to stalling can be calculated explicitly for some "typical" two and three-dimensional chaotic maps.

With $\varrho^h_{\min}(x^*) = \inf_{\mu,\alpha} \varrho_{x^*}(\alpha, \mu)$ denoting the rescaled stability of the linearization for the optimal parameter values, we calculated the functions

$$\overline{\rho}_h(p) = 1 - \min_{x^* \in \mathrm{Fix}^*_h(f,p)} \varrho^h_{\min}(x^*), \tag{3.12a}$$

$$\rho_h(p) = 1 - \frac{1}{\mathrm{card}(\mathrm{Fix}^*_h(f,p))} \sum_{x^* \in \mathrm{Fix}^*_h(f,p)} \varrho^h_{\min}(x^*), \tag{3.12b}$$

$$\underline{\rho}_h(p) = 1 - \max_{x^* \in \mathrm{Fix}^*_h(f,p)} \varrho^h_{\min}(x^*) \tag{3.12c}$$

numerically in the same fashion as (3.3) to asses the scaling of optimal asymptotic convergence speed of Stalled Predictive Feedback Control for a given chaotic map across different periods. That is, for every periodic orbit of f of minimal period p

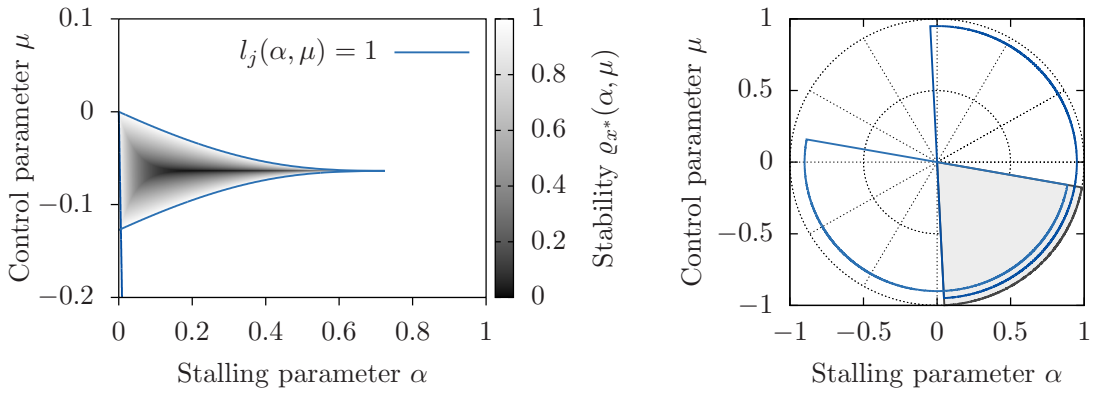

Figure 3.6.: Stability analysis for a periodic orbit of period $p = 5$ of the map (3.4) with local stability given by $\lambda = (\lambda_1, \lambda_2) = (1.46 \cdot 10^{-9}, 16.698)$ yields a region in parameter space in which it is stable. Panel (a) shows the stability function (3.8) and the lines defined by $l_j(\alpha, \mu) = 1$ with l_j as given by (3.7). The domain of stability C_λ around $(\alpha, \mu) = 0$ is depicted in Panel (b). Note that this periodic orbit cannot be stabilized using the PFC method.

we calculated the spectral radius at the optimal parameter values and then took the minimum, maximum, and mean of these values. In particular, $1 - \underline{\rho}_h$ is the upper limit and $1 - \overline{\rho}_h$ is the lower limit for the best asymptotic convergence speed of all SPFC-stabilizable periodic orbits of a given period p rescaled to one evaluation of f_p.

The increase of the number of stabilizable orbits for PFC and SPFC can be quantified by looking at the fractions of stabilizable periodic orbits that are given by

$$\nu_h(p) = \frac{\operatorname{card}(\operatorname{Fix}_h^*(f,p))}{\operatorname{card}(\operatorname{Fix}(f,p))} \qquad \text{and} \qquad \nu_g(p) = \frac{\operatorname{card}(\operatorname{Fix}_g^*(f,p))}{\operatorname{card}(\operatorname{Fix}(f,p))}, \tag{3.13a}$$

respectively.

Stabilizability for Chaotic Maps

Consider the two-dimensional neuromodule (3.4) discussed above and let x^* be some periodic orbit. The stability function describes local stability at x^*; cf. Figure 3.6. The region of stability in (α, μ)-parameter space is bounded by the lines $l_j(\alpha, \mu) = 1$ where $j = 1, 2$. The intersection of the half planes defined by the lines (3.9) gives the sector C_λ that describes stability around $(\alpha, \mu) = 0$ where $\lambda = (\lambda_1, \lambda_2)$ are the eigenvalues of $\mathrm{d}f_p|_{x^*}$; cf. Section 3.2. Note that for fixed α, the range of μ which yields stability becomes smaller for larger α.

To compare the scaling of the spectral radius across periods, we plotted the functions (3.3) and (3.12) in Figure 3.7. The original PFC method exhibits asymptotic con-

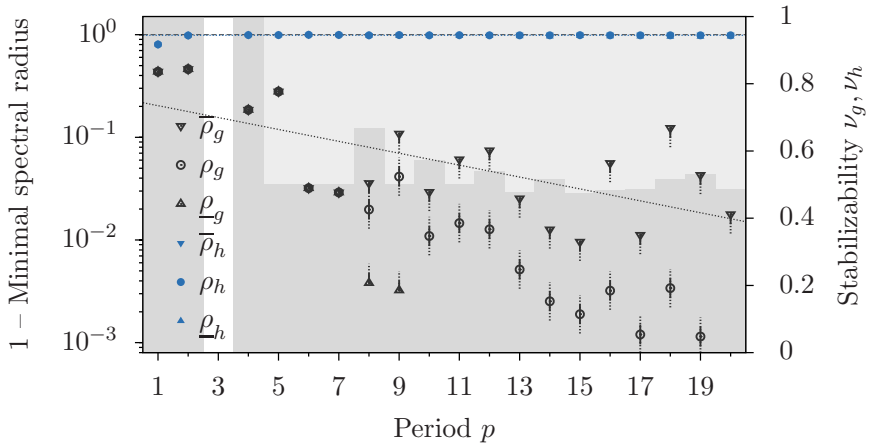

Figure 3.7.: Stalling PFC increases optimal asymptotic convergence speed for the 2D-Neuromodule (3.4). SPFC yields period-independent asymptotic convergence speed. At the same time, more periodic orbits can be stabilized. The fraction of stabilizable orbits is shaded in gray; dark indicates stabilizability for both with and without stalling, light indicates stabilizability for SPFC only.

vergence speeds that approach one exponentially for increasing period. A fit of $\underline{\rho}$, corresponding to the best asymptotic convergence speed, by a function $\phi(x) = a\exp(-bx)$ yields a slope of $b = 0.1334$. By contrast, stalling the control significantly improves this scaling. We obtain values close to zero for all periods $p \in \{1, \ldots, 20\}$ and hence period-independent asymptotic convergence speed in terms of evaluations of f_p. A fit with an exponential function of $\underline{\rho}_h(p)$, i.e., the worst convergence speed, yields an exponent of $b = 3.8112 \cdot 10^{-8}$.

Qualitatively similar results are obtained for other two-dimensional chaotic maps such as the Hénon map [45] (see [12] for more details) and the Ikeda map [53] (not shown).

As an example of a three-dimensional system, we analyzed a three-dimensional extension of the Hénon map [9] given by

$$f(x_1, x_2, x_3) = \left(a - x_2^2 - bx_3, x_1, x_2\right) \tag{3.14}$$

with parameters $a = 1.76, b = 0.1$. Stability properties of a periodic orbit of period $p = 6$ are depicted in Figure 3.8.

Due to additional constraints on stabilizability, the situation is different compared to the two-dimensional example above. In our example, the periodic orbits have a two-dimensional unstable manifold. If both eigenvalues corresponding to that manifold are real, the regime of stability depends on their sign and distance. If they have opposite signs, the periodic orbit cannot be stabilized, neither with nor without stalling. In case both eigenvalues have the same sign, the situation is depicted in Figure 3.8; there is a

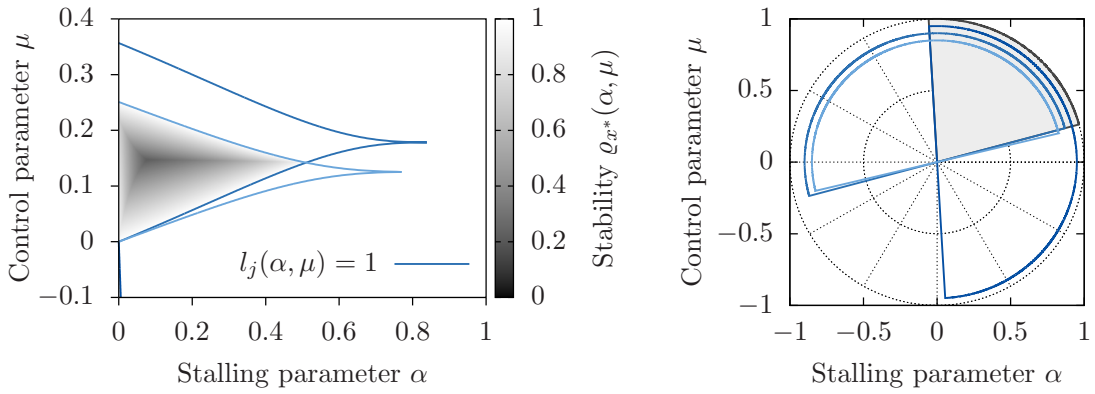

Figure 3.8.: Stability properties for a fixed point of period $p = 6$ of the three-dimensional Hénon map (3.14) with local stability given by $\lambda = (\lambda_1, \lambda_2, \lambda_3) = (3.1125 \cdot 10^{-8}, -4.6072, -6.9734)$ show a region where stabilization is successful. The stability function (3.8) is depicted in Panel (a) and the domain of stability C_λ in Panel (b); cf. Figure 3.6.

maximal value for α beyond which stabilization fails. For a pair of complex conjugate eigenvalues, the stability properties depend on the quotient of the real and imaginary part; cf. Figure 3.11. In particular, if the imaginary part is large, optimal asymptotic convergence speed is achieved for the PFC method, i.e., for a choice of $n = 0$.

When looking at the scaling of optimal asymptotic convergence speed across periods we have to distinguish between two cases (Figure 3.9). For even periods, we obtain a period-invariant scaling of both the mean and the best optimal asymptotic convergence speed similar to the two-dimensional system. While the upper bound on convergence speed will also increase to one due to the existence of periodic orbits with complex conjugate pairs, it will typically stay above the best convergence speed for the original PFC method. For odd periods, the number of periodic orbits with complex conjugate pairs of eigenvalues corresponding to the unstable directions is large. Therefore, we see the same performance as for the PFC method. Interestingly, for larger odd periods $p > 10$ stalling becomes more effective at increasing optimal asymptotic convergence speed, boosting the best speed close to one.

A similar scaling behavior is present in other three-dimensional examples; period-independent scaling for even periods p is observed for a three-dimensional neuromodule [80] (not shown).

Convergence Speed in Applications

The scaling of the spectral radius indicates only the best possible asymptotic convergence speed for Stalled Predictive Feedback Control, i.e., the speed for the linearized dynamics. We ran simulations to compare the convergence speed for the full nonlinear

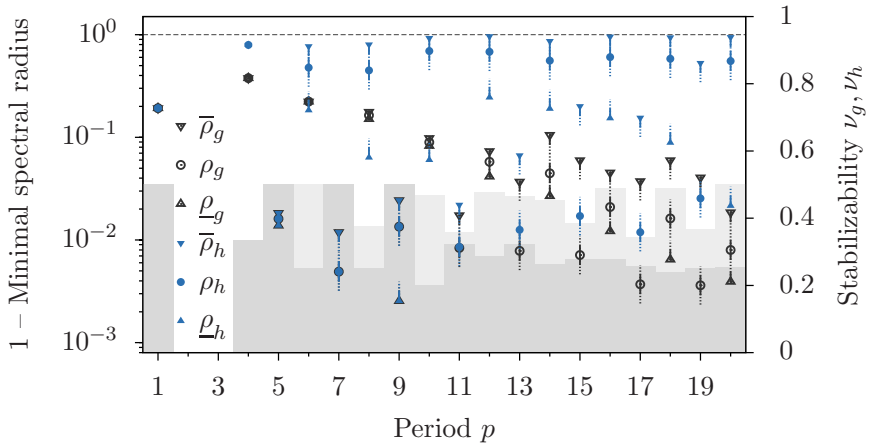

Figure 3.9.: Stalling Predictive Feedback Control yields period-independent scaling for periodic orbits of even period for the three-dimensional Hénon generalization (3.14). Effectivity of stalling for odd periods increases with increasing period. The number of stabilizable periodic orbits (3.13) roughly doubles for higher periods as indicated by the shading; cf. Figure 3.7.

system with the theoretical results for the linearized dynamics. In order to approximate a real-world implementation where control is turned on at a "arbitrary point in time" initial conditions were distributed randomly on the attractor according to the chaotic dynamics; cf. Section 2.2.

To evaluate convergence speed of Stalled Predictive Feedback Control, we compared the speed of $g_{\mu,p} = h^0_{\mu,p}$ with $h^\alpha_{\mu,p}$ for both $\alpha = 3^{-1}$ and $\alpha = (p+1)^{-1}$. In terms of the parameters m, n, a value of $\alpha = 3^{-1}$ corresponds to $m = 2$, $n = 1$ and $\alpha = (p+1)^{-1}$ to $m = p$, $n = 1$. In our implementation, convergence time is the first time T satisfying

$$\|x_T - \psi(x_T)\| \leq \theta_{\text{conv}}, \tag{3.15}$$

where ψ is one of the functions above; refer to Appendix A.2 for details on the algorithm. Convergence was only achieved if the criterion was fulfilled before a timeout of $T_{\text{timeout}} = 3000$ iterations. The convergence times were rescaled to evaluations of f_p to make them comparable. To calculate the best theoretical convergence time, we calculated the smallest spectral radius

$$\underline{\rho}^\alpha(p) = \min_{x^* \in \text{Fix}^*_h(f,p)} \inf_\mu \varrho(\mathrm{d}h^\alpha_{\mu,p}|_{x^*})$$

for all periodic orbits of a given period p with variable μ while keeping the stalling parameter $\alpha(m,n)$ fixed. Convergence time for the linear system may be approximated by $\|x^* - x_\tau\| = \|x^* - x_0\|(\underline{\rho}^\alpha(p))^\tau$. For an initial separation $\|x^* - x_0\| = d_{\text{ini}}$, a quick calculation yields that the convergence criterion (3.15) is first satisfied for

$$T = \left(\ln\left(\frac{\theta_{\text{conv}}}{d_{\text{ini}}}\right) - \ln\left(1 - \underline{\rho}^\alpha(p)\right)\right) \ln\left(\underline{\rho}^\alpha(p)\right)^{-1} =: \tau^\alpha(p). \tag{3.16}$$

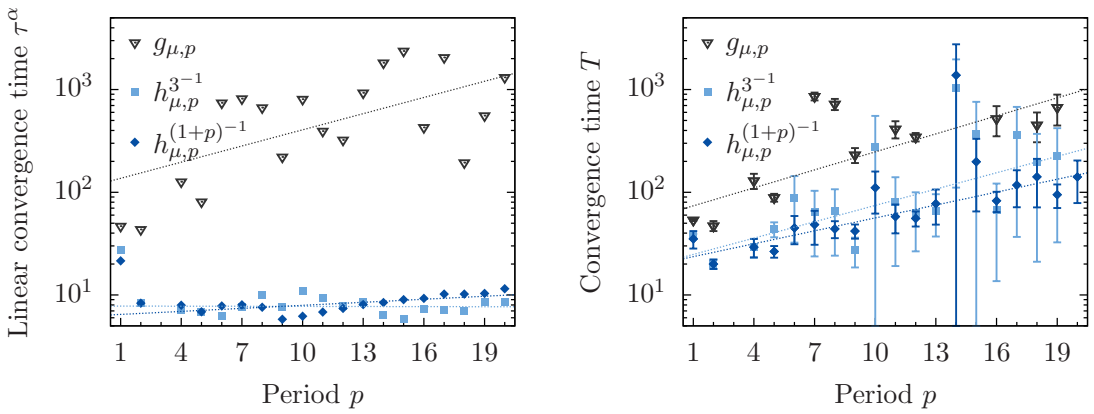

(a) Theoretical optimum (b) Numerical simulations

Figure 3.10.: Although the best convergence times obtained from numerical simulations as shown in Panel (b) cannot match the theoretical values of the linearized system given by (3.16), (Panel (a)), stalling PFC increases both the overall convergence times as well as the scaling across periods. Numerical simulations for the two-dimensional neuromodule (3.4) were performed with initial conditions distributed randomly on the chaotic attractor. Dashed lines represent an approximate fit with an exponential function solely for visual orientation to indicate the general scaling behavior. Note that in the numerical simulations convergence of PFC fails for some periods.

Thus, $\tau^{\alpha}(p)$ is the convergence time of the linearized system with convergence criterion (3.15) for an initial condition x_0 with (period-independent) initial separation d_{ini}. For the simulations presented here, we chose $\theta_{\text{conv}} = 10^{-13}$ and $d_{\text{ini}} = 0.1$.

The results are shown in Figure 3.10. The errorbars depict mean and standard deviation for all 500 runs with initial conditions given by transient iteration of random length on the attractor; cf. Appendix A.2. The value of the control parameter μ in the numerical simulations was chosen for each period to be the optimal value that yielded at least a fraction of 0.95 of convergent initial conditions. In other words, μ was chosen to yield the optimal speed with at least 95% reliability.

As predicted by the calculation of the spectral radius, stalling PFC leads to an increase in convergence speed across all periods. A scaling of convergence times (scaling is indicated by dashed lines) which is almost period-independent as observed in the theoretical calculations cannot be achieved in our simulations. This is due to several factors. First, in contrast to the linearized dynamics, the numerical simulations take the full nonlinear system into account. This includes the influence of the transient dynamics and the increasing complexity of the phase space (the number of fixed points increases with increasing period) on convergence times. Second, in the theoretical calculations we consider only the fixed point for which convergence is fastest. However,

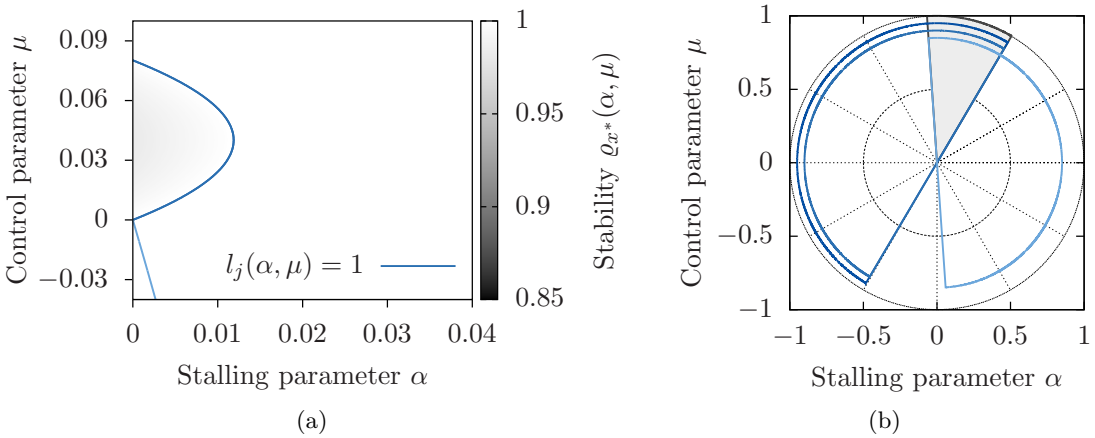

Figure 3.11.: For periodic orbits with unstable directions given by a pair of complex conjugated eigenvalues only few choices of the stalling parameter allow for stabilization (in particular for $m \gg 1$). The local stability of this period $p = 5$ orbit of the three-dimensional Hénon map (3.14) orbit are determined by $\lambda = (\lambda_1, \lambda_2, \lambda_3) = (0.0933 + 4.6673i, 0.0933 - 4.6673i, 0)$. Optimal performance is achieved for the PFC method, i.e., with $n = 0$; cf. Figures 3.6 and 3.8

even in our simulations, stalling improves both absolute convergence times was well as their scaling across periods compared to classical PFC. Furthermore, it increases the number of periods that can be stabilized. For some periods, only Stalled Predictive Feedback Control yields convergence within a reasonable time. The scaling of the convergence speeds is independent of whether the stalling parameter is fixed or scales with p. However, a period-dependent stalling parameter will generally reduce the standard deviation of the different convergence times.

Relation to Earlier Results

Stalled Predictive Feedback Control as defined in Definition 3.2.1 is a proper extension of the PFC method. In fact, the iteration of $h_{\mu,1}^{(1,1)}$ has been considered before in the context of Predictive Feedback Control when trying to overcome the odd number limitation [73, 96] as well as in the context of an experimental setup where measurements are time-delayed [18]. These studies were only concerned with whether or not fixed points can be stabilized, completely ignoring the aspect of convergence speed. Although for systems of dimension $N < 3$ stalling control increases the number of fixed points that can be stabilized; even for $N = 3$ there are points that can be stabilized using PFC but not using SPFC when the stalling parameter α is as large as in [18, 73, 96] (Figure 3.11). Hence, the introduction of an arbitrary stalling parameter is the key to both maximizing the number of fixed points subject to stabilization through PFC as well as minimizing the convergence speed.

The idea of periodically turning control on and off has been mentioned before in the literature on control theory; both "act-and-wait" control [54] and "intermittent" control [37] are stated for linear control problems in discrete and continuous time. At the same time, for linear control problems with many control parameters, "pole placement" techniques [101] are used to control the eigenvalues of the linearization. By contrast, SPFC aims at stabilizing many unstable periodic orbits of a given nonlinear system maintaining the simplicity of the simple one-parameter feedback control scheme. The situation where control is turned on at an arbitrary point in time as described above is of particular interest; here, the system is likely to be far from the linear regime. As shown above, stalling PFC improves performance even in this situation.

Stalling Predictive Feedback Control is also related to a recent application of chaos control [102]. Because of implementation restraints, Steingrube et. al. effectively iterated $f \circ g_{\mu,p}$. In some sense, this is similar to iterating $h_{\mu,p}^{(p,1)}$, but the stability analysis is not straightforward since one has to keep track of the (changing) point on the periodic orbit to be stabilized. Moreover, both SPFC and the method employed in [102] are related to an effort by Polyak [86] to introduce a generalized PFC method, which is able to stabilize periodic orbits with an arbitrary small perturbation. This method, however, is limited in applicability, because the control perturbation depends on predictions of the state of the system many time steps in the future.

3.4. Adaptation for Stalled Predictive Feedback Control

In the previous sections, we showed that for an optimal choice of parameters the asymptotic convergence speed of Predictive Feedback Control can be significantly increased by stalling control. This speedup is not only of theoretical nature, but also persists in an implementation with random initial conditions. The question that arises naturally is how to find the set of optimal parameter values for a given chaotic map f. If no a priori estimates are available, we show that adaptation methods provide a way to tune the control parameters online for optimal convergence speed.

Here, we focus on the case where the stalling parameter $\alpha = (p+1)^{-1}$ (corresponding to a choice of $m = p$, $n = 1$) is fixed and $\mu \geq 0$ is subject to adaptation. Thus, within this section, consider the iteration of

$$h_{\mu,p} = h_{\mu,p}^{(p,1)}.$$

We review a simple adaptation scheme before proposing a hybrid gradient adaptation rule. Both adaptation mechanisms are explored numerically and we find that the latter scheme leads to fast and highly reliable adaptation across different periods for initial conditions distributed randomly on the chaotic attractor.

Simple and Gradient Adaptation

First, recall a simple adaptation scheme proposed, for example, in [102]. Suppose that the period p is fixed within this subsection. A suitable objective function for finding a

periodic point of period p is given by

$$G_1(x,p) = \|f_p(x) - x\|^2.$$

for some vector norm $\|\cdot\|$ on $\mathbb{R}^N$. For $\mu = 0$ the map $h_{0,p}$ reduces to some iterate of f and adaptation should lead to sequences $x_k \to x^*$ and $\mu_k \to \mu^*$ with $x^* \in \mathrm{Fix}(f_p)$ and $\varrho_h(\alpha, \mu^*) < 1$. The objective function above suggests a simple adaptation rule (SiA) with

$$\Delta\mu_k = \nu(p) G_1(x_k, p) \tag{3.17}$$

where $\nu(p)$ is the (possibly period-dependent) adaptation parameter and dynamics of μ given by

$$\mu_0 = 0, \quad \mu_{k+1} = \mu_k + \Delta\mu_k. \tag{3.18}$$

This adaptation rule increases the control parameter μ monotonically. Suppose that x^* is a fixed point of f, i.e., $f_p(x^*) = x^*$. If we have a converging sequence $x_k \to x^*$ as $k \to \infty$ then the sequence $\Delta\mu_k$ tends to zero. In other words, adaptation stops in the vicinity of a fixed point x^* of f_p.

For this adaptation mechanism, the quantity $\Delta\mu_k$ is extremely easy to calculate and yields decent results in applications [102]. Adaptation, however, strongly depends on the choice of the adaptation parameter $\nu(p)$. If $\nu(p)$ is too small, it will take a long time to reach a regime in which convergence takes place. On the other hand, if $\nu(p)$ is too large and the interval M of possible values of μ in which convergence takes place is rather narrow, it is possible that $\mu_k > \sup M$ for some k, even if $\mu_l \in M$ for some values $l < k$. Hence, it is possible for the control parameter to "jump out of" the range of stability. Also, note that by construction, this simple adaptation will not optimize for asymptotic convergence speed. For small $\nu(p)$, adaptation will stop close to the boundary of the convergent regime, leading to slow asymptotic convergence speed.

Adaptation may be improved, if the objective function takes local stability into account. For some matrix norm $\|\cdot\|$, such an objective function is given by

$$G_2(x,\mu,p) = \|\mathrm{d}h_{\mu,p}|_x\|$$

Since any matrix norm is an upper bound for the spectral radius, minimizing the norm potentially leads to increased convergence speed as discussed in Chapter 2. At the same time, for a generic point on the attractor, this objective function is highly non-convex with steep slopes (Figure 3.12) making straightforward minimization through, for example, gradient descent [35] difficult.

We therefore propose an adaptation rule that combines aspects of simple adaptation as reviewed above and the objective function G_2. Let ∂_μ denote the derivative with respect to μ, and define $\Theta(x) = \tanh\left((pG_1(x,p))^{-1}\right)$. Consider the modified gradient adaptation rule (GrA) given by (3.18) with

$$\Delta\mu_k = \lambda(p)\left(G_1(x,p) - p\tanh\left(\Theta(x_k)\partial_\mu G_2(h_{\mu,p}(x_k),\mu,p)\right)\right). \tag{3.19}$$

This adaptation rule has the following properties. For $G_1(x,p) \gg 0$, i.e., away from a period p orbit $x^* \in \mathrm{Fix}(f_p)$, we have $\Theta(x) \approx 0$. Therefore, adaptation is dominated by

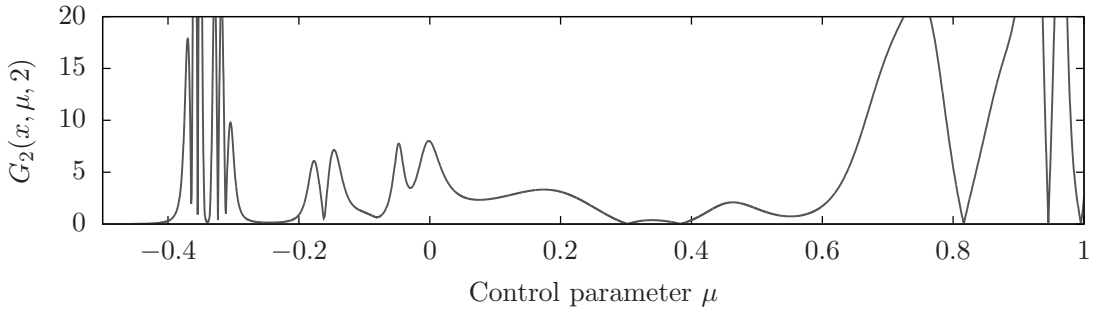

Figure 3.12.: The objective function $G_2(x, \mu, p)$ is nonconvex for a generic point x on the attractor leading to a difficult optimization problem.

the first term and leads to adaptation as given by the simple adaptation rule (3.17) to increase μ to reach a regime of convergence. On the other hand, in the vicinity of a fixed point we have $\Theta(x) \approx 1$ and $G_1(x, p) \approx 0$. Hence, adaptation occurs by bounded gradient descent and the dynamics of the control parameter μ are perpendicular to the level sets of the objective function G_2 towards a (local) minimum. The bound induced by the tanh prevents large fluctuations of the objective function G_2 from leading to a too large change of the control parameter μ.

The adaptation parameter $\nu(p)$ again determines the size of the adaptation steps. In contrast to the simple adaptation method, the modified gradient adaptation adapts bidirectionally in order to minimize both objective functions G_1 and G_2 as depicted in Figure 3.13(a). Clearly, the control parameter is adapted to the regime of stability of a periodic orbit by the modified gradient adaptation and $\Delta\mu_k \to 0$ as optimal asymptotic convergence speed is achieved. Statistics for a large number of initial conditions show that the population mean $\langle \mu_k \rangle$ for many runs is already close to the optimal value after only 70 iterations; cf. Figure 3.13(b).

Convergence Reliability

To assess the performance of the adaptive Stalled Predictive Feedback Chaos Control algorithm in a real-world application we performed large scale numerical simulations for the two-dimensional neuromodule (3.4). The setup was as described in Section 3.3 with the incorporation of the adaptation mechanisms just discussed; cf. Appendix A.2 for more details on the algorithm. The scaling of the adaptation parameter was given by $\nu(p) = \frac{\nu_0}{p}$ and for every ν_0 we iterated for 500 initial conditions on the chaotic attractor. To determine reliability, i.e., the fraction of runs where the trajectory converged to a periodic orbit of the desired period, we checked the period of the limiting periodic orbit (if any) to a threshold of $\theta = 10^{-6}$.

As discussed above, the adaptation parameter ν_0 influences both speed and reliability. The results for period $p = 5$ are plotted in Figure 3.14. Gradient adaptation not only decreases the total number of time steps needed to fulfill the convergence criterion but it also decreases the overall variation across runs (the standard deviation is depicted

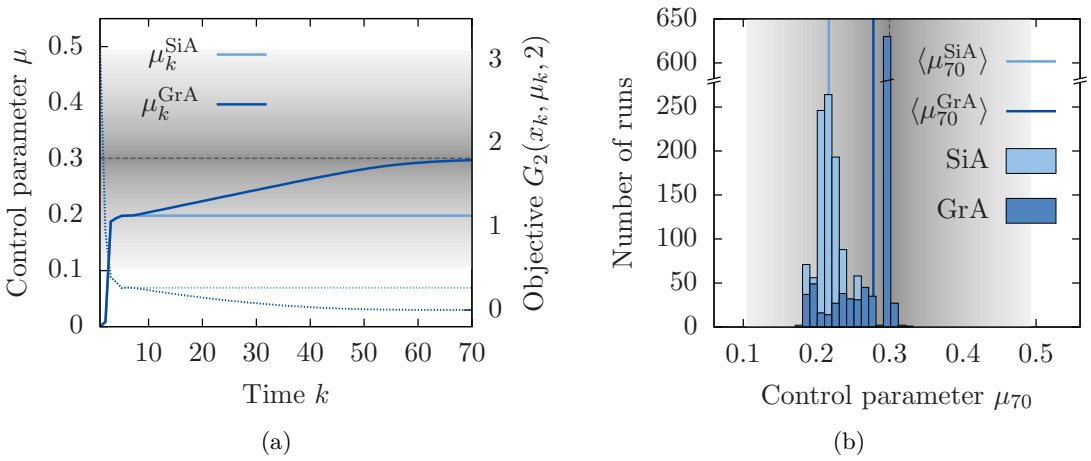

Figure 3.13.: In contrast to simple adaptation (SiA), gradient adaptation tunes the control parameter to the value where optimal convergence speed is achieved. The dynamics for a single run are shown in Panel (a) and the dotted lines depict the value of the objective function G_2. Statistics for 1000 runs are shown in Panel (b). The shading indicates values of the stability function smaller than one and the value yielding optimal asymptotic convergence speed is depicted by a dashed line. The target period was $p = 2$ for the two-dimensional neuromodule (3.4) with adaptation parameter $\nu = 10^{-3}$ and $n = 1$, $m = 2$. Here, $\langle \cdot \rangle$ denotes the population mean.

as an error bar). Of particular interest for applications is the range where convergence is highly reliable. In contrast to the simple adaptation scheme, for gradient adaptation the range of adaptation parameter values leading to highly reliable convergence is broadened. On the one hand, the gradient adaptation method optimizes for convergence speed, thereby increasing the chance that the convergence criterion is fulfilled before the timeout. At the same time, the bidirectional adaptation prevents the control parameter from leaving the regime of convergence. Gradient adaptation therefore improves both overall convergence speed while reducing the variation and increasing overall reliability.

The improvement of reliability compared to the simple adaptation scheme can be seen across all periods; cf. Figure 3.15. The broad range of adaptation parameters giving highly reliable convergence allows for the choice of an adaptation parameter ν_0 that will lead to reliable convergence across different periods, effectively eliminating this parameter.

Similar results are obtained for numerical simulations for other two- as well as three-dimensional chaotic maps (not shown). Convergence speed of μ_k to the optimal parameter value can be further increased by using higher order methods, such as Newton's method (not shown). The use of higher order methods (also with respect to compar-

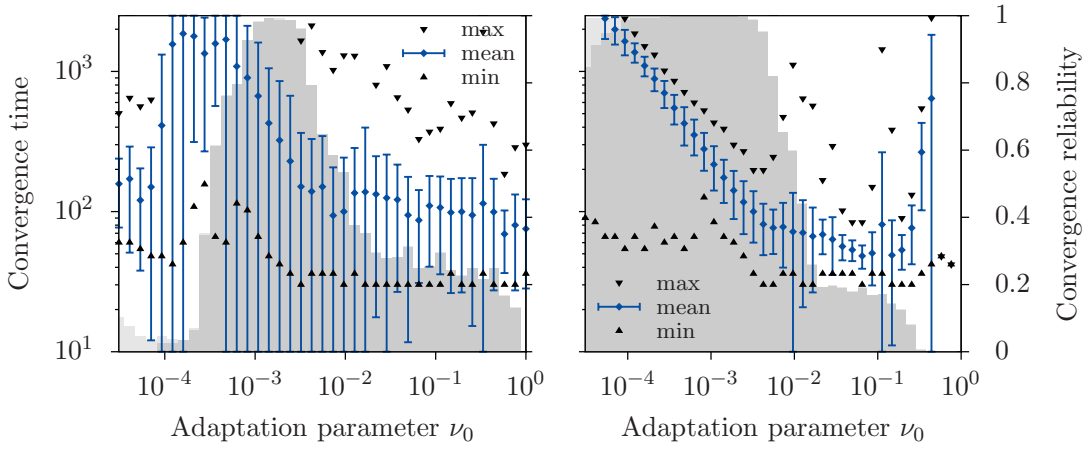

(a) Simple Adaptation (b) Gradient Adaptation

Figure 3.14.: Gradient adaptation decreases the overall convergence times and the variation thereof when compared to simple adaptation for target period $p = 5$. Furthermore, the range of reliable convergence, depicted by the shading in the background, is broadened. The fraction of convergent runs to a periodic orbit of the correct period is shaded in dark gray (reliable convergence) and to an incorrect period in light gray.

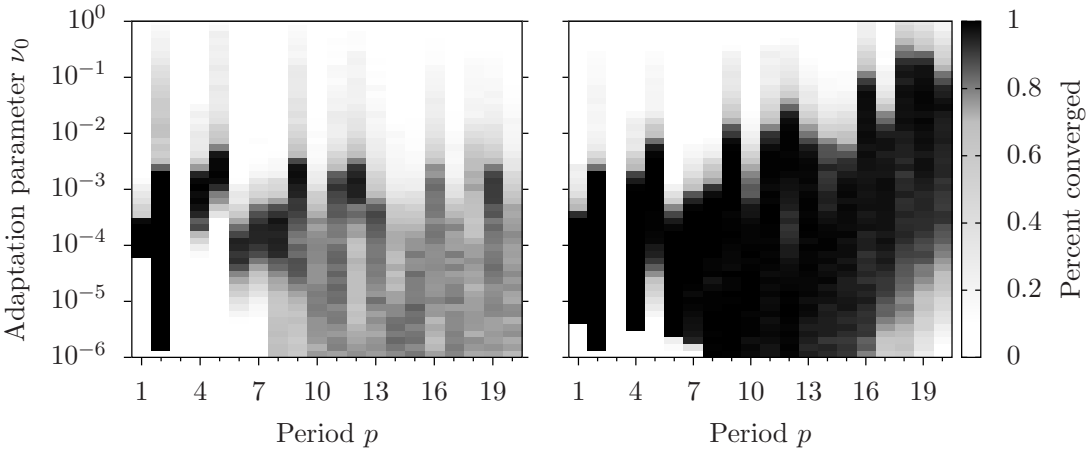

(a) Simple Adaptation (b) Gradient Adaptation

Figure 3.15.: Gradient adaptation increases the overall reliability of convergence across periods compared to simple adaptation. Reliability, i.e., the percentage of convergent runs to periodic orbits of the target period p, is depicted by the color of the shading for the adaptation parameter ν_0 and hence more dark areas correspond to higher overall reliability.

ing simple and gradient adaptation) comes with a higher absolute computational cost. For any implementation the improvement always needs to be related to the effective improvement.

3.5. Discussion

Stalling control is a way to overcome the inherent speed limit of Predictive Feedback Control. Optimal convergence speed of Predictive Feedback Control decreases for increasingly unstable periodic orbits. Thus, Predictive Feedback Control yields poor performance for periodic orbits of large periods which are typically highly unstable. In this chapter, we introduced Stalled Predictive Feedback Control, an extension of classical Predictive Feedback Control, which may overcome this limitation. It is motivated by the local dynamics that are the cause of the slowdown in the first place and makes use of the uncontrolled dynamics. As an extension of Predictive Feedback Control, it not only inherits certain desirable features from Predictive Feedback Control but it is also capable of stabilizing more periodic orbits. Stalled Predictive Feedback Control thus provides a noninvasive and easy-to-implement control scheme to stabilize periodic orbits, those, for example, which are embedded in chaotic attractors. Again, our method also applies to continuous time dynamics if suitably discretized (e.g., through a Poincaré map).

As discussed above, Stalled Predictive Feedback Control is related to approaches that have been put forward before. We derived conditions for stabilizability with respect to the local stability properties of a given periodic orbit as well as the control and stalling parameters. Whereas for certain similar ideas the choice of stalling parameters was rather ad hoc, our analysis allows for a suitable choice of parameters; cf. Section 3.3. We also showed that for certain "typical" dynamical systems, Stalled Predictive Feedback Control yields an almost period-independent performance in the linear regime. In contrast to classical linear control theory, we highlighted that this improvement in performance predicted for the linearized dynamics also carries over to the full nonlinear system with initial conditions distributed randomly on the chaotic attractor. Moreover, for a fixed stalling parameter, Stalled Predictive Feedback Control is still a one-parameter control scheme.

Adaptation mechanisms may further improve chaos control as they provide a way to tune the adaptation parameter online to a suitable value. We have seen that they not only reduce the need for such a priori parameter determination but they also allow for an increase in both speed and reliability. In contrast to previously proposed adaptation [63, 102], the hybrid algorithm presented here also adapts for optimal convergence speed. A broad range of parameters allows for a period-independent choice of the adaptation parameter, hence giving a chaos control method with a set of parameters for which many periodic points of most periods can be quickly and reliably stabilized. Adaptation using the objective function (3.17) also prevents the system from converging to one of the periodic orbits potentially induced by stalling control. However, as our adaptation method merely serves as a proof of concept, it still leaves room for improvement. In particular, the cap of adaptation speed through the sigmoidal function

is a major source of slowdown. Moreover, adaptation could be extended to the stalling parameter α.

For an efficient implementation, one might like to keep the stalling parameters m, n as small as possible since they directly influence the number of evaluations of f_p needed for a single time step for SPFC. This may be accomplished, for instance, by taking $m+n$ into account when choosing the stalling parameter. Such a penalty directly translates into an ordering of possible stalling parameters α. A different approach is given by extending Stalled Predictive Feedback Control to a "fractional stalling parameter," i.e., to allow for stalling by composing the PFC transformed map with $f^{\circ q}$ for $q < p$. With such stalling, however, one needs to track the point of the periodic orbit, as discussed in Section 3.3, rendering the theoretical analysis more cumbersome.

With increasing dimension of the dynamical system the number of constraints on the local stability properties as given by (3.7) to stabilize periodic orbits also increases. In contrast to two-dimensional systems, even with a nonzero stalling parameter not all the periodic orbits can be stabilized. However, the qualitative results regarding convergence speed remain the same as indicated by the three-dimensional example with periodic orbits with two-dimensional unstable manifold. First, there is a large subset of stabilizable periodic orbits for which asymptotic convergence speed is essentially period-independent as described above. Second, stalling Predictive Feedback Control increases the number of stabilizable periodic orbits. A priori estimates of the local stability properties and calculation of attractor dimensions would be desirable for a determination of the efficiency of Stalled Predictive Feedback Control.

The problems induced by the additional constraints in higher dimensions could potentially be overcome by tuning the eigenvalue corresponding to some eigenvector separately, for example by increasing the number of control parameters. From a mathematical point of view, a different approach would be to allow the control parameter to take complex values, turning the problem into one of complex dynamics in several complex variables as discussed in Chapter 2.

Conversely, the local stability properties and the resulting shape of the stability function may actually be exploited. On the one hand, the local stability conditions may provide "attractor design principles" such that the attractor contains many unstable periodic orbits that our Stalled Predictive Feedback Control method is capable of stabilizing. On the other hand, one may stabilize specific periodic orbits through the choice of stalling parameters. The range of control parameters μ that allow for stabilization for any given stalling parameter $\alpha > 0$ becomes more narrow as the stalling parameter α increases towards one. As a result, different local stability properties of the unstable periodic orbits allow for the stabilization of a specific set of periodic orbits.

Further exploration of these important questions, however, is beyond the scope of this thesis and should be addressed in further research.

Outlook

In this thesis, we took two distinct points of view to understand the properties of chaotic dynamical systems. In the first part we studied what restrictions symmetry imposes on dynamical systems with respect to the emergence of chaos. We took a different perspective in Part II, one which focused more on the practically useful features of chaotic dynamics: chaos may be exploited in applications through so-called "chaos control" which we studied with respect to convergence speed. The properties of chaotic dynamics link these two distinct points of view on the same topic. In this section, we discuss some aspects concerning both dynamical systems with symmetry and chaos control before giving some open questions and future perspectives.

Recently, there have been efforts to combine the two aspects of symmetry and chaos control [88]. Dynamical systems with symmetry have specific properties imposed by the action of the symmetry group. These properties may actually be taken advantage of when it comes to stabilizing periodic orbits in equivariant dynamical systems. Thus, one might additionally be able to exploit symmetry to raise convergence speed. For example, are any symmetries particularly useful in terms of fast stabilization of symmetric chaos? Hence, combining the two aspects of symmetry and chaos control will likely bear new, interesting questions for further research.

Uniformly hyperbolic dynamical systems are an important class of differentiable dynamical systems which may exhibit chaotic dynamics since global aspects are related to local properties. Recall that a system is uniformly hyperbolic if its local dynamics are characterized by distinct expanding and contracting directions at every point [56, 98]. For iterated maps this means that the derivative has no eigenvalue on the unit circle. The condition is similar for systems defined by vector fields, but in addition we have a neutrally stable direction in the direction of the trajectory. Hence, to a certain extent, local expansion and contraction are uniform on the whole set on which the dynamical system is defined since no changes in local stability are possible. Recently, computer-aided ways to prove hyperbolicity have been developed [2, 51] which may be applicable to our system of coupled phase oscillators studied in Part I of this thesis. Even though an implementation is beyond the scope of this thesis, this may be a way to rigorously prove hyperbolicity of the chaotic attractors we have found.

Uniform hyperbolicity is also an advantageous property for the application of Predictive Feedback Control and Stalled Predictive Feedback Control; cf. Part II of this thesis. Recall that Predictive Feedback Control is applicable only if the eigenvalues of the derivative at the periodic orbit are not equal to one. This condition is always satisfied for uniformly hyperbolic dynamical systems. Furthermore, a large number of periodic orbits is desirable for certain applications such as the robot for which a periodic orbit is mapped to a behavioral pattern [102]. Under some additional assumptions, the

number of periodic orbits of hyperbolic dynamical systems increases exponentially with increasing period. The Fatou conjecture states that hyperbolicity is a "common" property of dynamical systems [34, 41]. Originally stated for quadratic maps on the Riemann sphere, it claims that hyperbolicity is dense for an open set of parameters. However, it is believed that the conjecture is true for a wider class of dynamical systems. If the Fatou conjecture is true, this means that Predictive Feedback Control and its extensions are in fact applicable to a large class of dynamical systems.

The individual aspects covered in the two parts of this thesis motivate further investigation by themselves. Some questions were already formulated and discussed in the respective chapters. Within the remainder of this section, we highlight a few open problems that we find to be of particular interest.

In Chapter 1 we found that there are coupling functions for which the dynamical system defined by generalized Kuramoto equations (1.5) exhibits chaotic dynamics. For the family of coupling functions given in the first chapter, however, attractive chaos was found only for some smaller dimensions, namely for $N = 4, 5, 7$. Even though there is chaos in flow-invariant subsets for larger dimensions it is likely that this chaos is transversally repelling. Thus, the question remains whether there are coupling functions that give rise to chaotic attractors for larger N, or whether there is a "universal chaos function," i.e., a function for which there are chaotic attractors for the system (1.5) for all, or at least an infinite number of dimensions N. And if there are such functions, what are their fundamental building blocks? Furthermore, the relationship between the continuum limit and the finite dimensional case needs to be clarified. For coupling functions with only one Fourier mode, i.e., the classical Kuramoto equations, the Ott–Antonsen ansatz [77, 78] has implications for the dynamics in finite dimensions [68]. What are the limitations imposed by more than one nontrivial Fourier component regarding the applicability of this ansatz?

For even coupling functions, it would be desirable to uncover the origin of the regularity of the solutions seen for the case of four oscillators. Since we were unsuccessful at finding a constant of motion for four or more oscillators the question remains whether there exist one or more constants of motion at all. Recall that for coupling functions with a single Fourier mode, we have $N - 2$ constants of motion. Moreover, if the coupling function is even then for $N = 3$ oscillators this constant of motion generalizes to a constant of motion for an arbitrary even coupling function as shown in Section 1.3. Is there a way to interpolate between these two cases? As discussed above, uncovering such a constant of motion might be a way to predict the bifurcation structure when the reversing symmetry is broken.

In Chapter 3 we demonstrated that stalling Predictive Feedback Control has a positive effect on convergence speed. At the same time, we noted that the number of constraints on the eigenvalues of the periodic orbits to be stabilized grows with the system dimension. Is there a way to effectively predict the efficiency of Stalled Predictive Feedback Control for a given map, for example through the estimation of the entirety of local stability properties? Conversely, one might want to ask what properties a map has to have for its periodic orbits to be optimally stabilizable. From the results above it

seems that periodic orbits with "clustered" local stability properties, i.e., those with eigenvalues that are contained in as few small balls as possible in the complex plane, have the best optimal asymptotic convergence speed.

Adaptation methods for Stalled Predictive Feedback Control were introduced merely as a proof of concept. Our implementation and the choice of parameters still leave room for improvement. Even though the hybrid gradient adaptation method is motivated by convergence results for gradient adaptation methods [35], a more rigorous treatment would be desirable. For instance, a proof of convergence as presented for the adaptation method presented in Chapter 2 might clarify the overall impact of adaptation on the system's dynamics. Also note that when evaluating the overall effect of a speedup achieved through adaptation, one has to take numerical efficiency into account. In particular for dynamical systems of larger dimension, any objective function that involves the numerical evaluation of derivatives is numerically costly. In some cases, it might be more efficient in terms of overall performance to retain a simpler adaptation scheme since the higher numerical cost of any more involved adaptation is not compensated by the improvement in convergence speed due to adaptation.

Although our chaos control methods were stated for discrete time dynamical systems, they may be applied to continuous time dynamics through discretization by, for instance, a Poincaré map. Then again, it would be desirable to optimize existing chaos control methods, such as Pyragas control [89, 90], used to control continuous time dynamics directly for convergence speed. It turns out that through the analysis of delay differential equations [103] one may obtain an objective function that takes local stability of an unstable equilibrium close to a Hopf bifurcation into account. Adaptation with respect to this objective function might be a first step towards an adaptive method to accelerate chaos control of continuous time dynamical systems; a full treatment however is beyond the scope of this thesis.

In conclusion, the analysis of the emergence of chaos and its control may be seen as two different approaches to understanding the dynamics on chaotic attractors. Not only does each approach engender a complementary set of research questions but also the combination of both gives rise to interesting problems. Phase coupled oscillators provide an example of systems which exhibit rich dynamics despite strong structural constraints. Then again, the intricate properties of chaotic attractors may be exploited by effective chaos control methods. Further progress will no doubt come from continuing to pursue questions about both the structural as well as the practically useful properties of network dynamical systems.

A. Numerical Implementation

Although some comments on the numerics were already given in the main text above, this section covers some more details on the implementation of the numerical simulations. In the first section, we cover some implementation aspects of the calculations performed in Part I. These include the integration of the variational equation to calculate the maximal Lyapunov exponent, some properties of the projection Π which was used to plot solutions of the dynamical equations, and finally some details on the calculation of the symmetry groups of the chaotic attractors. The second section covers some aspects from Part II, in particular Chapter 3. We elaborate on the algorithm used to perform the simulations for Stalled Predictive Feedback Control with and without adaptation.

A.1. Chaos in Oscillators

Calculation of the maximal Lyapunov exponent $\lambda_{\max}$. To calculate the maximal Lyapunov exponent, we integrate the variational equation (1.3),

$$\frac{\mathrm{d}v}{\mathrm{d}t} = A(t)v, \tag{A.1}$$

where $A(t) = \mathrm{d}X(t)$ denotes the Jacobian along a given trajectory. Write the perturbation v as $v = \exp(r)u$ with (logarithmic) length $r(t) \in \mathbb{R}$ and direction $u(t) \in \mathbf{S}^N := \{x \in \mathbb{R}^N \mid \|x\| = 1\}$ on the unit sphere. With this substitution, Equation (A.1) is equivalent to

$$\frac{\mathrm{d}u}{\mathrm{d}t} + u\frac{\mathrm{d}r}{\mathrm{d}t} = A(t)u.$$

Taking the Euclidean scalar product $\langle \cdot, \cdot \rangle$ with u we obtain

$$\frac{\mathrm{d}r}{\mathrm{d}t} = \langle A(t)u, u\rangle - \left\langle \frac{\mathrm{d}u}{\mathrm{d}t}, u \right\rangle = \langle A(t)u, u\rangle$$

since we have $\langle x, p\rangle = 0$ for all $p \in \mathbf{S}^N$ and $x \in T_p\mathbf{S}^N$, i.e., any tangent space at a given point p of the sphere is perpendicular to the vector defining this point. Note that r is the logarithmic length of the perturbation and its integrated value corresponds to the maximal Lyapunov exponent for all most all initial conditions $v(0)$. Hence, the system (A.1) is equivalent to

$$\frac{\mathrm{d}r}{\mathrm{d}t} = \langle A(t)u, u\rangle \tag{A.2}$$

$$\frac{\mathrm{d}u}{\mathrm{d}t} = A(t)u - u\frac{\mathrm{d}r}{\mathrm{d}t} \tag{A.3}$$

which provides an efficient way to calculate the maximal Lyapunov exponent $\lambda_{\max}$ as the length of the perturbation is given in logarithmic scale already.

A program to solve this set of equations was implemented in C/C++ with the GSL[1] classes and functions. A standard Runge–Kutta scheme with a fixed time step (typically $\Delta t = 0.05$ time units) was employed to solve the dynamical equations numerically. Integration to determine the maximal Lyapunov exponent ranged within 25000–30000 time units. Fixed initial conditions were given by an ad hoc choice of $\varphi(0) = (\varphi_1, \ldots, \varphi_N)$ with

$$\varphi_j = \begin{cases} j+1 & \text{for } N \leq 6 \\ \frac{6.2(j+1)}{N-1} & \text{for } N > 6. \end{cases}$$

For simulation with random initial conditions, the initial conditions were sampled uniformly on the canonical invariant region $\mathcal{C}$; cf. Section 1.1. Before the calculation of the maximal Lyapunov exponent, a transient of some length was discarded to allow the dynamics to converge to an attractor.

There is a possibility of stable heteroclinic cycles lying on the flow-invariant boundary of the canonical invariant region $\mathcal{C}$. These will cause the numerically calculated maximal Lyapunov exponent to take positive values. To take this into account we calculated the closest approach to the boundary $\partial\mathcal{C}$ after discarding the transient. If the closest approach was less then a threshold of 10^{-3} was set to zero. However, this criterion was not fulfilled in the calculations performed for any of the figures shown in this thesis.

Properties of the projection Π. Consider a system of four oscillators, i.e., $N = 4$, and recall the following definitions from Chapter 1. The action of $\mathbb{Z}/4\mathbb{Z}$ on the canonical invariant region $\mathcal{C}$ is generated by

$$\xi : (0, \psi_2, \ldots, \psi_N) \mapsto (0, \psi_3 - \psi_2, \ldots, \psi_N - \psi_2, 2\pi - \psi_2)\,;$$

cf. Equation (1.9). Note that the group $\mathbb{Z}/N\mathbb{Z}$ is isomorphic to the group of Nth roots of unity. Let $\zeta := \exp\left(-\frac{\pi i}{2}\right)$ denote one of the primitive fourth roots of unity that generates $\mathbb{Z}/4\mathbb{Z}$, i.e., $\mathbb{Z}/4\mathbb{Z} \cong \langle\zeta\rangle$. The group $\mathbb{Z}/4\mathbb{Z}$ acts on $\mathbb{R}^2 = \mathbb{C}$ by complex multiplication, i.e., the group action is given by

$$\begin{aligned} a : \mathbb{Z}/4\mathbb{Z} \times \mathbb{C} &\to \mathbb{C}, \\ (k, z) &\mapsto \zeta^k z. \end{aligned} \tag{A.4}$$

Let $I := [0, 1]$ denote the unit interval. Thus, the group $\mathbb{Z}/4\mathbb{Z}$ acts on $\mathbb{R}^2 \times I$ through the map $a \times \mathrm{id}$.

These group actions give rise to a $\mathbb{Z}/4\mathbb{Z}$-equivariant (noninjective) map

$$\begin{aligned} \Pi : \mathcal{C} &\to \mathbb{R}^2 \times I, \\ \psi &\mapsto (y(\psi), |R(\psi)|) \end{aligned} \tag{A.5}$$

[1] GNU Scientific Library, available online at http://www.gnu.org/software/gsl/.

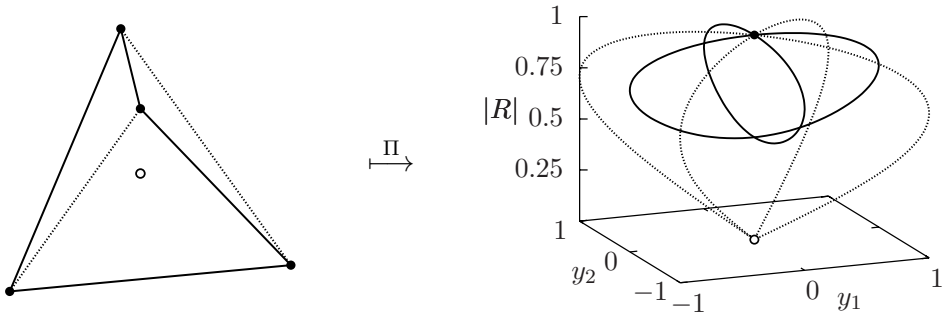

Figure A.1.: Image of the edges of the canonical invariant region $\mathcal{C}$ in $\mathbb{R}^2 \times I$. The line styles are the same as in Figure 1.1. Note that two opposite solid lines are mapped onto the same solid line since $\Pi(E_0(\mathbf{T})) = \Pi(E_2(\mathbf{T}))$ and $\Pi(E_1(\mathbf{T})) = \Pi(E_3(\mathbf{T}))$.

as defined in Chapter 1, Equation (1.13), where R denotes the order parameter (1.2). One easily verifies that the diagram

$$\begin{array}{ccc} \mathcal{C} & \xrightarrow{\xi^{\circ k}} & \mathcal{C} \\ {\scriptstyle\Pi}\downarrow & & \downarrow{\scriptstyle\Pi} \\ \mathbb{C} \times I & \xrightarrow[\zeta^k \times \mathrm{id}]{} & \mathbb{C} \times I \end{array}$$

commutes for any $k \in \mathbb{Z}/4\mathbb{Z}$. Thus, the action of the group $\mathbb{Z}/4\mathbb{Z}$ on the canonical invariant region $\mathcal{C}$ corresponds to a rotation of the complex plane $\mathbb{C}$ by an angle of $-\frac{\pi}{2}$.

For four oscillators, the canonical invariant region is a three-dimensional simplex whose edges may be parametrized by a parameter $\alpha \in \mathbf{T}$ through the functions

$$\begin{aligned} E_0(\alpha) &= (0, \alpha, \alpha, \alpha), \\ E_1(\alpha) &= (0, 0, 0, -\alpha), \\ E_2(\alpha) &= (0, 0, -\alpha, 0), \\ E_3(\alpha) &= (0, -\alpha, 0, 0) \end{aligned}$$

which correspond to edges with instantaneous symmetry group S_{N-1} and

$$\begin{aligned} E_4(\alpha) &= (0, 0, \alpha, \alpha), \\ E_5(\alpha) &= (0, \alpha, \alpha, 0) \end{aligned}$$

with instantaneous symmetry $S_2 \times S_2$. Note that the group action of $\mathbb{Z}/4\mathbb{Z}$ permutes the edges. With indices in $\mathbb{Z}/4\mathbb{Z}$, we have $E_{k+1} = \xi \circ E_k$. Furthermore, for the last two edges we have $E_5 = \xi \circ E_4$ and $-E_4 = \xi \circ E_5$. The images of the edges under the projection Π are curves in $\mathbb{R}^2 \times I$ as depicted in Figure A.1. For the fully synchronized state and the splay state, we have

$$\begin{aligned} \Pi(\varphi^{\mathrm{sync}}) &= (0, 0, 1), \\ \Pi(\varphi^{\mathrm{splay}}) &= (0, 0, 0). \end{aligned}$$

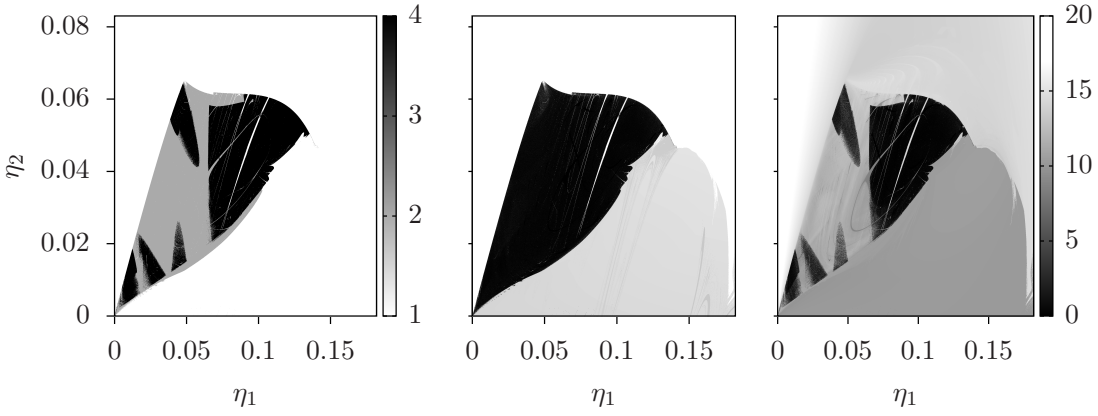

(a) Approximation $\widetilde{\Sigma}$ (b) Average $|Q_2^{\mathrm{a}}|$ (c) Average $|Q_4|$

Figure A.2.: A comparison of the approximation of the size of the group of symmetries on average (A.6) (cf. Figure 1.3) with the ergodic averages Q_2^{a} and Q_4 shows good agreement; values close to zero in Panels (b) and (c) indicate the presence of $\mathbb{Z}/2\mathbb{Z}$ and $\mathbb{Z}/4\mathbb{Z}$ symmetry, respectively.

Symmetries of the attractor. We use the projection (A.5) to calculate the symmetry of chaotic attractors. Suppose that $p_j = \zeta^{-j}(1+i)$, $j = 1, \ldots, 4$, and define $d_k(\varphi, T) := \min_{t<T} |a(\varphi(t)) - p_k|$. Calculate

$$P(\varphi, T) = (d_1(\varphi, T), d_2(\varphi, T), d_3(\varphi, T), d_4(\varphi, T)) \in \mathbb{R}^4.$$

For $A = \omega(\varphi)$, $P(\varphi, T) = (P_1, P_2, P_3, P_4)$ and given threshold $\theta > 0$ evaluate the function

$$\widetilde{\Sigma}(A, T) = \operatorname{card}\left\{ j \;\middle|\; \left| P_j - \min_{k=1,\ldots,4} P_k \right| < \theta \right\}. \tag{A.6}$$

The value of $\widetilde{\Sigma}(A, T)$ is some measure of symmetry for the group S_4 acting on $\mathbb{R}^4$ by permuting indices and served as an approximation for the size of the group of symmetries on average in Figure 1.3.

The value of $\widetilde{\Sigma}(A)$ for a threshold of $\theta = 10^{-2}$ is in good agreement with the ergodic averages of the image under the equivariant projection Π; cf. Figure A.2 for a comparison with fixed initial conditions. These are given by

$$Q_2^{\mathrm{a}}(\varphi) = \frac{1}{T} \int_0^T \sin(\varphi_1(t) - \varphi_3(t))\, \mathrm{d}t \tag{A.7}$$

$$Q_2^{\mathrm{b}}(\varphi) = \frac{1}{T} \int_0^T \sin(\varphi_2(t) - \varphi_4(t))\, \mathrm{d}t \tag{A.8}$$

$$Q_4(\varphi) = \frac{1}{T} \int_0^T \sin(\varphi_1(t) - \varphi_3(t)) \sin(\varphi_2(t) - \varphi_4(t))\, \mathrm{d}t. \tag{A.9}$$

The functions Q_2^j with $j \in \{\mathrm{a}, \mathrm{b}\}$ take the average over either one component of the projection (A.5) and Q_4 takes a combined average. Hence, Q_2 encodes $\mathbb{Z}/2\mathbb{Z}$ symmetry

Parameter	Description	Value in simulations
θ_{div}	Divergence threshold	10^6
θ_{conv}	Convergence threshold	10^{-13}
θ_{same}	Tolerance for two points to be the same	10^{-6}
μ_{cap}	Adaptation parameter divergence threshold	5
T_{timeout}	Maximum number of iterations	3000

Table A.1.: Parameters for the numerical simulations to evaluate the performance of stalling Predictive Feedback Control and adaptation.

and Q_4 symmetry with respect to $\mathbb{Z}/4\mathbb{Z}$. A value close to zero of these averages indicates the presence of the corresponding symmetries; see for example [4, 39] for a more comprehensive treatment of these so-called detectives.

A.2. Chaos Control

Implementation of large scale simulations. To evaluate the performance of Stalled Predictive Feedback Control we performed numerical simulations. The software was implemented in C/C++ making use of the GSL libraries. In particular, derivatives were calculated numerically using the GSL built-in functions.

A given number of runs was performed for a given $h^{\alpha}_{\mu,p}$. The control parameter μ may be subject to adaptation with adaptation parameter ν_0 and $\nu(p) = \frac{\nu_0}{p}$ as explained above. The parameters of the simulation algorithm are summarized in Table A.1. Each run consists of the following steps where k is the index of the current time step.

Step 0 *(Initialization)*:

(1) Initialize adaptation according to the current adaptation rule (3.18). No adaptation corresponds to $\mu_0 = \nu(p)$ and $\Delta\mu_k = 0$ for all k.

(2) Sample $\hat{x} \in \mathbb{R}^N$ from a probability distribution with support on some (map dependent) subset of the basin of attraction of the chaotic attractor. Sample T'_{trans} uniformly from the set $\{1, \ldots, 2000\}$. Calculate the initial condition

$$x_0 = f^{\circ(T_{\text{trans}})}(\hat{x}),$$

with $T_{\text{trans}} = T'_{\text{trans}} + 250$, after some transient iteration. Thus, the minimal transient iteration is 251 time steps to allow the orbit to converge to the attractor. Set $k := 0$.

While $K < T_{\text{timeout}}$ and $\|x_K\| < \theta_{\text{div}}$ repeat the following steps.

Step 1 *(Iterate)*: Calculate $x_{k+1} = h^{\alpha}_{\mu,p}(x_k)$, $\mu_{k+1} = \mu_k + \Delta\mu_k$, and $k := k + 1$.

Step 2 *(Divergence check)*: End loop if $\|x_k\| > \theta_{\text{div}}$ (divergence) or $\mu_k > \mu_{\text{cap}}$ (divergence of the control parameter). In this case return convergence failure.

Step 3 *(Convergence check)*: If $\|x_k - x_{k-1}\| < \theta_{\text{conv}}$ and $\|f_p(x_{k-1}) - x_{k-1}\| < \theta_{\text{same}}$ then execute the following steps. The second condition ensures convergence to a periodic orbit of f. Note that this additional condition does not lead to any extra numerical cost as $f_p(x_k)$ is needed to evaluate $h^{\alpha}_{\mu,p}(x_k)$. Refer to Section 3.5 for a discussion of the role of adaptation.

(1) Calculate periodic orbit $x_k, f(x_k), \ldots, f^{\circ p}(x_k)$.

(2) If $\|f^{\circ q}(x_k) - x_k\| > \theta_{\text{same}}$ for $1 \leq q < p-1$ and $\|f^{\circ p}(x_k) - x_k\| < \theta_{\text{same}}$ then return successful convergence. Otherwise return convergence to incorrect period.

If the loop ends without a result then return convergence failure. The resulting convergence times were rescaled to the number of evaluations of f_p before any statistic was evaluated.

Acknowledgements

First of all, I would like to express my gratitude towards Marc Timme for giving me the chance to write my thesis under his supervision. I am very thankful for the friendly and relaxed atmosphere in which I was able to work and pursue my own ideas. At the same time, I have to thank Laurent Bartholdi who took the role to represent the Institute for Mathematics. In addition to their constant support all matters regarding science, I would also like to thank for all the valuable comments that helped to improve the presentation of the results presented here.

Thanks also go to Theo Geisel and the whole Department of Nonlinear Dynamics and the Network Dynamics Group at the Max Planck Institute for Dynamics and Self-Organization. They have provided a superb working environment which has been my home for the past three years and there are many people who have contributed to this work in some way or the other. I am very thankful for wonderful discussion on and off topic. In particular, our retreats have proven not only to be scientifically inspiring but also great fun. There are too many awesome individuals who have made my time worthwhile to name them all. I would also like to thank all the administrative staff that has been very helpful sorting out any matter.

I am indebted to Michael Monteforte and Christoph Kolodziejski who have been way more to me than just my officemates.

Outside of Göttingen, I would like to thank Peter Ashwin and the University of Exeter for their hospitality for almost half a year. It was an enriching experience both scientifically and personally. My gratitude also goes to Mikhail I. Rabinovich and the whole BioCircuits Institute for hosting me and the continuing support and friendship. These extended stays would not have been possible without funding from the German Academic Exchange Service (DAAD) through multiple short-term scholarships.

Throughout the years I have had the honor to meet and discuss with great scientists from around the world whom I met along the way. All these discussions have greatly influenced my work and my thinking. In particular, I would like to thank Peter Ashwin, Jonathan Dawes, Alexander Fradkov, Rainer Lauterbach, Yuri Maistrenko, Arkady Pikovsky, Mikhail I. Rabinovich, Eckehard Schöll, and Sebastian Wieczorek for helpful discussions. Moreover, I would also like to thank all the people outside of science that I have met along the way all over the globe. You have taught me a lot and all the discussions have shaped my view of the world, helped me to see things I might not have been able to see otherwise.

In the last years there have been several occasions where I realized what an amazing group of friends I have. This is one of the most precious things in life. At or outside

of the Institute, in Germany and many other places. Thank you for your hospitality, wine, cheese, coffee, tea, beer, whiskey, food, dancing, and much, much more. Thank you for sharing the pleasures, but sometimes also the hardships of life with me. Too many to name, you know who you are and how much I appreciate your friendship.

Last but not least I would like to thank my parents and my brother for their continuing support in every respect. This thesis is dedicated to my mother who, unfortunately, did not live to see it completed.

List of Symbols

$\overline{A}$	Topological closure of a set A, page 16
∂A	Topological boundary of a set A, page 29
$\mathbb{C}$	Field of complex numbers, page 41
$\hat{\mathbb{C}}$	Riemann sphere, page 50
$\mathbb{C}^\times$	Nonzero complex numbers, page 63
$\mathbb{C}[z]$	Polynomial with complex valued coefficients, page 50
$\mathcal{C}$	Canonical invariant region as a subset of $\mathbf{T}^{N-1}$, page 19
$\mathrm{card}(S)$	Cardinality of a set S, page 42
$\mathrm{d}f\|_x$	Total derivative of a differentiable function f at x, page 16
$\mathcal{F}(\mu_0, p)$	Class of functions with at least one stabilizable period p orbit for control parameter μ_0, page 42
$F(f)$	Fatou set of a meromorphic function $f : \hat{\mathbb{C}} \to \hat{\mathbb{C}}$, page 50
$\mathrm{Fix}(f)$	Set of fixed points of a map f, page 40
$\mathrm{Fix}^\bullet(f)$	Stabilized fixed points for $f \in \mathcal{F}(\mu_0, 1)$, page 43
$\mathrm{Fix}(f, p)$	Fixed points of f of minimal period p, page 58
$\mathrm{Fix}_g^*(f, p)$	PFC stabilizable fixed points of f of minimal period p, page 58
$\mathrm{Fix}_h^*(f, p)$	SPFC stabilizable fixed points of f of minimal period p, page 62
$f^{\circ p}$	pth iterate of a map f, page 40
Γ	A group, typically acting on a smooth manifold $\mathfrak{M}$, page 17
i	Imaginary unit, page 15
id	Identity element of a group or identity map, page 40
$J(f)$	Julia set of a meromorphic function $f : \hat{\mathbb{C}} \to \hat{\mathbb{C}}$, page 50
$\lambda_{\max}$	Maximal Lyapunov exponent, page 17
$\mathfrak{M}$	Smooth manifold, page 16

$T_p\mathfrak{M}$	Tangent space of $\mathfrak{M}$ at $p \in \mathfrak{M}$, page 16
$\mathbb{N}$	Set of natural numbers, page 16
$\mathbb{N}_0$	Set of natural numbers including zero, page 61
$\mathbb{R}$	Field of real numbers, page 16
$\varrho(M)$	Spectral radius of a matrix M, page 41
$\Sigma(A)$	Group of symmetries on average of a set A in Γ, page 18
$\mathbf{S}^1$	Unit circle, page 63
S_N	Group of permutations of N symbols, page 19
$\mathrm{Stab}(A)$	Stabilizer of the set A in Γ, page 18
$\mathbf{T}^N$	N-dimensional torus, page 16
X	Vector field on a smooth manifold $\mathfrak{M}$, page 16
$\mathbb{Z}$	Ring of integers, page 16
$\mathbb{Z}/N\mathbb{Z}$	Cyclic group with N elements, page 19

Bibliography

[1] J. Acebrón, L. Bonilla, C. Pérez Vicente, F. Ritort, and R. Spigler, *The Kuramoto model: A simple paradigm for synchronization phenomena*, Reviews of Modern Physics **77** (2005), no. 1, 137–185, doi:10.1103/RevModPhys.77.137.

[2] Z. Arai, *On Hyperbolic Plateaus of the Hénon Map*, Experimental Mathematics **16** (2007), no. 2, 181–188, doi:10.1080/10586458.2007.10128992.

[3] P. Ashwin, J. Buescu, and I. Stewart, *From attractor to chaotic saddle: a tale of transverse instability*, Nonlinearity **9** (1996), no. 3, 703–737, doi:10.1088/0951-7715/9/3/006.

[4] P. Ashwin and M. Nicol, *Detection of symmetry of attractors from observations I. Theory*, Physica D **100** (1997), no. 1, 58–70, doi:10.1016/S0167-2789(96)00175-3.

[5] P. Ashwin, G. Orosz, and J. Borresen, *Heteroclinic Switching in Coupled Oscillator Networks: Dynamics on Odd Graphs*, Nonlinear Dynamics and Chaos: Advances and Perspectives (M. Thiel, J. Kurths, M. C. Romano, G. Károlyi, and A. Moura, eds.), Understanding Complex Systems, Springer, Berlin, Heidelberg, 2010, pp. 31–50.

[6] P. Ashwin, G. Orosz, J. Wordsworth, and S. Townley, *Dynamics on Networks of Cluster States for Globally Coupled Phase Oscillators*, SIAM Journal on Applied Dynamical Systems **6** (2007), no. 4, 728, doi:10.1137/070683969.

[7] P. Ashwin and J. W. Swift, *The dynamics of n weakly coupled identical oscillators*, Journal of Nonlinear Science **2** (1992), no. 1, 69–108, doi:10.1007/BF02429852.

[8] D. Auerbach, P. Cvitanović, J.-P. Eckmann, G. Gunaratne, and I. Procaccia, *Exploring Chaotic Motion Through Periodic Orbits*, Physical Review Letters **58** (1987), no. 23, 2387–2389, doi:10.1103/PhysRevLett.58.2387.

[9] G. Baier and M. Klein, *Maximum hyperchaos in generalized Hénon maps*, Physics Letters A **151** (1990), no. 6–7, 281–284, doi:10.1016/0375-9601(90)90283-T.

[10] L. Barreira and Y. B. Pesin, *Lyapunov exponents and smooth ergodic theory*, University Lecture Series, vol. 23, American Mathematical Society, Providence, RI, 2002.

[11] C. Bick, C. Kolodziejski, and M. Timme, *On Adaptive Stalled Predictive Feedback Chaos Control*, In Prep. (2012).

[12] C. Bick, C. Kolodziejski, and M. Timme, *Stalling Chaos Control Accelerates Convergence*, Submitted (2012).

[13] C. Bick, M. Timme, and P. Ashwin, *Dynamics and Bifurcations in Symmetric Kuramoto Systems with Generalized Coupling Functions*, In Prep. (2013).

[14] C. Bick, M. Timme, and C. Kolodziejski, *Adapting Predictive Feedback Chaos Control for Optimal Convergence Speed*, SIAM Journal on Applied Dynamical Systems **11** (2012), no. 4, 1310–1324, doi:10.1137/120861618.

[15] C. Bick, M. Timme, D. Paulikat, D. Rathlev, and P. Ashwin, *Chaos in Symmetric Phase Oscillator Networks*, Physical Review Letters **107** (2011), no. 24, 244101, doi:10.1103/PhysRevLett.107.244101.

[16] M. E. Brewster and R. Kannan, *Nonlinear Successive Over-Relaxation*, Numerische Mathematik **44** (1984), no. 2, 309–315, doi:10.1007/BF01410114.

[17] E. Brown, J. Moehlis, and P. Holmes, *On the Phase Reduction and Response Dynamics of Neural Oscillator Populations.*, Neural Computation **16** (2004), no. 4, 673–715, doi:10.1162/089976604322860668.

[18] J. C. Claussen and H. G. Schuster, *Improved control of delayed measured systems*, Physical Review E **70** (2004), no. 5, 056225, doi:10.1103/PhysRevE.70.056225.

[19] J. J. Crofts and R. L. Davidchack, *Efficient Detection of Periodic Orbits in Chaotic Systems by Stabilizing Transformations*, SIAM Journal on Scientific Computing **28** (2006), no. 4, 1275–1288, doi:10.1137/050623401.

[20] J. J. Crofts and R. L. Davidchack, *On the use of stabilizing transformations for detecting unstable periodic orbits in high-dimensional flows*, Chaos **19** (2009), no. 3, 033138, doi:10.1063/1.3222860.

[21] P. Cvitanović, *Periodic orbits as the skeleton of classical and quantum chaos*, Physica D **51** (1991), no. 1–3, 138–151, doi:10.1016/0167-2789(91)90227-Z.

[22] P. Cvitanović, R. Artuso, R. Mainieri, G. Tanner, and G. Vattay, *Chaos: Classical and Quantum*, ChaosBook.org, Niels Bohr Institute, Copenhagen, 2009.

[23] H. Daido, *Generic scaling at the onset of macroscopic mutual entrainment in limit-cycle oscillators with uniform all-to-all coupling*, Physical Review Letters **73** (1994), no. 5, 760–763, doi:10.1103/PhysRevLett.73.760.

[24] H. Daido, *Onset of cooperative entrainment in limit-cycle oscillators with uniform all-to-all interactions: bifurcation of the order function*, Physica D **91** (1996), no. 1–2, 24–66, doi:10.1016/0167-2789(95)00260-X.

[25] R. Davidchack and Y.-C. Lai, *Efficient algorithm for detecting unstable periodic orbits in chaotic systems*, Physical Review E **60** (1999), no. 5, 6172–6175, doi:10.1103/PhysRevE.60.6172.

[26] M. de Sousa Vieira and A. Lichtenberg, *Controlling chaos using nonlinear feedback with delay*, Physical Review E **54** (1996), no. 2, 1200–1207, doi: 10.1103/PhysRevE.54.1200.

[27] F. K. Diakonos and P. Schmelcher, *On the construction of one-dimensional iterative maps from the invariant density: the dynamical route to the beta distribution*, Physics Letters A **211** (1996), no. 4, 199–203, doi:10.1016/0375-9601(95)00971-X.

[28] F. K. Diakonos, P. Schmelcher, and O. Biham, *Systematic Computation of the Least Unstable Periodic Orbits in Chaotic Attractors*, Physical Review Letters **81** (1998), no. 20, 4349–4352, doi:10.1103/PhysRevLett.81.4349.

[29] E. J. Doedel, *AUTO: A Program for the Automatic Bifurcation Analysis of Autonomous Systems*, Congressus Numerantium **30** (1981), 265–384.

[30] E. J. Doedel, R. C. Paffenroth, A. R. Champneys, T. F. Fairgrieve, Y. A. Kuznetsov, B. E. Oldeman, B. Sandstede, and X. J. Wang, *AUTO2000 : Software for Continuation and Bifurcation Problems in Ordinary Differential Equations*, Tech. report, California Institute of Technology, Pasadena, CA, 2000.

[31] B. Doyon and L. Dubé, *Targeting unknown and unstable periodic orbits*, Physical Review E **65** (2002), no. 3, 1–4, doi:10.1103/PhysRevE.65.037202.

[32] H. Dullin, *Personal Communication.*

[33] J.-P. Eckmann and D. Ruelle, *Ergodic theory of chaos and strange attractors*, Reviews of Modern Physics **57** (1985), no. 3, 617–656, doi: 10.1103/RevModPhys.57.617.

[34] P. Fatou, *Sur les équations fonctionnelles*, Bulletin de la Société Mathématique de France **48** (1920), 33–94.

[35] A. L. Fradkov and A. Y. Pogromsky, *Introduction to Control of Oscillations and Chaos*, World Scientific, 1998.

[36] A. Garfinkel, M. Spano, W. Ditto, and J. Weiss, *Controlling cardiac chaos*, Science **257** (1992), no. 5074, 1230–1235, doi:10.1126/science.1519060.

[37] P. Gawthrop, *Act-and-Wait and Intermittent Control: Some Comments*, IEEE Transactions on Control Systems Technology **18** (2010), no. 5, 1195–1198, doi: 10.1109/TCST.2009.2034403.

[38] M. Golubitsky, M. Krupa, and C. Lim, *Time-Reversibility and Particle Sedimentation*, SIAM Journal on Applied Mathematics **51** (1991), no. 1, 49–72, doi: 10.1137/0151005.

[39] M. Golubitsky and I. Stewart, *The Symmetry Perspective*, Progress in Mathematics, vol. 200, Birkhäuser Verlag, Basel, 2002.

[40] M. Golubitsky, I. Stewart, and D. G. Schaeffer, *Singularities and Groups in Bifurcation Theory. Vol. II*, Springer-Verlag, New York, 1988.

[41] J. Graczyk and G. Świątek, *The Real Fatou Conjecture*, Annals of Mathematics Studies, Princeton University Press, Princeton, NJ, 1998.

[42] J. Guckenheimer and P. Holmes, *Nonlinear Oscillations, Dynamical Systems, and Bifurcations of Vector Fields*, Applied Mathematical Sciences, vol. 42, Springer-Verlag, New York, 1983.

[43] V. Hakim and W.-J. Rappel, *Dynamics of the globally coupled complex Ginzburg-Landau equation*, Physical Review A **46** (1992), no. 12, R7347–R7350, doi:10.1103/PhysRevA.46.R7347.

[44] B. Hasselblatt and Y. Pesin, *Hyperbolic dynamics*, Scholarpedia **3** (2008), no. 6, 2208, doi:10.4249/scholarpedia.2208.

[45] M. Hénon, *A two-dimensional mapping with a strange attractor*, Communications in Mathematical Physics **50** (1976), no. 1, 69–77, doi:10.1007/BF01608556.

[46] P. Holmes, *History of dynamical systems*, Scholarpedia **2** (2007), no. 5, 1843, doi:10.4249/scholarpedia.1843.

[47] A. J. Homburg, H. Kokubu, and V. Naudot, *Homoclinic-Doubling Cascades*, Archive for Rational Mechanics and Analysis **160** (2001), no. 3, 195–243, doi:10.1007/s002050100159.

[48] A. J. Homburg and B. Krauskopf, *Resonant Homoclinic Flip Bifurcations*, Journal of Dynamics and Differential Equations **12** (2000), no. 4, 807–850, doi:10.1023/A:1009046621861.

[49] A. J. Homburg and B. Sandstede, *Homoclinic and heteroclinic bifurcations of vector fields*, Handbook of Dynamical Systems Vol. 3 (H. W. Broer, T. Floris, and B. Hasselblatt, eds.), Elsevier, 2010, pp. 379–524.

[50] A. S. Householder, *Minimal Matrix Norms*, Monatshefte für Mathematik **63** (1959), no. 4, 344–350, doi:10.1007/BF01299549.

[51] S. L. Hruska, *A Numerical Method for Constructing the Hyperbolic Structure of Complex Henon Mappings*, Foundations of Computational Mathematics **6** (2006), no. 4, 427–455, doi:10.1007/s10208-006-0141-2.

[52] J. H. Hubbard and R. W. Oberste-Vorth, *Hénon mappings in the complex domain I: The global topology of dynamical space*, Publications Mathématiques de L'Institut des Hautes Scientifiques **79** (1994), no. 1, 5–46, doi:10.1007/BF02698886.

[53] K. Ikeda, H. Daido, and O. Akimoto, *Optical Turbulence: Chaotic Behavior of Transmitted Light from a Ring Cavity*, Physical Review Letters **45** (1980), no. 9, 709–712, doi:10.1103/PhysRevLett.45.709.

[54] T. Insperger and G. Stépán, *Act-and-wait control concept for discrete-time systems with feedback delay*, IET Control Theory & Applications **1** (2007), no. 3, 553–557, doi:10.1049/iet-cta:20060051.

[55] E. M. Izhikevich, *Dynamical Systems in Neuroscience: The Geometry of Excitability and Bursting*, MIT Press, Cambridge, Massachusetts, 2007.

[56] A. Katok and B. Hasselblatt, *Introduction to the Modern Theory of Dynamical Systems*, Encyclopedia of Mathematics and its Applications, vol. 54, Cambridge University Press, Cambridge, 1995.

[57] A. Klebanoff and E. Bollt, *Convergence analysis of Davidchack and Lai's algorithm for finding periodic orbits*, Chaos, Solitons & Fractals **12** (2001), no. 7, 1305–1322, doi:10.1016/S0960-0779(00)00099-0.

[58] H. Kori, C. G. Rusin, I. Z. Kiss, and J. L. Hudson, *Synchronization engineering: theoretical framework and application to dynamical clustering*, Chaos **18** (2008), no. 2, 026111, doi:10.1063/1.2927531.

[59] Y. Kuramoto, *Chemical Oscillations, Waves and Turbulence*, Springer, New York, 1984.

[60] Y. A. Kuznetsov, *Elements of applied bifurcation theory*, third ed., Applied Mathematical Sciences, vol. 112, Springer-Verlag, New York, 2004.

[61] J. S. W. Lamb and J. A. G. Roberts, *Time-reversal symmetry in dynamical systems: A survey*, Physica D **112** (1998), no. 1–2, 1–39, doi:10.1016/S0167-2789(97)00199-1.

[62] J. M. Lee, *Introduction to Smooth Manifolds*, Graduate Texts in Mathematics, vol. 218, Springer New York, New York, NY, 2012.

[63] J. Lehnert, P. Hövel, V. Flunkert, P. Y. Guzenko, A. L. Fradkov, and E. Schöll, *Adaptive tuning of feedback gain in time-delayed feedback control*, Chaos **21** (2011), no. 4, 043111, doi:10.1063/1.3647320.

[64] X.-B. Lin, *Lin's method*, Scholarpedia **3** (2008), no. 9, 6972, doi:10.4249/scholarpedia.6972.

[65] E. N. Lorenz, *Deterministic Nonperiodic Flow*, Journal of the Atmospheric Sciences **20** (1963), no. 2, 130–141, doi:10.1175/1520-0469(1963)020<0130:DNF>2.0.CO;2.

[66] S. Luccioli and A. Politi, *Irregular Collective Behavior of Heterogeneous Neural Networks*, Physical Review Letters **105** (2010), no. 15, 158104, doi:10.1103/PhysRevLett.105.158104.

[67] R. Mañé, *Ergodic theory and differentiable dynamics*, Ergebnisse der Mathematik und ihrer Grenzgebiete (3), vol. 8, Springer-Verlag, Berlin, 1987.

[68] S. A. Marvel, R. E. Mirollo, and S. H. Strogatz, *Identical phase oscillators with global sinusoidal coupling evolve by Möbius group action*, Chaos **19** (2009), no. 4, 043104, doi:10.1063/1.3247089.

[69] J. Milnor, *On the concept of attractor*, Communications in Mathematical Physics **99** (1985), no. 2, 177–195, doi:10.1007/BF01212280.

[70] J. Milnor, *On the concept of attractor: Correction and remarks*, Communications in Mathematical Physics **102** (1985), no. 3, 517–519, doi:10.1007/BF01209298.

[71] J. Milnor, *Dynamics in one complex variable*, third ed., Annals of Mathematics Studies, vol. 160, Princeton University Press, Princeton, NJ, 2006.

[72] J. Moehlis and E. Knobloch, *Equivariant dynamical systems*, Scholarpedia **2** (2007), no. 10, 2510, doi:10.4249/scholarpedia.2510.

[73] O. Morgül, *Stabilization of unstable periodic orbits for discrete time chaotic systems by using periodic feedback*, International Journal of Bifurcation and Chaos **16** (2006), no. 2, 311–323, doi:10.1142/S0218127406014824.

[74] N. Nakagawa and Y. Kuramoto, *Collective Chaos in a Population of Globally Coupled Oscillators*, Progress of Theoretical Physics **89** (1993), no. 2, 313–323, doi:10.1143/PTP.89.313.

[75] N. Nakagawa and Y. Kuramoto, *From collective oscillations to collective chaos in a globally coupled oscillator system*, Physica D **75** (1994), no. 1–3, 74–80, doi:10.1016/0167-2789(94)90275-5.

[76] E. Ott, *Chaos in Dynamical Systems*, Cambridge University Press, New York, 2002.

[77] E. Ott and T. M. Antonsen, *Low dimensional behavior of large systems of globally coupled oscillators*, Chaos **18** (2008), no. 3, 037113, doi:10.1063/1.2930766.

[78] E. Ott and T. M. Antonsen, *Long time evolution of phase oscillator systems*, Chaos **19** (2009), no. 2, 023117, doi:10.1063/1.3136851.

[79] E. Ott, C. Grebogi, and J. A. Yorke, *Controlling Chaos*, Physical Review Letters **64** (1990), no. 11, 1196–1199, doi:10.1103/PhysRevLett.64.1196.

[80] F. Pasemann, *Complex dynamics and the structure of small neural networks*, Network: Computation in Neural Systems **13** (2002), no. 2, 195–216, doi:10.1080/net.13.2.195.216.

[81] A. Pikovsky and P. Rosenau, *Phase compactons*, Physica D **218** (2006), no. 1, 56–69, doi:10.1016/j.physd.2006.04.015.

[82] A. Pikovsky, M. Rosenblum, and J. Kurths, *Synchronization: A Universal Concept in Nonlinear Sciences*, Cambridge University Press, 2003.

[83] D. Pingel, P. Schmelcher, and F. K. Diakonos, *Stability transformation: a tool to solve nonlinear problems*, Physics Reports **400** (2004), no. 2, 67–148, doi:10.1016/j.physrep.2004.07.003.

[84] D. Pingel, P. Schmelcher, F. Diakonos, and O. Biham, *Theory and applications of the systematic detection of unstable periodic orbits in dynamical systems*, Physical Review E **62** (2000), no. 2, 2119–2134, doi:10.1103/PhysRevE.62.2119.

[85] H. Poincaré, *Sur le problème des trois corps et les équations de la dynamique*, Acta Mathematica **13** (1890), 1–270.

[86] B. T. Polyak, *Stabilizing Chaos with Predictive Control*, Automation and Remote Control **66** (2005), no. 11, 1791–1804, doi:10.1007/s10513-005-0213-z.

[87] O. V. Popovych, Y. L. Maistrenko, and P. A. Tass, *Phase chaos in coupled oscillators*, Physical Review E **71** (2005), no. 6, 65201, doi:10.1103/PhysRevE.71.065201.

[88] C. M. Postlethwaite, G. Brown, and M. Silber, *Feedback control of unstable periodic orbits in equivariant Hopf bifurcation problems*, submitted (2012).

[89] K. Pyragas, *Continuous control of chaos by self-controlling feedback*, Physics Letters A **170** (1992), no. 6, 421–428, doi:10.1016/0375-9601(92)90745-8.

[90] K. Pyragas, *Delayed feedback control of chaos.*, Philosophical transactions. Series A, Mathematical, physical, and engineering sciences **364** (2006), no. 1846, 2309–34, doi:10.1098/rsta.2006.1827.

[91] M. I. Rabinovich and H. D. I. Abarbanel, *The role of chaos in neural systems*, Neuroscience **87** (1998), no. 1, 5–14, doi:10.1016/S0306-4522(98)00091-8.

[92] P. Schmelcher and F. K. Diakonos, *Detecting Unstable Periodic Orbits of Chaotic Dynamical Systems*, Physical Review Letters **78** (1997), no. 25, 4733–4736, doi:10.1103/PhysRevLett.78.4733.

[93] P. Schmelcher and F. K. Diakonos, *General approach to the localization of unstable periodic orbits in chaotic dynamical systems*, Physical Review E **57** (1998), no. 3, 2739–2746, doi:10.1103/PhysRevE.57.2739.

[94] E. Schöll, *Neural control: Chaos control sets the pace*, Nature Physics **6** (2010), no. 3, 161–162, doi:10.1038/nphys1611.

[95] E. Schöll and H. G. Schuster (eds.), *Handbook of Chaos Control*, Wiley-VCH Verlag GmbH & Co. KGaA, Weinheim, Germany, 1999.

[96] H. G. Schuster and M. Stemmler, *Control of chaos by oscillating feedback*, Physical Review E **56** (1997), no. 6, 6410–6417, doi:10.1103/PhysRevE.56.6410.

[97] A. J. Schwartz, *A Generalization of a Poincaré-Bendixson Theorem to Closed Two-Dimensional Manifolds*, American Journal of Mathematics **85** (1963), no. 3, 453, doi:10.2307/2373135.

[98] S. Smale, *Differentiable dynamical systems*, Bulletin of the American Mathematical Society **73** (1967), no. 6, 747–818, doi:10.1090/S0002-9904-1967-11798-1.

[99] D. A. Smith, W. F. Ford, and A. Sidi, *Extrapolation Methods for Vector Sequences*, SIAM Review **29** (1987), no. 2, 199–233, doi:10.1137/1029042.

[100] P. So, E. Ott, S. Schiff, D. Kaplan, T. Sauer, and C. Grebogi, *Detecting Unstable Periodic Orbits in Chaotic Experimental Data*, Physical Review Letters **76** (1996), no. 25, 4705–4708, doi:10.1103/PhysRevLett.76.4705.

[101] E. D. Sontag, *Mathematical control theory*, second ed., Texts in Applied Mathematics, vol. 6, Springer-Verlag, New York, 1998.

[102] S. Steingrube, M. Timme, F. Wörgötter, and P. Manoonpong, *Self-organized adaptation of a simple neural circuit enables complex robot behaviour*, Nature Physics **6** (2010), no. 3, 224–230, doi:10.1038/nphys1508.

[103] G. Stépán, *Retarded dynamical systems: stability and characteristic functions*, Pitman Research Notes in Mathematics Series, vol. 210, Longman Scientific & Technical, Harlow, 1989.

[104] S. H. Strogatz, *From Kuramoto to Crawford: exploring the onset of synchronization in populations of coupled oscillators*, Physica D **143** (2000), no. 1–4, 1–20, doi:10.1016/S0167-2789(00)00094-4.

[105] S. H. Strogatz, *Sync: The Emerging Science of Spontaneous Order*, Penguin, 2004.

[106] J. W. Swift, S. H. Strogatz, and K. Wiesenfeld, *Averaging of globally coupled oscillators*, Physica D **55** (1992), no. 3–4, 239–250, doi:10.1016/0167-2789(92)90057-T.

[107] S. Watanabe and S. H. Strogatz, *Integrability of a globally coupled oscillator array*, Physical Review Letters **70** (1993), no. 16, 2391–2394, doi:10.1103/PhysRevLett.70.2391.

[108] S. Watanabe and S. H. Strogatz, *Constants of motion for superconducting Josephson arrays*, Physica D **74** (1994), no. 3–4, 197–253, doi:10.1016/0167-2789(94)90196-1.

[109] D. Yang and P. Yang, *Numerical instabilities and convergence control for convex approximation methods*, Nonlinear Dynamics **61** (2010), no. 4, 605–622, doi:10.1007/s11071-010-9674-x.